國立交通大學

分子科學研究所

碩士論文

聯氨與四氧化二氮自燃反應機制的研究

Ab Initio Study of the Mechanism for the Hypergolic Reaction of Hydrazine with Dinitrogen Tetroxide

研究生　賴科余

指導教授　林明璋 院士

中華民國 九十八 年 十一 月

聯氨與四氧化二氮自燃反應機制的研究

Ab Initio Study of the Mechanism for the Hypergolic Reaction of Hydrazine with Dinitrogen Tetroxide

研 究 生：賴科余　　Student：Ke-Yu Lai

指導教授：林明璋 院士　　Advisor：Prof. M.C. Lin

國 立 交 通 大 學

分子科學研究所

碩 士 論 文

A Thesis

Submitted to Institute of Molecular Science

Department of Applied Chemistry, College of Science, National Chiao Tung University

in partial Fulfillment of the Requirements

for the Degree of

Master

in

Applied Chemistry

September 2009

Hsinchu, Taiwan, Republic of China

中華民國九十八年十一月

Acknowledgement

首先感謝院士在這兩年中的指導，無論是在研究上或是在做人處事上，常常都指引著我向前，並且提供許多的資源讓我進行研究，與許多實驗室的合作也讓我學到如何溝通與協調，非常感謝老師當初讓我有這個機會可以進入這間實驗室學習。另外，感謝帶我進入量子計算的欣聰學長，不厭其煩地讓我常常纏著問問題,以及感謝禎翰學長在實驗上的指導與教導我如何處理人生道路上的起起伏伏，很懷念與你們在工作一整天後的夜晚，在便利商店外喝著飲料討論問題與談天的日子;感謝雯妃學姊在研究上的許多協助，能找到可以一起討論研究到眼睛發亮的同伴真好；感謝 AD 總是一起熬夜做實驗，最欣賞你的直言直語，可以讓我們暢所欲言，還有小結巴廢彬，帶給大家那麼多的歡樂；感謝志翰與冠霖讓我不是孤軍奮戰，雖然總是被我碎碎念，還是非常認真地做實驗，與你們一起做實驗讓我信心十足!還有雯傑一起討論，一起做手指運動紓發壓力，是我們最好的夥伴。總是一起相約去打球的老王、馬哥、阿布、偉志、巨砲還有 Alonso，感謝你們的照顧，跟你們學習到很多不同領域的知識與解決問題的想法，在做實驗時你們總是最棒的友軍!雖然跟小朱還有欣瑜領域不同，不過與你們相處很開心，很高興與你們一起走過這兩年；另外感謝林鵬老師與文碩學長在實驗上毫不保留地教導。跟老師一起爬山出遊、與大夥一起打球賽、一起熬夜做實驗、還有每天收不停地失敗計算，這些日子非常感謝大家的照顧與陪伴，有你們真好!

最後我要感謝我的父母，不論在什麼時候都守護著我，感謝你們的栽培!以及在英國求學的怡孜，在我挫折的時候，提供我溫暖的支持，陪我一起走過。有許許多多的人在這段時間中幫助我、砥礪我、陪伴我，非常感謝你們讓我成長、一起擁有歡笑!

Abstract

Hydrazine and dinitrogen tetroxide reaction is a spontaneously ignited combustion reaction, and the propellants are practically used in the space shuttle of NASA. However, the mechanism of this hypergolic combustion system is still unknown theoretically and experimentally. In the practical system, the reactants are not only composed of $N_2H_4(C_2)$ and $N_2O_4(D_{2h})$ molecules, and they also contain trans-$ONONO_2(C_s)$, cis-$ONONO_2(C_s)$ and $NO_2(C_{2v})$ molecules which can react with hydrazine when the liquid N_2O_4 oxidizer is ejected into reaction chamber with high velocity. We consider these four bimolecular reactions by using ab-initio calculations with the Gaussian03 code. The geometries of all stationary points on the potential energy surfaces (PESs) are optimized by B3LYP/6-311++G(3df,2p). Moreover, the single-point calculations, including G3B3, CCSD(T), and G2M methods, correct the relative energies to give better values for the kinetic calculations. The G2M method provides the good prediction as CCSD(T)/6-311++G(3df,2p), and it also has smaller differences comparing with experimental data. The G2M(CC1) and G2M(CC3) schemes are chosen for the smaller and larger reaction system, respectively.

The geometries of cis- and trans-$ONONO_2$ molecules are unknown experimentally. The PES of N_2O_4 isomerization has been studied; the energy barrier between the cis-isomer and $N_2O_4(D_{2h})$ is lower than that between the trans-isomer and $N_2O_4(D_{2h})$ by 20.15 kcal/mol. The energy of transition state (TS) between cis- and trans-$ONONO_2$ is only 1.71 kcal/mol; thus cis-trans isomerization can occur rapidly.

In the bimolecular reactions, the major and lower-energy channels are the hydrogen abstraction reactions, and the mechanism for breaking the N-O bond of NO_2 or N_2O_4 molecule needs much higher energies. In the N_2H_4 + NO_2 reaction, the lowest-energy channel produces the N_2H_3 and cis-HONO via the TS with a 7.57

kcal/mol barrier. The rate constant predicted by transition state theory is $3.20\times10^{-25}T^{3.74}\exp(-1662.5/T)$ $cm^3/(molecule \cdot sec)$ at 100K - 4000K. In the N_2H_4 + N_2O_4 reaction, the hydrogen transfer reaction accompanies with bonds breaking and forming via a ring-like TS. The energy barriers of transition state in most of the reaction channels are higher than 10 kcal/mo; however, the N_2H_4 + trans-$ONONO_2$ reaction occurs by hydrogen transfer via a six-member ring TS without an intrinsic barrier. In this lowest-energy channel, the energy of transition state is predicted to be lower than intermediate by 2.66 kcal/mol at the G2M(CC3) level. However the difference is only 0.16 kcal/mol at the B3LYP/6-311++G(3df,2p) level, which is confirmed by IRC calculation; therefore, it may be caused by the zero-point energy correction and computational errors. This lowest-energy channel produces $HONO_2$ + $H_2NN(H)NO$ with 15.57 kcal/mol exothermicity. Moreover, another lower-energy channel of N_2H_4 + $N_2O_4(D_{2h})$ reaction is also exothermic, and the products are trans-HONO and $H_2NN(H)NO_2$. Furthermore, the decomposition reactions of $H_2NN(H)NO$ and $H_2NN(H)NO_2$ molecules provide another possibility producing the active species. The direct dissociation reaction to form N_2H_3 and NO radicals is the most possible path for $H_2NN(H)NO$ molecule, where it needs to overcome a small rotation TS with 6.28 kcal/mol barrier height and undergoes the dissociation reaction with 27.83 kcal/mol energy. On the other hand, the $H_2NN(H)NO_2$ can overcome a five-member ring TS, with a barrier is 26.6 kcal/mol barrier, and decompose to trans-N_2H_2 and trans-HONO. Besides, it is also possible to directly dissociate to N_2H_3 and NO_2 with 38.23 kcal/mol energy.

The hypergolic reaction of N_2O_4 with N_2H_4 is therefore believed to be initiated by the reaction of trans-$ONONO_2$ with N_2H_4 which is shown to occur barrierlessly.

Table of Contents

I. Introduction 1

1.1 Chemical properties of hydrazine and dinitrogen tetroxide 2

1.2 Review of NASA reports 6

1.3 Isomers of N_2O_4 11

1.3.1 Isomerization of N_2O_4 11

1.3.2 Temperature induced autoionization 13

1.3.3 Ab-initio studies of N_2O_4 isomers 15

1.4 References 18

II. Computation Methods 20

2.1 Ab-initio Calculations 20

2.1.1 Modified GAUSSIAN-2 (G2M) 21

2.1.2 Gaussian-3 theory using DFT geometries and zero-point energies (G3B3) 24

2.2 Kinetic Calculation 26

2.3 Reference 27

III. Results and Discussions 28

3.1 N_2H_4+NO_2 reaction 28

3.1.1 Molecular Geometries of hydrazine and nitrogen dioxide 28

3.1.2 PES of the $N_2H_4 + NO_2$ reaction 29

3.1.3 Kinetic calculation 34

3.2 N_2O_4 isomerization reaction 46

3.2.1 The geometries of N_2O_4 isomers 46

3.2.2 PES of N_2O_4 isomerization 50

3.3 N_2H_4+N_2O_4 reaction 68

3.3.1 N_2H_4 + trans-$ONONO_2$ and N_2H_4 + cis-$ONONO_2$ reactions 68

3.3.2 Decomposition of $H_2NN(H)NO$ molecule 86

3.3.3 N_2H_4+N_2O_4 (D_{2h}) reaction 97

3.3.4 Decomposition of $H_2NN(H)NO_2$ molecule 107

3.3.5 The single-point energies in N_2H_4+N_2O_4 isomeric reactions 118

3.4 Reference 120

IV. Conclusion 123

Appendix I. Geometries of Stationary Points in Reactions 125

List of Tables

Table1-1: Physical properties of N_2H_4, N_2O_4, and NO_2 1

Table1-2: The equilibrium constant of $2NO_2 \rightleftarrows N_2O_4$ at three temperatures 3

Table1-3: Equilibrium distance (in Å), bond angle (in deg), harmonic frequencies (in cm^{-1})and zero-point vibrational energies (kcal/mol) for NO_2. 5

Table1-4: Bond distance (in Å), bond angle (deg), harmonic frequencies (cm^{-1}), zero-point vibraional energies (kcal/mol) for the N_2O_4 dimer. 5

Table1-5: Energetics (in kcal/mol) of the reaction 6

Table1-6: Gas evolution from the low temperature reaction of N_2H_4+N_2O_4 7

Table1-7: The correspondence between D and D'. 12

Table1-8: Frequency and vibrational assignment of infrared bands of $ONONO_2$ (D) in an oxygen matrix. (NO_2 refers to the nitro group, and O=N-O- to the nitrite group of D). 12

Table1-9: Estimated activation barrier (kcal/mol) at the QCI and DFT (in parentheses) level of theories. 16

Table2-1: Formulas for the recommended G2M methods. 22

Table2-2: Comparison of the accuracy and the range of applicability for various modified Gaussian-2 (G2M) methods. 23

Table2-3: Steps in G3, G3(MP2), G3//B3LYP, and G3(MP2)//B3LYP methods. 25

Table2-4: Comparison of average absolute deviations in kcal/mol. 25

Table3-1: Moments of inertia (I_A, I_B, I_C) and vibration frequencies of the species computed at the B3LYP/6-311++G(3df,2p) level 39

Table3-2: Relative energies of species predicted at various theoretical levels. 41

Table3-3: Comparison of geometries (bond length in Å and bond angle in deg) of N_2H_4 by different computational methods and experimental results. 42

Table3-4: Calculated and Experimental Vibrational Frequencies (in cm^{-1}) of N_2H_4 43

Table3-5: Calculated and Experimental bond lengths (in Å), bond angles (in deg), and vibrational Frequencies (in cm^{-1}) of NO_2. 44

Table3-6: Fitting expressions for the rate constants of the N_2H_4+NO_2 reactions employing transition-state theory. 44

Table3-7: Moments of inertia (I_A, I_B, I_C) and vibration frequencies of the species in N_2O_4 isomerization computed at B3LYP/6-311++G(3df,2p). 58

Table3-8: Relative energies of species in N_2O_4 isomerization reaction at various theoretical levels. 59

Table3-9: The heat of dissociation for N_2O_4 to $2NO_2$ at 0K and one atmosphere. 60

Table3-10: Comparison of geometries (bond length in Å and bond angle in deg) of N_2O_4 by different computational methods and experimental results. 61

Table3-11: Calculated and Experimental Vibrational Frequencies (in cm^{-1}) of N_2O_4 62

Table3-12: Calculated (B3LYP) and Experimental Vibrational Frequencies (in cm^{-1}) of cis-$ONONO_2$. 63

Table3-13: Calculated Vibrational Frequencies (in cm^{-1}) of the cis-$ONONO_2$ and cis-$ONONO_2$_2 structures. 64

Table3-14: Calculated Vibrational Frequencies (in cm^{-1}) of the cis-$ONONO_2$_3 structures. 65

Table3-15: Computational and Experimental Vibrational Frequencies (in cm^{-1}) of trans-$ONONO_2$ 66

Table3-16: Moments of inertia (I_A, I_B, I_C) and vibration frequencies of the species in trans-$ONONO_2$ + N_2H_4 and cis-$ONONO_2$ + N_2H_4 reactions computed at B3LYP/6-311++G(3df,2p). 81

Table3-17: Relative energies of species in trans-$ONONO_2$ + N_2H_4 reaction and cis-$ONONO_2$ + N_2H_4 reaction predicted at various theoretical levels. 83

Table3-18: Moments of inertia (I_A, I_B, I_C) and vibration frequencies of the species in the major channel of trans-$ONONO_2$ + N_2H_4 reaction computed at PW91PW91/6-311++G(3df,2p). 84

Table3-19: Relative energies of species in the major channel of the trans-$ONONO_2$ + N_2H_4 reaction at various theoretical levels. 85

Table3-20: Moments of inertia (I_A, I_B, I_C) and vibration frequencies of the species in

$H_2NN(H)NO$ decomposition computed at B3LYP/6-311++G(3df,2p) 94

Table3-21: Relative energies of species in $H_2NN(H)NO$ decomposition computed at various theoretical levels. 95

Table3-22: Moments of inertia (I_A, I_B, I_C) and vibration frequencies of the species in the N_2O_4 (D_{2h}) + N_2H_4 reaction computed at B3LYP/6-311++G(3df,2p). 104

Table3-23: Relative energies of species in N_2O_4 (D_{2h}) + N_2H_4 reaction computed at various theoretical levels. 106

Table3-24: Moments of inertia (I_A, I_B, I_C) and vibration frequencies of the species in $H_2NN(H)NO_2$ decomposition computed at B3LYP/6-311++G(3df,2p). 115

Table3-25: Relative energies of species in $H_2NN(H)NO_2$ decomposition computed at various theoretical levels. 117

Table3-26: The heats of formation based on experimental and computational studies. 119

Table3-27: The heats of reaction of N_2H_4+NO_2 and N_2H_4+N_2O_4 reaction computed by the values from Table3-24. 119

List of Figures

Fig1-1: Measured data for equilibrium constant of at 25, 35, and 45℃. 4

Fig1-2: The infrared spectrum of N_2O_4 (high concentration) at -196℃ 6

Fig1-3: Separation model for the impinging hypergolic stream 9

Fig1-4: Parallel injector spray pattern in the combustion reaction. 9

Fig1-5: Typical spray photographs for (a) stream mixing for high pressure, (b) stream separation for high pressure. 10

Fig1-6: The D structure can undergo a cis-trans isomerization to form D'. 12

Fig1-7: Structures of N_2O_4 isomers 15

Fig3-1: The geometries in the PES are determined by B3LYP/6-311++G(3df,2p). 38

Fig 3-2: Potential Energy Surface of the N_2H_4+NO_2 reaction, whose energies are calculated by G2M(CC1)//B3LYP/6-311++G(3df,2p). 40

Fig3-3: Arrhenius plots of the calculated rate constants for various channels of the N_2H_4+NO_2 reaction. 45

Fig3-4: (a) The geometries in the PES of N_2O_4 isomerization are determined at B3LYP/ 6-311++G(3df,2p) level, (b) PW91PW91/6-311++G(3df,2p) level, (c) BHandHLYP/ 6-311++G(3df,2p) level, and (d) CCSD/6-311+G(d,p) The value in parentheses is noted for Mulliken charge. 56

Fig3-5: The PES of N_2O_4 isomerization, whose energies are calculated by

G2M(CC1)//B3LYP/6-311++G(3df,2p). 57

Fig3-6: Arrhenius plots and three-parameters fitting expressions for the rate constants. (a) The faster reaction is N_2O_4 to cis-$ONONO_2$ via i-TS2, and the lower one is N_2O_4 to trans-$ONONO_2$ via i-TS1. 67

Fig3-7: (a) The stationary points in the PES of trans-$ONONO_2$ + N_2H_4 reaction and cis-$ONONO_2$ + N_2H_4 reaction are optimized by B3LYP/6-311++G(3df,2p), and (b) the stationary points on the major channel of trans-$ONONO_2$ + N_2H_4 reaction optimized by PW91PW91 /6-311++G(3df,2p). 77

Fig3-8: Potential Energy Surface of trans-$ONONO_2$ + N_2H_4 reaction and cis-$ONONO_2$ + N_2H_4 reactions, whose energies are calculated by G2M(CC3) // B3LYP/6-311++G(3df,2p). 78

Fig3-9: The IRC calculation of C_s-TS1 is determined by B3LYP/6-311++G(3df,2p) for reverse direction. The highest point is the position of C_s-TS1, and the lowest point is approaching to the C_s-Complex1. The energy difference is 0.00027 Hartree (0.17 kcal/mol). 79

Fig3-10: The comparison for the major channel of trans-$ONONO_2$ + N_2H_4 reaction optimized by B3LYP/6-311++G(3df,2p) and PW91PW91/ 6-311++G(3df,2p). 80

Fig3-11: The stationary points in the PES of $H_2NN(H)NO$ decomposition are optimized

by B3LYP/6-311++G(3df,2p) 92

Fig3-12: Potential Energy Surface of $H_2NN(H)NO$ decomposition, whose energies are calculated by G2M(CC1) // B3LYP/6-311++G(3df,2p). 93

Fig3-13: The stationary points in the PES of N_2O_4 (D_{2h}) + N_2H_4 reaction are optimized by B3LYP/6-311++G(3df,2p) 102

Fig3-14: Potential Energy Surface of the N_2O_4 (D_{2h}) + N_2H_4 reaction, whose energies are calculated by G2M(CC3) // B3LYP/6-311++G(3df,2p). 103

Fig3-15: The stationary points in the PES of $H_2NN(H)NO_2$ decomposition are optimized by B3LYP/6-311++G(3df,2p). 113

Fig3-16: Potential Energy Surface of $H_2NN(H)NO_2$ decomposition, whose energies are calculated by G2M(CC1) // B3LYP/6-311++G(3df,2p). 114

I. Introduction

$RNHNH_2$ and N_2O_4 (R = H, CH_3, (CH_2-CH_3)) reaction systems have been continuously used as propellants for rocket propulsions into space by NASA nowadays. [1] The hydrazine (N_2H_4) and dinitrogen tetroxide (N_2O_4) reaction has an extremely hypergolic property, which ignites spontaneously upon mixing without a source of ignition. A great many reports discussed this important reaction in early NASA research [2-6], and most of them highlighted the combustion process of the rocket, whose fuel and oxidizer are hydrazine and dinitrogen tetroxide, respectively. This reaction contains many complex and rapid reactions, which make up a kind of huge chemical soup of reactions, and the spectra of these reactions make it very difficult to separate the signals originating from many species. To our best knowledge, there is no recent paper which discusses the mechanism or kinetics of this reaction computationally or experimentally.

The hydrazine and dinitrogen tetroxide have critical chemical properties as a combustion fuel and oxidizer, respectively, and some of their basic physical properties are presented in table1-1.

Table1-1: Physical properties of N_2H_4, N_2O_4, and NO_2

	Hydrazine (N_2H_4)	Dinitrogen tetroxide (N_2O_4)	Nitrogen dioxide (NO_2)
Melting Point	1 °C (274 K, anhydrous) -51.7 °C (hydrate)	−11.2 ℃ (261.9 K)	11.2 °C (62 K)
Boiling Pont	114 °C (387 K, anhydrous) 119 °C (hydrate)	21.1 ℃ (294.3 K)	21.1 °C (294 K)
Density(g/cm^3)	1.0045 (anhydrous) 1.032 (hydrate)	1.443 (liquid,21 ℃)	1.449 (liquid,20 ℃) 3.4 (gas, 22 ℃)
Appearance	colorless liquid	colorless gas	brown gas
Solubility in water	miscible	miscible	miscible
Refractive index	1.46044 (22 °C, anhydrous) 1.4284 (hydrate)	1.00112	1.449 (20 °C)
Molecular shape	C_2	planar, D_{2h}	bent, C_{2v}

1.1 Chemical properties of hydrazine and dinitrogen tetroxide

Hydrazine (N_2H_4) is a toxic, flammable caustic liquid and strong reducing agent. Its odor is similar to that of ammonia, but less strong. It is soluble in water, methanol, ethanol, UDMH (Unsymmetrical Dimethyl hydrazine ($(CH_3)_2NNH_2$)), and ethylenediamine, and therefore, it can be used with UDMH in the bi-fuel system. Hydrazine is found early and used as a storable liquid fuel, and it is replaced gradually by UDMH and MMA (Monomethyl hydrazine (CH_3NHNH_2)). Currently, it is used as a monopropellant for satellite motors. Hydrazine can be made by different methods, and these are briefly described below.

Raschig Process:

$$NH_3 + OCl^- \rightarrow NH_2Cl + OH^-$$
$$NH_2Cl + OH^- + NH_3 \rightarrow N_2H_4 + Cl^- + H_2O \quad (1.1)$$

Bayer Process:

$$2NH_3 + OCl^- + 2Me_2C{=}O \rightarrow Me_2C{=}N-N{=}CMe_2 + 3H_2O + Cl^-$$
$$Me_2C{=}N-N{=}CMe_2 + 2H_2O \rightarrow N_2H_4 + 2Me_2C{=}O \quad (1.2)$$

Produits Chimiques Ugine Kuhlmann Process (PCUK)

$$2NH_3 + H_2O_2 + 2R_2C{=}O \rightarrow R_2C{=}N-N{=}CR_2 + 4H_2O$$
$$R_2C{=}N-N{=}CR_2 + 2H_2O \rightarrow N_2H_4 + 2R_2C{=}O \quad (1.3)$$

The MMA and UDMA originate from hydrazine in which one and two hydrogen atoms are replaced by one or two methyl groups, respectively. These two species are also easy to manufacture as N_2H_4, and are applied as common rocket fuels nowadays.

On the other hand, dinitrogen tetroxide (N_2O_4) is a powerful oxidizer, highly toxic and corrosive, and it is manufactured by the catalytic oxidation of ammonia, in which steam is used as a diluting agent in order to reduce the reaction temperature. Next, the gases are cooled, and most of the water is condensed and removed. Furthermore, the nitric oxide (NO) is oxidized into nitrogen dioxide (NO_2), and the remainder of the

water is removed as nitric acid. The above process is represented by eq. (1.4). This almost pure nitrogen dioxide gas is cooled to a low temperature and condensed into liquid, which keeps the equilibrium towards dinitrogen tetroxide (N_2O_4) as the temperature decreased. The last cooling step is called a dimerization reaction, which is the eq. (1.5).

$$\begin{aligned} &4NH_3+5O_2 \xrightarrow[750\sim900^oC]{\text{Pt catalyst}} 4NO+6H_2O \\ &2NO+O_2 \rightarrow 2NO_2 \end{aligned} \tag{1.4}$$

Therefore, the NO_2 exists in equilibrium with N_2O_4.

$$2NO_2 \rightleftarrows N_2O_4 \tag{1.5}$$

This equilibrium is famous, and is often used as a good example in many text books. Verhoek and Daniels [7] studied this effect in 1931, and the following equation is the representation of the dissociation constant, $K_{N_2O_4}$. Fig1-1 and Table1-2 represent the equilibrium constant in this study.

$$K_{N_2O_4}=\frac{4\alpha^2 P}{1-\alpha^2}$$

where the P is the measured pressure in atmosphere
and α is the degree of dissociation.

$$\alpha=\frac{P-P^o_{N_2O_4}}{P^o_{N_2O_4}}; \quad P^o_{N_2O_4}=\frac{g}{M}\frac{RT}{V} \tag{1.6}$$

in which g is the weight of nitrogen tetroxide, M is the molecular weight and R, T, and V have their usual meanings.

Table1-2: The equilibrium constant of $2NO_2 \rightleftarrows N_2O_4$ at three temperatures. [7]

$N_2O_4 \rightleftarrows 2NO_2$

Temp., °C.	Equilibrium constants ($C^0_{N_2O_4}$ = total weight/92.02 × volume in liters)
25	$K_p = 0.1426 - 0.7588 \times C^0_{N_2O_4}$
35	$K_p = .3183 - 1.591 \times C^0_{N_2O_4}$
45	$K_p = .6706 - 3.382 \times C^0_{N_2O_4}$

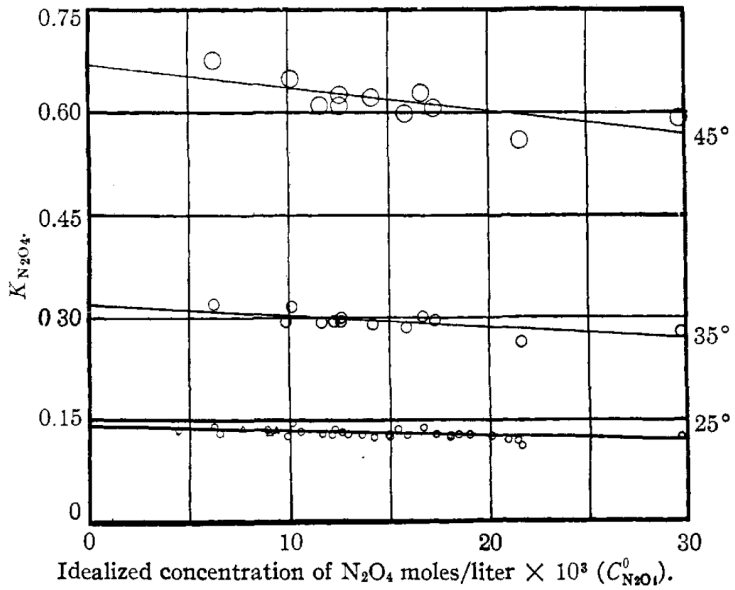

Fig1-1: Measured data for equilibrium constant $2NO_2 \rightleftarrows N_2O_4$ of at 25, 35, and 45℃. [7]

Many papers discuss the N_2O_4 single molecule or the unimolecular dissociation reaction. The most stable N_2O_4 geometry is D_{2h}, and the N-N bond distance varies between 1.772 and 1.776, which is much longer than the N-N bond distance of hydrazine (1.434-1.449). [8,9] The weak N-N bond is also evidenced by the low values of the enthalpies of the dissociation reaction, which are 12.7-12.9 kcal/mol at 0K[10,11] and 13.1-13.7 kcal/mol at 298K. [10-12] The activation energy barrier is also low. The dissociation energy, the reaction is very fast, and the experimental rate constants for the limiting low-concentration (k_0) and high-concentration (k_∞) regions are 4.5×10^6 cm^3/mol^{-1} sec^{-1} and 1.7×10^5 1/sec at 298K, respectively.[13] The reason for the high rate constant is that the weak N-N bond undergoes an internal rotation (torsion) with a barrier height of about 3 kcal/mol. [14,15]

This dissociation reaction have been also calculated by an ab-initio calculation method (CCSD(T)/cc-PVTZ) to determine the rate constants, which are 0.62×10^1, 1.90×10^3, and 1.66×10^5 1/sec at 250, 298.15, and 350K. [16] The following tables are the

geometries of NO_2, N_2O_4, and the energetic properties of the reaction $N_2O_4 \rightarrow 2NO_2$.

Table1-3: Equilibrium distance (in Å), bond angle (in deg), harmonic frequencies (in cm^{-1})and zero-point vibrational energies (kcal/mol) for NO_2. [16]

Method	r_e(NO)	∠ONO	ω_1	ω_2	ω_3	ZPVE
CASSCF/cc-pVDZ	1.209	133.8	1640	1328	751	5.32
CASSCF/cc-pVTZ	1.205	133.9	1626	1319	757	5.29
CCSD(T)/cc-pVDZ	1.207	134.1	1759	1370	735	5.53
CCSD(T)/aug-cc-pVDZ	1.210	134.0	1751	1367	693	5.45
CCSD(T)/cc-pVTZ	1.199	134.2	1668	1348	658	6.91
Experimental	1.1939[a]	133.5[a]	1655.5[b]	1357.8[b]	756.8[b]	

Table1-4: Bond distance (in Å), bond angle (deg), harmonic frequencies (cm^{-1}), zero-point vibraional energies (kcal/mol) for the N_2O_4 dimer. [16]

Method	r_e(N–N)	r_e(N–O)	∠ONO
CASSCF/cc-pVDZ	1.806	1.171	134.4
CASSCF/cc-pVTZ	1.806	1.168	134.1
CASSCF-CI/cc-pVTZ	1.746	···	···
CASSCF/QT[a]	1.803	1.167	134.0
CASPT2/QT[a]	1.794	1.191	134.8
CCSD(T)/TZP2f[b]	1.752	1.195	134.7
CCSD(T)/cc-pVDZ	1.776	1.200	135.2
CCSD(T)/aug-cc-pVDZ	1.780	1.204	134.7
CCSD(T)/cc-pVTZ	1.744	1.194	134.8
Expt.[c](ED)[d]	1.776(4)	1.191(4)	134.6(5)
Expt.[c](X-D)[e]	1.712(17)	1.189(12)	134.8(15)
Expt.[c](ND)[f]	1.7561(9)	1.1893(5)	134.40(7)
Expt.[c](IRR)[g]	1.756(10)	1.196(5)	133.7(5)

Mode	CASSCF	CASSCF	CCSD(T)	CCSD(T)	CCSD(T)	CCSD(T)	Expt.[a,b]	Expt.[a,c]
	cc-pVDZ	cc-pVTZ	DZP[d]	cc-pVDZ	aug-cc-pVDZ	cc-pVTZ		
ω_1 (b_{2u})	2067	2035	1786	1834	1788	1813	1818	1757
ω_2 (b_{3g})	2043	2013	1760	1803	1741	1782	1777	1724
ω_3 (a_g)	1558	1538	1385	1414	1389	1398	1413	1383
ω_4 (b_{1u})	1457	1439	1286	1301	1273	1288	1294	1261
ω_5 (a_g)	877	884	798	820	804	829	826	812
ω_6 (b_{1u})	826	831	738	759	737	763	776	751
ω_7 (b_{2g})	682	716	677	677	677	711	707	676
ω_8 (b_{3g})	482	502	495	495	463	512	484	480
ω_9 (b_{3u})	430	454	434	434	429	454	441	425
ω_{10} (a_g)	221	246	278	279	273	302		282
ω_{11} (b_{2u})	210	230	240	232	222	249		265
ω_{12} (a_u)	98	93	86	95	80	92		82
ZPVE	15.7	15.6	14.2	14.5	14.1	14.6		14.1

Table1-5: Energetics (in kcal/mol) of the reaction $N_2O_4 \rightarrow 2NO_2$. Values in parentheses include the BSSE correction (basis set superposition error) in kcal/mol. [16]

Method	ΔE^a	ΔH_0^{0b}	ΔH_{298}^0	ΔG_{298}^0	BSSE
CCSD(T)/cc-pVDZ[i]	12.16(6.74)	8.70(3.28)	9.64(4.22)	−3.08(−8.50)	5.42
CCSD(T)/aug-cc-pVDZ	14.61(10.25)	11.39(7.03)	12.29(7.93)	−0.30(−4.66)	4.36
CCSD(T)/cc-pVTZ[i]	15.36(12.65)	14.61(11.90)	14.47(12.76)	+2.81(0.10)	2.71
CCSD(T)/TZ2P[e]	15.0	9.9			
CCSD(T)/TZ2P+f/TZ2P[e]	16.0	10.9(7.2)			3.70
CASPT2/QT[d]	13.2	9.6			
CASSCF/cc-pVDZ[i]					
CASSCF/cc-pVTZ[i]					
CASSCF-CI/cc-pVTZ[e,i]	15.4	10.8			
Expt.		12.7,[f] 12.9[g]	13.6,[f] 13.7,[g] 13.1[h]	1.1[j]	

1.2 Review of NASA reports

Weiss [2] studied the dinitrogen tetroxide and hydrazine reaction with an infrared spectrum at a low temperature, and he found some important elements of note, the first of which was, that the NO_2 exists in pure N_2O_4 liquid at -196℃,which is shown in Fig1-2. Although this situation is normal due to the equilibrium, it suggested that NO_2 is also one of the important liquid oxidants for this combustion reaction.

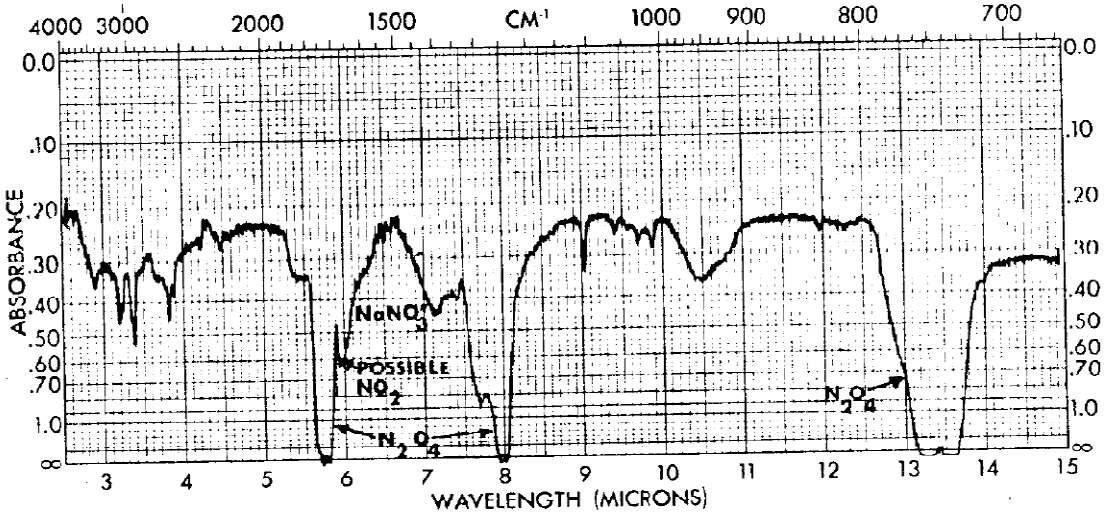

Fig1-2: the infrared spectrum of N_2O_4 (high concentration) at -196℃ [2]

By means of the experiment at low temperature, this reaction could occur under control. The experiment was started at -196℃ and slowly warmed up, and the infrared spectra began to change at around -78℃. After continuously increasing the temperature, the concentration of NO_2 increased more than the quantity in the equilibrium state, and the spectra was more complex than it was at a lower temperature. However, the heat of the system did not increase to the same temperature until at -54℃. Therefore, comparing the results of the infrared spectrum and the calorimeter; Weiss suggests that

(1) the initial formation of adducts in the lower temperature made the spectrum change,

(2) increasing the concentration of NO_2 may be the result of adduct formation,

(3) the decomposition of adducts made the free-radical reaction occur and a large amount of heat and gas was released. Table1-6 presents the summary of the species in the spectrum at different temperatures. However, Weiss also indicates that there are contradictions between the results and the assumptions of the reaction mechanism. Furthermore, there were some species in the spectra which could be not identified.

Table1-6: Gas evolution from the low temperature reaction of N_2H_4+N_2O_4 [2]

Temperature	Gas Evolved (m. moles x 10^{-3})		Species Found
	Noncondensable*	Condensable*	
-126°	.13		NO, N_2
		10.3	NO_2, N_2O
- 50°	.52		N_2
		30.5	N_2O, NO_2 + unknown
- 30°	.25		N_2
		.27	NO_2
- 25°	.02		N_2
		.16	NO_2
Total millimoles Gas Evolved	.92	41.2	

In the end, the simple miscibility experiments had been done, and there were some principle factors when the N_2H_4-N_2O_4 impinging jets were diverted by the interaction between the two propellants. The factors causing this phenomenon were:

(1) Immiscibility of two reactants,

(2) Rapid reaction rate between N_2O_4 and N_2H_4,

(3) The high heat evolution and large gas volume generated by the reaction, and the heat can make the product gases expand and the propellants vaporize.

Therefore, the way to resolve the immiscibility problem is to increase the ratio of the contact surface and the volume of the two reactants as much as possible, since this would be very important for achieving better performance of the combustion system. This part is a different topic from the reaction kinetic, and another NASA reports [3-6] tried to solve it. Although these reports did not focus on the reaction mechanism, they could still offer the experimental conditions to make a better computational assumption. In the real rocket system, the N_2O_4 and N_2H_4 are in the liquid phase, which stays with the cooler system, and are ejected into the combustion chamber with a high flow velocity. In order to achieve the best performance by means of a good mix of two propellants, the ratio of N_2O_4/ N_2H_4 should be optimized, and the type of the injector, including the arrangement of the injector positions of the two propellants and the impingement angles of the injecting direction for every injector.[3-5] Furthermore, the injecting velocity and temperature of the propellants, the size of the nozzle, and the pressure of the combustion chamber are also very important elements which affect the performance.[6] Therefore, it can be understood that the combustion reaction occurs as the N_2O_4 and N_2H_4 collide with each other at very high momentum, and it also combines with the phased transformation of propellants from a liquid to gas

phase. The temperature of the chamber is over 3000℃ after continuous reaction. The following figures are the photographs of the combustion reaction.

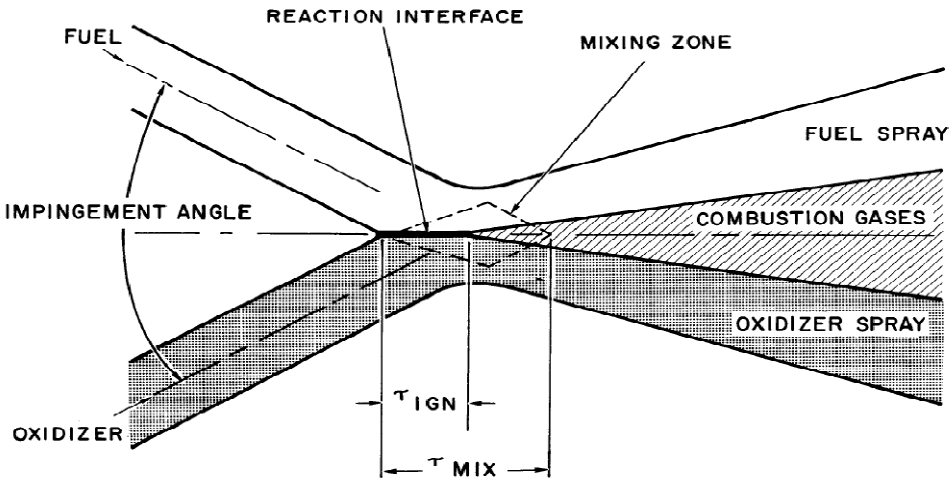

Fig1-3: Separation model for the impinging hypergolic stream [4]

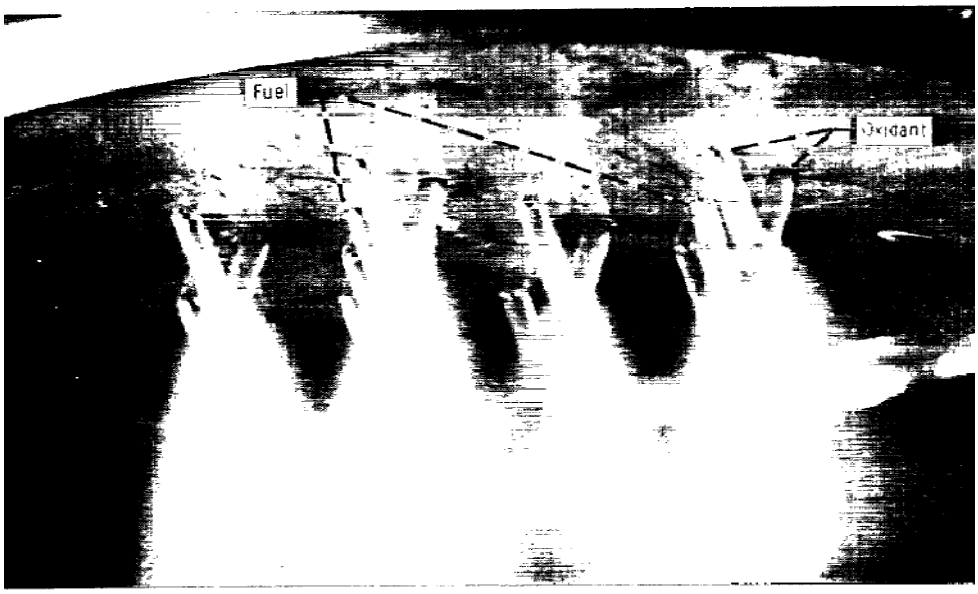

Fig1-4: Parallel injector spray pattern in the combustion reaction. [3]

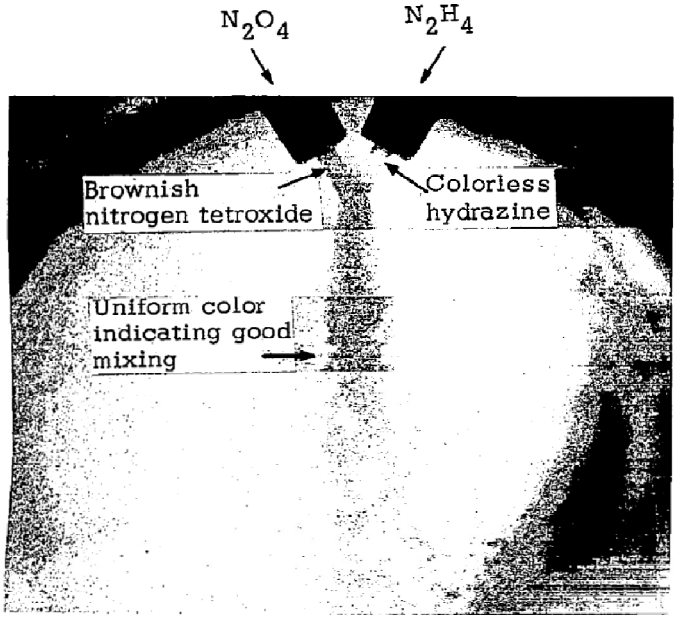

	OX	Fuel
Temp (°F)	100	71
Velocity (ft/sec)	54.8	46.2
Pressure (Psia)	162	
$\rho_f u_f^2 / \rho_o u_o^2$	.98	
O/F	1.24	
Orifice	.040"	
Nozzle	.283"	
Test Number	242	

(a)

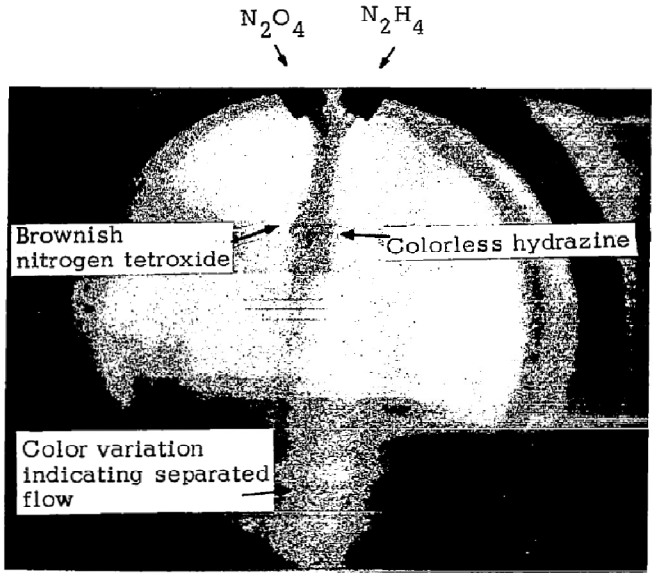

	OX	Fuel
Temp (°F)	93	104
Velocity (ft/sec)	31.66	36.76
Pressure (Psia)	422.7	
$\rho_f u_f^2 / \rho_o u_o^2$	.95	
O/F	1.22	
Orifice	.040"	
Nozzle	.128"	
Test Number	259	

(b)

Fig1-5: Typical spray photographs for (a) stream mixing for high pressure, (b) stream separation for high pressure. [6]

1.3 Isomers of N_2O_4

In the gas phase, the association of NO_2 produces the N_2O_4 dimer, which is a stable molecule. Infrared and Raman spectral techniques were used to record the vibrational frequencies of the molecules. The existence of unstable forms of the dinitrogen tetroxide was proposed by Fateley, Bent, and Crawfold [17], and they studied NO_2 at helium temperature in six types of matrices. Apart from bands belonging to NO_2 and stable N_2O_4 (D_{2h}), other bands were assigned to an unstable isomer of N_2O_4. Baldeschwieler [18] repeated Fateley's work, which was a similar work at liquid-hydrogen temperature. Furthermore, Hisatune, Devlin, and Wada [19] reported that unstable molecules appeared to be formed when pure NO_2 gas was deposited at liquid-nitrogen temperature.

1.3.1 Isomerization of N_2O_4

St. Louis and Crawford [20] used infrared spectra to study NO_2 suspended in oxygen and argon matrices at helium temperature, and assign the absorption spectra of NO_2, N_2O_4 (D_{2h}), and three unstable forms of N_2O_4, including N_2O_4 (D_{2d}) and another two ONO-NO_2 isomers based on the relative optical density measurements and the temperature dependence of the bands. They called the two conformers of ONO-NO_2 as D and D', where D and D' are notations for cis-ONO-NO_2 and trans-ONO-NO_2. However, it is actually difficult to identify which one is cis- or trans- $ONONO_2$. Subsequent papers have applied the same notation, but sometimes the meanings of the notation would change from each other. They assumed that the ONO-NO_2 molecule is planar as in similar cases of stable N_2O_4 and stable N_2O_2, and they calculated the vibrational symmetry species for the molecule in terms of the symmetry group Cs. They

also assumed the bonding structures, as Fig1-6, and most subsequent researchers followed this assumption. After warming up from the temperature of existence D, they also found another isomer D', and the bands of D' were near to D. It appeared that D was isomerized to D', a molecule with a structure close to D. The following tables are the absorption spectra of D and D'.

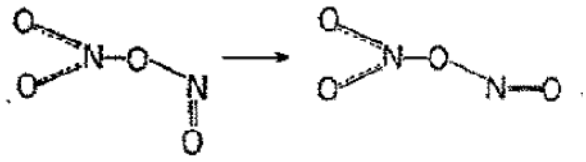

Fig1-6: The D structure can undergo a cis-trans isomerization to form D'.

Table1-7: The correspondence between D and D'.

$D(ONONO_2)$		D'
1829 cm^{-1}		1889–1899 cm^{-1}
1645		1584
1291		1290
905	→	916
783		794
644		660
488		524

Table1-8: Frequency and vibrational assignment of infrared bands of $ONONO_2$ (D) in an oxygen matrix. (NO_2 refers to the nitro group, and O=N-O- to the nitrite group of D).

Observed band (cm^{-1})	Assignment
2132	1645+488=2133
1829	ν_1; N=O stretch
1645	ν_2; NO_2 asymmetric stretch
1291	ν_3; NO_2 symmetric stretch
905	ν_4; N–O stretch in O=N–O–
783	ν_5; NO_2 bend
642	ν_6; O=N–O– bend
488	ν_7 or ν_{10}; NO_2 rock (in-plane) or wag (out-of-plane)

1.3.2 Temperature induced autoionization

Parts and Miller [21] first observed that the heterolytic dissociation of ONO-NO_2 produced the nitrosonium-nitrate $NO^+NO_3^-$ complex in a solid state form by the infrared spectra. Bouduan, Jodi, and Loewenschuss [22] also observed this complex by the Raman spectra, and $NO^+NO_3^-$ complex could produce as spontaneously as N_2O_4 trapping in an Ne matrix. They suggested that autoionization is an intermolecular rather than intramolecular process. The results indicate that, when a solid matrix is warmed to about 180K, an almost complete conversion occurs to the ionic $NO^+NO_3^-$ which remains stable over the full temperature range of 15-180K. There was no evidence that the unsymmetrical forms, D and D' of ONO-NO_2, are observed prior to the transformation to the ionic form. Even though the unsymmetrical isomers exist in the matrix, all unsymmetrical and symmetrical N_2O_4 still undergo the temperature induced ionization in the mean time.

However, Jones, Swanson, and Agnew [23] also reported a similar experiment with the infrared spectra, but they indicated the mechanism of the temperature induced autoionzation was intramolecular, contrary to that of Bolduan *et al.* [22] The experiment used the gas which was an equilibrium mixture of NO_2 and N_2O_4 at room temperature to make the low pressure deposition at various temperatures onto a CsBr window. The spectra were observed as the matrix samples were heated to different temperatures. The results showed that temperature induced that autoionization only occurred with the two less stable isomers of ONO-NO_2, D and D' existing. The frequencies of these isomers were shifted towards those $NO^+NO_3^-$ relative to the more stable nitrite form. In addition, the bulk of N_2O_4 did not undergo autoionization at low pressure and at temperatures below 200K.

In fact, the band assignments for the solid N_2O_4 isomers in the matrix are far less conclusive than N_2O_4 (D_{2h}) gas. In earlier researches, there is no systematic correlation between the different conditions as the solid sample is formed, such as its composition and the effect of the temperature cycling on such solid samples. Therefore, A. Givan and A. Loewenschuss[24-27] have also tried to solve this open question, and the results appear to clarify some of the conflicting points. In their work, the Raman and Fourier transform infrared spectra had been used to detect the matrices which included different preparation processes, such as controlling deposition rates, substrate material, deposition temperatures, and temperature cycling as parameters. They found similar results as Jones *et al*[23] that there was no evidence of the conversion to the ionic form of either an ordered or disordered $N_2O_4(D_{2h})$ layer, and the existence in the solid of the D' isomer was directly related to the formation of ionic nitrosonium nitrate ($NO^+NO_3^-$) and nitrogen dioxide (NO_2). With temperature cycling, up to 150K, the NO_3^- bands increased in intensity while the D' features decreased. On the other hand, the summary of the relationship between the deposition rate and temperature for the species appearing in the solid matrix was that lowering the deposition temperature increased the relative amount of the monomer, and increasing the deposition temperature favored the D' formation in the solid. Givan and Loewenschuss also suggested a mechanism of the formation of D and D',[24,25] and proposed that the formation of temperature induced autoionization is an intermolecular process. Although these experimental results offered different mechanisms of autoionization, it is still open to question, because of the uncertain assignments for the results of the Raman or infrared spectra. The existence of D and D' isomers (cis- and trans-$ONONO_2$) and the NO^+NO3^- complex appearing from temperature induced autionization could stand up by the above observations.

1.3.3 Ab-initio studies of N_2O_4 isomers

Stirling [28], McKee [29] and many other researchers [30-33] have calculated the conformations and characterizations of N_2O_4 isomers, which include O_2N-$NO_2(D_{2h})$, cis-ONO-$NO_2(C_s)$, trans-ONO-$NO_2(C_s)$, cis-perp-cis ONO-ONO(C_2), cis-perp-trans ONO-ONO(C_s), and trans-perp-trans ONO-ONO(C_2), and the geometries are shown in Fig1-7. McKee [29] also calculated the N_2O_4 Potential Energy Surface (PES) as Fig.1-8, and the estimated activation energy in Table1-9.

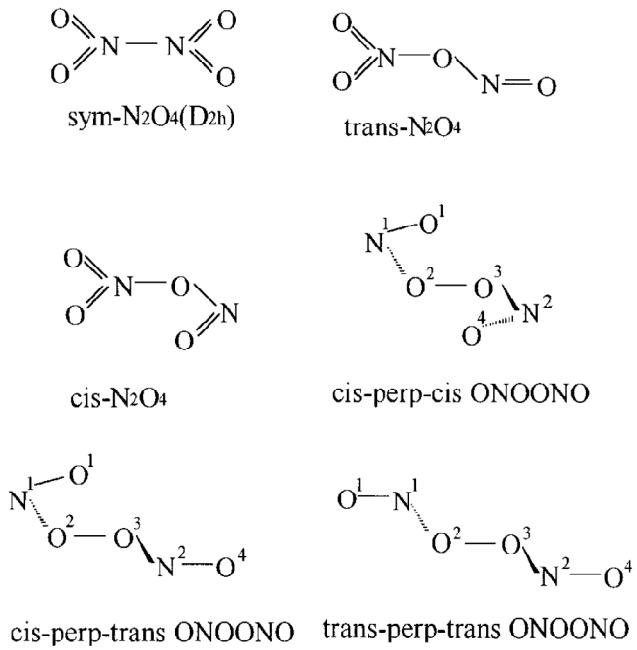

Fig1-7: Structures of N_2O_4 isomers [33]

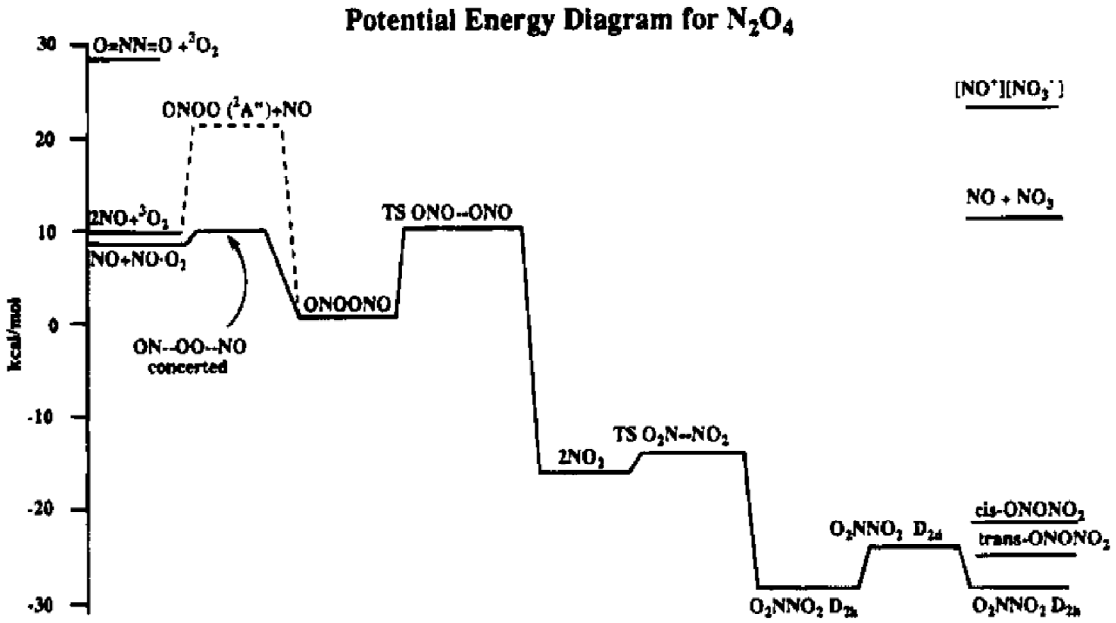

Fig1-7: Potential energy surface for the formation of ONO-ONO and N_2O_4 from $2NO+O_2$ at the QCI level theory. (29)

Table1-9: Estimated activation barrier (kcal/mol) at the QCI and DFT (in parentheses) level of theories. [a] (29)

reactant → TS	radicals at //reactant[b]	TS[c]	radicals at //TS[d]
ONOONO → ON- -OO- -NO	32.1 (27.7)	17.4	10.1
ONOONO → ONO- -ONO	53.7 (50.1)	28.0 (30.4)	10.9 (2.7)
O_2NNO_2 → O_2N- -NO_2	−0.1 (0.1)	1.7	1.1

[a] The first energy is at QCI = [QCISD(T)/6-31+G(2df)]//MP2/6-31G(d)+ZPC. The value in parentheses is DFT = Becke3LYP/6-31G(d)//Becke3LYP/6-31G(d)+ZPC. [b] The energy of the transition structure is assumed to be equal to radicals frozen in the geometry of the reactant. The zero-point energies are taken from optimized NO, O_2, and NO_2. [c] The energy of the transition structure is evaluated at the optimized transition structure. [d] The energy of the transition structure is assumed to be equal to radicals frozen in the geometry of the transition structure. The zero-point energies are taken from optimized NO, O_2, and NO_2.

These isomers are only the stationary points from computation, and only $N_2O_4(D_{2h})$, trans-$ONONO_2$, and cis-$ONONO_2$ have been observed in experiments. However, there is no direct measurement for the geometries of isomers in experiments, except for the

most stable state N_2O_4 (D_{2h}). Therefore, the computational work can only be compared with the results of the vibrational frequencies in the Raman or infrared spectra for cis-$ONONO_2$ and trans-$ONONO_2$ molecules. The geometries of cis-$ONONO_2$ and trans-$ONONO_2$ molecules are assumed to be planar and C_s symmetry, as discussed in section 1.3.1 [20]. No other papers discuss this important assumption further, and thus, it may be still an open question needing to be resolved in experiments.

Since there is a possibility of the existence of NO_2, trans-$ONONO_2$, and cis-$ONONO_2$ with the N_2O_4 (D_{2h}) as oxidizers, the N_2H_4+NO_2, N_2H_4+cis-$ONONO_2$, N_2H_4+trans-$ONONO_2$, and N_2H_4+N_2O_4(D_{2h}) reactions should be considered for this combustion system. After all, in order to account for the hypergolic phenomenon in the reactions, the products of these reactions have to be produced as reactive radicals fast and exothermically to make the reactions occur violently.

1.4 References

(1) Martin J. L. Turner, *Rocker and Spacecraft Propulsion*, 3rd ed (2009)., Springer Berlin Heidelberg.

(2) Harold G. Weiss, *Technical report: A basic study of the nitrogen tetroxide - hydrazine reaction*, Jet Propulsior Laboratory Contract No. BE4-229751 (1965)

(3) Martin Herscb, *Performance and stability characteristics of nitrogen tetroxide – hydrazine combustors*, NASA Technical Note D-4776 (1968)

(4) B.R. Lawver and B. P. Breen, *Hypergolic stream impingement phenomena – nitrogen tetroxide / hydrazine*, NASA-CR-72444 (1968)

(5) Marshall C. Burrows, *Mixing and reaction studies of hydrazine and nitrogen tetroxide using photographic and spectral trchniques*, NASA-TN-D-4467 (1968)

(6) L.B. Zung and J.R. White, *Combustion process of impinging hypergolic propellants*, NASA-CR-1704 (1971)

(7) Frank H. Verhoek and Ferrington Daniels, J. Am. Chem. Soc., 53 (4), 1250 (1931)

(8) F.B.C. Machado and O. Roberto-Nero, Chem. Phys. Lett., 352, 120 (2002)

(9) K. Kohata, T. Kukujama, and K. Kuchitsu, J. Phys. Chem. 86, 602 (1982)

(10) W.F. Giauque and J.D. Kemp, J. Chem. Phys., 6, 40 (1938)

(11) I.C. Hisatsune, J. Phys. Chem., 65, 2249 (1961)

(12) A. Gutman and S.S. Penner, J. Chem. Phys. 36, 98 (1962)

(13) M. Cher, J. Chem. Phys. 37, 2564 (1962)

(14) C.H. Bibart and G.E. Ewing, L. Chem. Phys., 61, 1284 (1974)

(15) L. Koput, J.W.G. Seibert, and B.P. Winnewisser, Chem. Phys. Lett. 204, 183 (1993)

(16) F,R. Ornellas, S.M. Resende, F.B.C. Machado, and O. Roberto-Neto, J. Chem.

Phys. 118, 4060 (2003)

(17) W.G. Fateley, H.A. Bent, and B. Crawford, J. Chem. Phys. 31, 204 (1959)

(18) J.D. Baldeschwieler, PhD. Thesis, University of California (Berkeley), 1959

(19) I.C. Hisatsune, J.P. Devlin, and Y. Wada, J. Chem. Phys., 33, 714 (1960)

(20) R. V. St. Louis and B. Craeford, J. Chem. Phys., 42, 857, 1965

(21) L. Parts and J.T. Miller, J. Chem. Phys. 43, 136 (1965)

(22) F. Bolduan, H.J. Jodi, and A. Loewenschuss, J. Chem. Phys., 80, 1739 (1984)

(23) L. H. Jones, B.I. Swanson, and S.F. Agnew, J. Chem. Phys., 82, 4389 (1985)

(24) A. Givan and A. Loewenschuss, J. Chem. Phys., 90, 6135 (1989)

(25) A. Givan and A. Loewenschuss, J. Chem. Phys., 91, 5126 (1989)

(26) A. Givan and A. Loewenschuss, J. Chem. Phys., 93, 866 (1990)

(27) A. Givan and A. Loewenschuss, J. Chem. Phys., 93, 7592 (1990)

(28) A. Stirling, I. Papai, J. Mink, J. Chem. Phys., 100, 2910 (1994)

(29) M.L. McKee, J. Am. Chem. Soc., 117, 1629-1637 (1995)

(30) E.D. Glendening and A.M. Halpern, J. Chem. Phys., 127, 164307 (2007)

(31) X. Wang, Q. Qin, K. Fan, J. Molecular Structure, 432, 55-62, (1998)

(32) I.I. Zakharov, A.I. Kolbasin, O.I. Zakharova, I.V. Kravchenko, and v.i. Dyshlovoi, Theoretical and Experimental Chemistry, 44, 26 (2008)

(33) X. Wang, Q. Qin, J. Molecular Structure, 76, 77-82 (2000)

(34) A.S. Pimentel, F.C.A. Lima, and A.B.F. da Silva, J. Phys. Chem. A, 111, 2913-2920 (2007)

II. Computation Methods

2.1 Ab-initio Calculations

The equilibrium geometries, including reactants, complexes, transition states (TS), and products, have been optimized at the B3LYP/6-311++G(3df,2p) level in both NO_2+N_2H_4 and N_2O_4+N_2H_4 reactions. The zero-point energies and the harmonic vibrational frequencies have been also determined by the B3LYP method, which is the Becke's three-parameter nonlocal exchange functional [(1)] with the nonlocal correlation functional of Lee, Yang, and Parr [(2)]. All the stationary points have been positively identified for local minima (number of imaginary frequencies NIMAG=0), transition states (NIMAG=1), and higher order top (NIMAG>1). In order to confirm that the transition states have connected between the correct complexes (intermediates), we use the intrinsic reaction coordinate [(3)] (IRC) calculations at the B3LYP/6-311++G(3df,2p) level.

In order to obtain the more reliable energies, we have used the higher level computational methods to calculate the single-point energies with structures optimized by B3LYP/6-311++G(3df,2p). In the NO_2+N_2H_4 reaction, the CCSD(T)/6-311+G(d,p), CCSD(T)/6-311G(3df,2p), the CC1 scheme of modified G2 (G2M) [(4)], and G3B3 [(5,6)] have been employed to achieve more reliable evaluation of energies. In the N_2O_4+N_2H_4 reaction, there are four nitrogen atoms, four oxygen atoms, and four hydrogen atoms; hence, the higher-level ab-initio calculations could only be done by a large amount of computational resources. Due to the limitation of the resource, we have only calculated the single-point energies by CCSD(T)/6-311+G(d,p) and the CC3 scheme of modified G2 (G2M) method. In the Potential Energy Surface (PES), the total energy of each equilibrium geometry is composed of the zero-point energy determined by

B3LYP/6-311++G(3df,2p) and the single-point energy calculated by high-level ab-initio calculations. All of the ab-initio calculations have been performed by the Gaussian03 program, and the calculation theories are summarized in Appendix II.

2.1.1 Modified GAUSSIAN-2 (G2M)

This method is developed by Mebel and coworkers; it improves the G2 method in many places. First, for the open shell species, G2 uses the unprojected MPn energies, but spin-projected MPn energies are expected to be more reliable than UMPn ones, especially for the systems with large spin contamination. However, the spin contamination problems occur not only on UMPn methods but also on the (unprojected) QCISD(T) method. On the other hand, the zero-point energy (ZPE) of the G2 method is from HF/6-31G* method, and it is better to include the electron correlations. Therefore, G2M method improves the G2 method by using PUMPn, CCSD(T) methods, and the ZPE at B3LYP levels. The following eq. is the G2M(CC1) and G2M(CC3) methods.

$$\mathrm{E(G2M(CC1))}=E_{bas}+\Delta E(+)+\Delta E(2df)+\Delta E(CC)+\Delta+\Delta E(HLC,CC1)+ZPE$$
$$E_{bas}=E[PMP4/6-311G(d,p)]$$
$$\Delta E(+)=E[PMP4/6-311+G(d,p)]-E_{bas}$$
$$\Delta E(2df)=E[PMP4/6-311G(2df,p)]-E_{bas}$$
$$\Delta E(CC)=E[CCSD(T)/6-311G(d,p)]-E_{bas}$$
$$\Delta=E[PMP2/6-311+G(2df,p)]-E[PMP2/6-311G(2df,p)]$$
$$-E[PMP2/6-311+G(d,p)]+E[PMP2/6-311G(d,p)]$$
$$\Delta E(HLC,CC1)=-xn_{\beta}-0.00019n_{\alpha}$$

where the PMPn stands for the spin-projected PUMPn energies for open shells and restricted RMPn energies for closed shell. The ΔE(HLC,CC1), the higher level correction, is defined by the number of α and β valence electrons, with $n_{\alpha}\geq n_{\beta}$. Furthermore, the x value for ΔE(HLC,CC1) is optimized for each of modified G2

schemes, minimizing the average absolute deviation of calculated atomization energies from experiment values for the G2 sample set of molecules. The ZPE is determined at the B3LYP level, which is the same method as geometry optimization. The G2M(CC3) is similar with G2M(CC1) but with some simplification.

$$\mathrm{E(G2M(CC3))}=E_{bas}+\Delta E(+)+\Delta' E(2df)+\Delta E(CC)+\Delta'+\Delta E(HLC,CC3)+ZPE$$

$$E_{bas}=E[PMP4/6-311G(d,p)]$$

$$\Delta E(+)=E[PMP4/6-311+G(d,p)]-E_{bas}$$

$$\Delta' E(2df)=E[PMP2/6-311G(2df,p)]-E[PMP2/6-311G(d,p)]$$

$$\Delta E(CC)=E[CCSD(T)/6-311G(d,p)]-E_{bas}$$

$$\Delta'=E[UMP2/6-311+G(2df,p)]-E[UMP2/6-311G(2df,p)]$$
$$-E[UMP2/6-311+G(d,p)]+E[UMP2/6-311G(d,p)]$$

$$\Delta E(HLC,CC3)=-xn_{\beta}-0.19n_{\alpha}$$

The following tables are the summary of the other branch methods in G2M, including the parameters.

Table2-1: Formulas for the recommended G2M methods.[4]

Model name	Necessary calculations	Formulas
G2M(RCC2) or G2M(RCC)	MP4(SDTQ)/6-311G(d,p) MP4(SDTQ)/6-311+G(d,p) MP4(SDTQ)/6-311G(2df,p) RCCSD(T)/6-311G(d,p) MP2/6-311+G(3df,2p)	$E_{\mathrm{pas}}=E$[PMP4/6-311G(d,p)] $\Delta E(+)=E$[PMP4/6-311+G(d,p)]$-E_{\mathrm{bas}}$ $\Delta E(2df)=E$[PMP4/6-311G(2df,p)]$-E_{\mathrm{bas}}$ ΔE(RCC)$=E$[RCCSD(T)/6-311G(d,p)]$-E_{\mathrm{bas}}$ $\Delta'=E$[MP2/6-311G(3df,2p)]$-E$[MP2/6-311G(2df,p)] $-E$[MP2/6-311+G(d,p)]$+E$[MP2/6-311G(d,p)] ΔE(HLC,RCC2)$=-5.71n_{\beta}-0.19n_{\alpha}$ E[G2M(RCC2 or RCC)]$=E_{\mathrm{bas}}+\Delta E(+)+\Delta E(2df)+\Delta E$(RCC) $+\Delta'+\Delta E$(HLC,RCC2)+ZPE
G2M(RCC5) or G2M(RCC,MP2)	MP4(SDTQ)/6-311G(d,p) RCCSD(T)6-311G(d,p) MP2/6-311+G(3df,2p)	$E_{\mathrm{bas}}=E$[PMP4/6-311G(d,p)] ΔE(RCC)$=E$[RCCSD(T)/6-311G(d,p)]$-E_{\mathrm{bas}}$ $\Delta E(+3df2p)=E$[MP2/6-311+G(3df,2p)]$-E$[MP2/ 6-311G(d,p)] ΔE(HLC,RCC5)$=-5.25n_{\beta}-0.19n_{\alpha}$ E[G2M(RCC5 or RCC,MP2)]$=E_{\mathrm{bas}}+\Delta E(+3df2p)+\Delta E$(RCC) $+\Delta E$(HLC,RCC5)+ZPE
G2M(RCC6) or G2M(rcc,MP2)	MP4(SDTQ)/6-311G(d,p) MP4(SDTQ)/6-31G(d,p) RCCSD(T)/6-31G(d,p) MP2/6-311+G(3df,2p)	$E_{\mathrm{bas}}=E$[PMP4/6-311G(d,p)] $\Delta' E$(RCC)$=E$[RCCSD(T)/6-31G(d,p)]$-E$[PMP4/6-31G(d,p)] $\Delta E(+3df2p)=E$[MP2/6-311+G(3df,2p)]$-E$[MP2/ 6-311G(d,p)] ΔE(HLC,RCC6)$=-4.93n_{\beta}-0.19n_{\alpha}$ E[G2M(RCC6 or rcc,MP2)]$-E_{\mathrm{bas}}+\Delta E(+3df2p)+\Delta' E$(RCC) $+\Delta E$(HLC,RCC6)+ZPE

Table2-2: Comparison of the accuracy and the range of applicability for various modified Gaussian-2 (G2M) methods.(4)

Method	Optim. E(HLC), (mhartree)	AAD[a] (kcal/mol)	$E_{calc}-E_{exp}$[b] (kcal/mol)	Largest calculation	Number of heavy atoms[c]	Number of basis functions[d]
G2M(RCC1)	$-5.68n_\beta-0.19n_\alpha$	0.878	Li_2:+2.55 C_2H_2:−2.36 O_2:−2.40	MP4(SDQ)/6-311 +$G(3df,2p)$	4	$168+9n_H$
G2M(CC1)	$-5.77n_\beta-0.19n_\alpha$	0.891	Li_2:+2.59 C_2H_2:−2.34 O_2:−2.26	MP4(SDQ)/6-311 +$G(3df,2p)$	4	$168+9n_H$
G2M(RCC2) or G2M(RCC)	$-5.71n_\beta-0.19n_\alpha$	0.883	Li_2:+2.57 C_2H_2:−2.36 O_2:−2.37	MP4(SDTQ)/6-311 $G(2df,p)$	4	$128+6n_H$
G2M(CC2) or G2M(CC)	$-5.78n_\beta-0.19n_\alpha$	0.890	Li_2:+2.59 C_2H_2:−2.38 O_2:−2.25	MP4(SDTQ)/6-311 $G(2df,p)$	4	$128+6n_H$
G2M(RCC3)	$-5.45n_\beta-0.19n_\alpha$	1.054	BeH:−2.42 $CH_2(^3B_1)$−2.24 Li_2:+2.88 C_2H_2:−3.47 C_2H_4:−2.13	MP4(SDQ)/6-311 $G(2df,p)$ RCCSD(T)/ 6-311G(d,p)	5	$160+6n_H$ $95+6n_H$
G2M(CC3)	$-5.63n_\beta-0.19n_\alpha$	1.042	BeH:−2.40 $CH_2(^3B_1)$−2.03 Li_2:+2.97 C_2H_2:−3.28	MP4(SDQ)/6-311 $G(2df,p)$ CCSD(T)/6-311G(d,p)	5	$160+6n_H$ $95+6n_H$
G2M(RCC4)	$-5.33n_\beta-0.19n_\alpha$	1.082	BeH:−2.42 $CH_2(^3B_1)$−2.19 Li_2:+2.80 C_2H_2:−3.38 C_2H_4:−2.12	RCCSD(T)/6-311 $G(d,p)$	6	$160+6n_H$
G2M(CC4)	$-5.37n_\beta-0.19n_\alpha$	1.067	BeH:−2.40 $CH_2(^3B_1)$−2.06 Li_2:+2.80 C_2H_2:−3.46 C_2H_4:−2.18	CCSD(T)/6-311 $G(d,p)$	6	$160+6n_H$
G2R(RCC5) or G2M(RCC,MP2)	$-5.25n_\beta-0.19n_\alpha$	1.149	BeH:−2.45 $CH_2(^3B_1)$:−2.16 Li_2:+2.76 C_2H_2:−3.27 C_2H_4:−2.03 CO:+2.17	RCCSD(T)/6-311 $G(d,p)$	6	$160+6n_H$
G2M(CC5) or G2M(CC,MP2)	$-5.30n_\beta-0.19n_\alpha$	1.134	BeH:−2.43 $CH_2(^3B_1)$:−2.02 Li_2:+2.76 C_2H_2:−3.33 C_2H_4:−2.06 CO:+2.02	CCSD(T)/6-311 $G(d,p)$	6	$160+6n_H$
G2M(RCC6) or G2M(rcc,MP2)	$-4.93n_\beta-0.19n_\alpha$	1.277	BeH:−2.67 $CH_2(^3B_1)$:−2.44 CH_3:−2.24 Li_2:+2.99 C_2H_2:−3.54 C_2H_4:−2.64 C_2H_6:−3.00 CO:+2.32 CO_2:+2.05	RCCSD(T)/6-31 $G(d,p)$ MP4(SDTQ)/ 6-311G(d,p) MP2/6-311+G $(3df,2p)$	7	$105+5n_H$ $133+6n_H$ $294+9n_H$
G2M(CC6) or G2M(cc,MP2)	$-5.05n_\beta-0.19n_\alpha$	1.246	BeH:−2.65 $CH_2(^3B_1)$:−2.27 CH_3:−2.06 Li_2:+2.54 C_2H_2:−3.45 C_2H_4:−2.49 C_2H_6:−2.77 CO:+2.30 CO_2:+2.01	CCSD(T)/6-31 $G(d,p)$ MP4(SDTQ)/ 6-311G(d,p) MP2/6-311+G $(3df,2p)$	7	$105+5n_H$ $133+6n_H$ $294+9n_H$

[a]Average absolute deviation from experimental atomization energies.
[b]For the worst cases where deviation of calculated atomization energy from experiment exceeds 2 kcal/mol.
[c]Maximum number of heavy atoms for which the method is practical on workstations at present.
[d]Number of basis functions required for the largest calculation for the maximum number of heavy atoms in the preceding column, computed for the basis set with $6d$ functions. n_H is the number of hydrogen atoms in the species.

2.1.2 Gaussian-3 theory using DFT geometries and zero-point energies (G3B3)

The G3B3 method [5] is based on the Gaussian-3 theory (G3) and used the geometries and zero-point energies by B3LYP calculations. The G3 method uses geometries by MP2(FC)/6-31G(d) and scaled zero-point energies by HF/6-31G(d) followed by a series of single-point energy calculations at the MP2, MP4, and QCISD(T) levels. The detail of the G3 method is presented in the Table2-3. It includes a spin-orbit correction and a higher-level correction; therefore, the average absolute derivation between experimental data and G3 theory for 299 energies is 1.01 kcal/mol. It performs much more accurate and requires less computation time than the G2 theory. In the modified version of the G2 method, such as G2M [4], G2(MP2) [7], G2(MP2,SVP) [8] methods, they use different methods to determine the geometries and zero-point energies for getting better computation results. They suggested that using B3LYP methods has many advantages. First, the frequencies and zero-point energies obtained at the B3LYP level have improved much more than those obtained at the HF level, and B3LYP geometries may be easier and cheaper to obtain than MP2 geometries for larger systems. The accuracy of density functional theory for calculation of geometries has been examined in several studies. [9,10] For the above reasons, Redfern's group presents variations of G3 and G3(MP2) theories that use the B3LYP density functional method for geometries and zero-point energies in place of the MP2/6-31G(d) geometries and scaled HF/6-31G(d) zero-point energies. These two variations were referred to as G3//B3LYP (G3B3) and G3(MP2)//B3LYP. On the other hand, there is another variation for zero-point energy calculations; that is introducing the new scaling factor. As the scaling factor is optimized (along with the high-level correction parameters), it gives a smallest average absolute derivation. The scaling factor in G3B3 is 0.925.

However, such a low scaling factor for B3LYP is clearly nonphysical and may compensate for other deficiencies. In the end, the new scaling factor for the zero-point energy was recommended to be 0.96. In the table2-3, we can realize clearly what the difference between G3 and G3B3 is.

Table2-3: Steps in G3, G3(MP2), G3//B3LYP, and G3(MP2)//B3LYP methods. [5]

	G3	G3//B3LYP	G3(MP2)	G3(MP2)//B3LYP
Geometry	MP2(FU)/6-31G(d)	**B3LYP/6-31G(d)**	MP2(FU)/6-31G(d)	**B3LYP/6-31G(d)**
Single-point energies	MP4(FC)/6-31G(d)	MP4(FC)/6-31G(d)	⋯	⋯
	MP4(FC)/6-31+G(d)	MP4(FC)/6-31+G(d)	⋯	⋯
	MP4(FC)/6-31G(2df,p)	MP4(FC)/6-31G(2df,p)	⋯	⋯
	QCISD(T,FC)/6-31G(d)	QCISD(T,FC)/6-31G(d)	QCISD(T,FC)/6-31G(d)	QCISD(T,FC)/6-31G(d)
	MP2(FU)/G3large	MP2(FU)/G3large	MP2(FC)/G3MP2large	MP2(FC)/G3MP2large
Spin-orbit correction (ΔSO)	Atomic species	Atomic species	Atomic species	Atomic species
Higher-level correction (ΔHLC)[d]	Molecules	Molecules	Molecules	Molecules
	A=6.386	A=6.760	A=9.279	A=10.041
	B=2.977	B=3.233	B=4.471	B=4.995
	Atoms	Atoms	Atoms	Atoms
	C=6.219	C=6.786	C=9.345	C=10.188
	D=1.185	D=1.269	D=2.021	D=2.323
Zero-point energy (ZPE)[e]	HF/6-31G(d)	**B3LYP/6-31G(d)**	HF/6-31G(d)	**B3LYP/6-31G(d)**

[a]FC=frozen core approximation for the correlation calculation, FU=all electrons included in the correlation calculation. Further details of G3 and G3(MP2) theories are in Refs. 1 and 5, respectively.
[b]E_o(G3)=E[MP4(FC)/6-31(d)]+Δ(+)+Δ(2df,p)+Δ(QCI)+Δ+ΔSO+ΔHLC+ZPE where
Δ(+)=E[MP4(FC)/6-31+G(d)−MP4(FC)/6-31G(d)],
Δ(2df,p) = E[MP4(FC)/6-31G(2df,p) − MP4(FC)/6-31G(d)],
Δ(QCI) = E[QCISD(T,FC)/6-31G(d) MP4(FC)/6-31G(d)],
Δ = [MP2(FU)/G3large−MP2(FC)/6-31G(2df,p)−MP2(FC)/6-31+G(d)+MP2/6-31G(d)].
[c]E_o[G3(MP2)] QCISD(T)/6-31G(d)+ΔE_{MP2}+ΔE(SO)+E(HLC)+E(ZPE) where
ΔE_{MP2}=[E(MP2/G3MP2large)]−[E(MP2/6-31G(d)].
[d]The IILC is $-An_\beta - B(n_\alpha - n_\beta)$ for molecules and $-Cn_\beta - D(n_\alpha - n_\beta)$ for atoms (including atomic ions). The n_β and n_α are the number of β and α valence electrons, respectively, with $n_\alpha \geq n_\beta$. The A, B, C, D are in mhartrees.
[e]Scale factor of 0.8929 used for HF/6-31G(d) and 0.96 for B3LYP/6-31G(d).

By the comparing with the experimental energies of 299 species, the average results for these four methods are given in the following table.

Table2-4: Comparison of average absolute deviations in kcal/mol.

	Average absolute deviation from experiment			
Type	G3	G3//B3LYP	G3(MP2)	G3(MP2)//B3LYP
Enthalpies of formation (148)	0.94	0.93	1.18	1.13
Nonhydrogen (35)	1.72	1.65	2.12	1.99
Hydrocarbons (22)	0.68	0.57	0.70	0.75
Subst. hydrocarbons (47)	0.56	0.70	0.74	0.70
Inorganic hydrides (15)	0.87	0.78	1.03	0.93
Radical (29)	0.84	0.76	1.23	1.18
Ionization energies (85)	1.13	1.10	1.41	1.37
Electron affinities (58)	0.98	0.95	1.46	1.44
Proton affinities (8)	1.34	1.22	1.02	0.89
All (299)	1.01	0.99	1.30	1.25

2.2 Kinetic Calculation

The canonical Transition State Theory (cTST) is employed to calculate the rate constants for the biomolecular and unimolecular reactions. In addition, the quantum tunneling effects are included in the rate constant calculations with the Eckart tunneling model. With the transition state theory, the thermal rate constant of a reaction can be expressed as

$$k(T) = \kappa(T)\sigma \frac{k_B T}{h} \frac{Q_{TS}(T)}{Q_r(T)} Exp[\frac{-\Delta E_{TS}}{k_B T}]$$

Where $\kappa(T)$ is the transmission coefficient accounting for the quantum tunneling effect; σ is the reaction symmetry number; $Q_{TS}(T)$ and $Q_r(T)$ are the total partition functions of the transition state and reactants, respectively; ΔE_{TS} is the classical energy barrier for the transition state at 0K. The conventional T, k_B, and h are temperature, Boltzmann constant and Planck constant, respectively. The details of partition functions are shown in Appendix 1.11. The kinetics of a reaction was computed by the Rate Program at the platform of Computational Science and Engineering Online (CSE-online)[11].

2.3 Reference

(1) (a) A. D. Becke, J. Chem. Phys. 98, 5648 (1993);

(b) 96, 2155 (1992); (c) 97, 9173 (1992)

(2) C. Lee, W. Yang, and R. G. Parr, Phys. Rev. B 37, 785 (1988)

(3) C. Gonzalez and H. B. Schlegel, J. Phys. Chem. 90, 2154 (1989)

(4) A. M. Mebel, K. Morokuma, and M. C. Lin, J. Chem. Phys. 103, 7414 (1995)

(5) A. G. Baboul, L. A. Curtiss, P. C. Redfern, and K. Raghavachari, J. Chem. Phys. 110, 7650 (1999)

(6) B. Anantharaman and C. F. Melius, J. Phys.Chem. A 109, 1734-1747 (2005)

(7) L. A. Curtiss, K. Raghavachari, and J. A. Pople, J. Chem. Phys. 98, 1293 (1993)

(8) (a) J. Smith and L. Radom, J. Phys. Chem. 99, 6468 (1995);

(b) L. A. Curtiss, P. Redfern, B. J. Smith, and L. Radom, J. Chem. Phys. 104, 5148 (1996)

(9) C. W. Bauschlicher, Chem. Phys. Lett. 246, 40 (1995)

(10) B. G. Johnson, P. M. W. Gill, and J. A. Pople, J. Chem. Phys. 98, 5612 (1993)

(11) Computational Science and Engineering Online. http://www.cse-online.net/

III. Results and Discussions

3.1 N_2H_4+NO_2 reaction

In the first section, we focus on N_2H_4 and NO_2 reaction, which is one of the possible reactions in the hydrazine and dinitrogen tetroxide combustion system, since the NO_2 always co-exists with N_2O_4 in the equilibrium state. The characteristic bond lengths and angles of optimized geometries in this reaction are discussed, including reactants, complexes, transitions states (TS), and products at the B3LYP / 6-311++G(3df,2p) calculation level, showed in Fig3-1. Next, we describe the reaction channels in the full potential surface energy surface (PES) of the N_2H_4+NO_2 reaction, whose energies obtained by G2M(CC1) calculation shown in Fig.3-2. Furthermore, the moments of inertia and vibrational frequencies are represented in Table3-1. Table3-2 displays the details of relative energies computed by various computational methods. Finally, we predict the rate constants for the reaction channels by mean of the Transition State Theory (TST).

3.1.1 Molecular Geometries of hydrazine and nitrogen dioxide

Reactants, hydrazine and nitrogen dioxide, are well-studied molecules, and we compare the geometries and vibrational frequencies with the computational and experimental data, as shown in Tables 3-3 to 3-5. In Table3-3, comparing with the experimental data, the N-N bond of N_2H_4 predicted by B3LYP is smaller by 0.015Å; at the CCSD(T) level the agreement between theory and experiment is very good. In the case of the bond angles, both B3LYP and CCSD(T) methods have good predictions.

Therefore, the geometry by B3LYP calculation is still reliable as CCSD(T) does. Furthermore, in Table3-4, the vibrational frequencies are over-predicted by the B3LYP, MP2, and CCSD(T) methods; the most serious difference results from the MP2 method. In the high frequency region, B3LYP and CCSD(T) give similar values. The B3LYP method has a much serious over-prediction problem in the low frequency region, which is higher than 40 cm^{-1} on average. On the other hand, for the N-O bond of the NO_2 molecule, the B3LYP method performs slightly better than the CCSD(T) and CASSCF methods. The errors of bond length between calculations and the experimental data are less than 0.01Å, and they have similar values in the bond angle. Moreover, the average error of vibrational frequencies predicted the B3LYP method is about 20 cm^{-1}, which is a reliable prediction. Comparing with DFT calculation, the CCSD(T) and CASSCF methods need much computational resources, and the MP2 method suffers from spin contamination in many cases. Therefore, according to comparison between the DFT method (B3LYP) and the MP2, CCSD(T), CASSCF methods for prediction of geometries and vibrational frequencies of N_2H_4 and NO_2 molecules, the former can not only save computational resources for larger molecular systems, it can also have a reliable prediction.

3.1.2 PES of the N_2H_4 + NO_2 reaction

There are four product channels in the N_2H_4+NO_2 reaction, are presented in Fig3-2. Three of them are hydrogen-abstraction reactions, and the other is the oxygen transfer reaction. In the hydrogen-abstraction channels, the products are similar, including cis-HONO+N_2H_3, trans-HONO+N_2H_3, and HNO_2+N_2H_3 for channel-1, channel-2, and channel-3 respectively. Nitrous acid (HONO) is a key reactive

intermediate in the combustion of many nitramine propellants, and hydrazinyl radical (N_2H_3) is very reactive with other species due to one unpaired electron in the open shell configuration. Therefore, the N_2H_3 radical and HNO_2 isomers can play an important role in the hypergolic combustion reaction. In the N_2H_4+NO_2 reaction, every channel starts to react from complex1, which originates from the physical attraction of the two reactants. This intermediate is lower in energy by 2.50 kcal/mol relative to the reactants at the G2M(CC1) level, and the closest distance of the two molecules is 2.494 Å. The hydrogen bond between O and H may be the reason for the decrease in the energy of complex1, and this makes the N-O bond of NO_2 and the N-N bond of N_2H_4 slightly longer. Moreover, the NO_2 and N_2H_4 in complex1 still maintain their symmetries.

In channel-1, in the beginning, complex1 is transformed to complex2 through TS1, the relative energy of which is 2.56 kcal/mol and is lower than complex2 by 0.81 kcal/mol. TS1 is a transition state to change the symmetry of N_2H_4, and the imaginary frequency is only 114 cm^{-1}, corresponding to a rotation motion. According to Table3-2, the energy difference between complex2 and TS1 is -0.7 to -0.8kcal/mol by single-point calculations. Therefore, we believe the small negative value should originate from a calculation error (less than 1 kcal/mol in normal situations). On the other hand, the increase in the energy of complex2 result from the structural change of N_2H_4 in complex2, from C_2 symmetry to its anti-form (C_{2h} symmetry)[21], the energy of C_{2h} form is much higher than that of C_2 symmetry. Therefore, the energy of complex2 is the balance between creating hydrogen bonds and the high energy conformation of N_2H_4. Since complex1 and complex2 are the physical attraction of the two reactant molecules, the bond lengths (N-H, N-N, and N-O) and bond angles (H-N-H) have only a small difference comparing with the separate single molecules, except that the bond angle of O-N-O decreases by 5 degrees due to the formation hydrogen bonds. To produce the

cis-HONO and N_2H_3, complex2 needs to cross over TS2, whose energy barrier is 4.2 and 7.6 kcal/mol at the G2M(CC1) level with respect to complex2 and the reactants, respectively. The intrinsic reaction coordinate (IRC) calculation of TS2 in the direction of the products indicates the formation of the O-H bond and the breaking N-H bond, resulting in the production of the cis-HONO and N_2H_3 radical. This hydrogen transfer breaks the symmetry of complex2 and elongates the N-O bond to connect with the hydrogen into an N-O-H form, but the change in the other N-O bond is less significant. In the mean time, the N-N bond shortens by 0.9 Å to balance the loss of one electron. At the next step, complex3, the association complex of cis-HONO and the N_2H_3 radical, dissociates to two independent molecules; with 8.4 and 9.5 kcal/mol energies predicted at G2M(CC1) and CCSD(T)/6-311G(3df,2p) levels of theory.

Comparing complex1 with complex2, the hydrogen is in a different position relating to NO_2. For complex2, the two hydrogen atoms are in the inner side of the N-O-N angle, whereas the hydrogen is in the outer side of O-N-O angle of complex1, as presented in Fig3-1. Therefore, the products are cis-HONO+N_2H_3 and trans-HONO+N_2H_3 in channel-1 and channel-2, respectively. In channel-2, complex1 directly goes through TS3, whose energy barrier is 15.5 and 13.0 kcal/mol with respect to complex1 and the reactants at the G2M(CC1) level, producing complex4 (trans-HONO and N_2H_3). TS2 and TS3 have similar hydrogen transfers, but the position of the hydrogen atom between the oxygen atom of NO_2 and nitrogen atom of N_2H_4 is different. The distances between the hydrogen and nitrogen of N_2H_4 are 1.144 Å and 1.083Å, and those between hydrogen and oxygen of NO_2 are 1.395Å and 1.528Å for TS2 and TS3, respectively. This means that the energy for hydrogen transfer will be higher as the hydrogen atom is closer to the nitrogen. On the other hand, TS2 and TS3 have the same tendencies in bond lengths and the bond angle of N_2H_3 and NO_2, as

discussed above. The last step is also a dissociation of complex4 into N_2H_3 and trans-HONO, whose energy is 10.5 and 12.2 kcal/mol predicted at the G2M(CC1) and CCSD(T)/6-311G(3df,2p) levels. Furthermore, the arrangement of the two molecules in complex3 and complex4 may mean that the hydrogen bonding in complex3 is weaker than in complex4. Therefore, the dissociate energy of complex4 is higher than that of complex3.

In channel-3, which also occurs by hydrogen transfer, it connects a hydrogen atom of N_2H_4 with the nitrogen atom of NO_2. Complex1 twists its N-N bond of N_2H_4 to form TS4, bringing the hydrogen atom closer to the nitrogen atom of NO_2. The energy of TS4 is 11.86 and 9.36 kcal/mol above complex1 and the reactants, respectively, at the G2M (CC1) level. The characteristic of bond lengths and angles in TS4 has the same trend as in TS2 and TS3. The IRC calculation of TS4 confirms the hydrogen transfer to form complex5, which is composed of N_2H_3 and HNO_2. The dissociation energy from complex5 to the two separated molecules is 11.8 and 13.7 kcal/mol predicted at the G2M(CC1) and CCSD(T)/6-311G(3df,2p) levels. Comparing the three products from channel-1 to channel-3, the dissociation energies are high and close. Therefore this infers that the physical attractions and the hydrogen bonding are similar and important in these three systems.

Channel-4 is the pathway in which oxygen is transferred to produce NO, instead of hydrogen transfer reaction; this process has to pass through a very high energy barrier via TS5, in which one N-O bond breaks in NO_2, creating another N-O bond with N_2H_4. The N-N bond in N_2H_4 decreases by 0.4Å, which is less than that in TS2, and the N-O bond not involved in the oxygen transfer increases by 0.5Å at TS5. Furthermore, the oxygen is located in the middle of the nitrogen atoms of NO_2 and the nitrogen atom of N_2H_4 with 1.610 and 1.465Å distance, respectively. The angle of N-O-N at TS5 is

106.5°, and the O-N-O angle of NO_2 molecule is decreased from 134.5 ° to 109.8°. Since the NO double bond in NO_2 is originally short (1.190Å), the elongation of this bond at TS5 by over 0.25Å makes the energy barrier (which is 48.47 and 45.97 kcal/mol relative to complex1 and reactants, respectively) very high comparing with the transition states for the hydrogen transfer. After passing through TS5, complex6 consisting of NO and $H_2NN(O)H_2$ molecule. The $H_2NN(O)H_2$ isomerizes to $H_2NN(H)OH$ via TS6, which is a more stable molecule obeying the Octet rule. The unimolecular reaction via TS6 involves hydrogen migration from the nitrogen to the oxygen with releasing of energy giving the more stable molecule, $H_2NN(H)OH$.

In this computational work, we use G3B3, CCSD(T),and G2M methods to improve single-point energies based on the geometries at B3LYP/6-311++G(3df,2p). In Table3-2, the energies predicted by these methods are slightly different, but with the same trends. Based on few experimental data, we only compare the heats of the reaction for the cis-HONO+N_2H_3 and trans-HONO+N_2H_3 products. The experimental reference for $\Delta_fH^o_T$ of the N_2H_3 radical is the experimental study of Ruscic and Berkowitz[22]. The heat of reaction in $N_2H_4 \rightarrow N_2H_3+H$ is 3.50±0.01 eV (80.8±0.3 kcal/mol), and ΔH_f of N_2H_3 would be 55.3±0.3 kcal/mol after calculation with the values of $\Delta H_f(N_2H_4)$ and $\Delta H_f(H)$. Moreover, if we use the values of $\Delta H_f(N_2H_4)$ and $\Delta H_f(H)$ given in the NIST database[23,24], the $\Delta H_f(N_2H_3)$ will be 55.333 kcal/mol, which is almost the same as the study of Ruscic. On the other hand, the $\Delta H_f(N_2H_3)$ is computed as 56.2 and 53.7 kcal/mol at 0K and 298K by Matus et al.[25], but they do not compare with the experimental data. After applying the ΔH_f(trans-HONO), ΔH_f(cis-HONO), and $\Delta H_f(N_2H_3)$, which are -17.36[23], -16.84[23], 55.333 kcal/mol, respectively, the heat of the reaction is 3.25 and 3.76 kcal/mol for the products trans-HONO+N_2H_3 and cis-HONO+N_2H_3, respectively. Comparing with the experimental data and

computational results, G3B3 and G2M(CC1) perform well, but the heat of reaction for trans-HONO+N_2H_3 is higher than that for cis-HONO+N_2H_3 at CCSD(T) /6-311G(3df,2p). However, since the difference of two CCSD(T) values are less with the trans product energy slightly higher than the cis-counterpart than 0.7 kcal/mol, which is within the accuracy of these methods. Comparing the experimental data, the errors of the computational result are -0.32, -0.33, and 0.66 kcal/mol for ΔH(cis-HONO+N_2H_3) and 0.68, -0.32, and 0.51 kcal/mol for ΔH(trans-HONO+N_2H_3) predicted at CCSD(T)/6-311G(3df,2p), G2M(CC1), and G3B3 methods, respectively.

3.1.3 Kinetic calculation

Based on the PES presented in the preceding section, we consider the N_2H_4+NO_2 reaction to proceed through TS2-TS4 and calculate the rate constants by employing the transition-state theory.[25,26] For these kinetic calculations, we use the barrier heights obtained at G2M(CC1) and molecular geometries of the reactants and transition states at B3LYP/6-311++G(3df,2p) presented in Table3-1. We use the conventional TST method with Eckart's tunneling corrections. The Arrhenius plots of various rate constants are shown in Fig3-3, and the three-parameters fitting expressions for the rate constants are presented in Table3-6.

The lowest-energy channel is channel-1,

N_2H_4+NO_2→complex1→TS1→complex2

→TS2→complex3→cis-HONO+N_2H_3 (channel-1)

The rate constant k_1, which is controlled mainly by TS2, is the highest at any temperature among the three channels. The activation energy is 7.6 kcal/mol, and channel-2 and channel-3 have similar reaction paths, namely

N_2H_4+NO_2→complex1→TS3→complex4→trans-HONO+N_2H_3 (channel-2)

$N_2H_4+NO_2 \rightarrow complex1 \rightarrow TS4 \rightarrow complex5 \rightarrow HNO_2+N_2H_3$ (channel-3)

The activation energy of Channel-4 is too high and therefore, we do not calculate its rate constant. In Fig.3-3, the rate constants of channel-3 (k_3) is higher than that of channel-2 (k_2) at a low temperature, whereas the k_2 is slightly lower than k_3 at a high temperature. Although the activation energy of channel-2 is higher than that of channel-3 by 3.6 kcal/mol, the A factor, which is also called the pre-exponential factor, and temperature dependence are also more important as temperature increases. Unfortunately, as mentioned in the introduction, there is no experimental result for comparison with our predicted values.

(a) Reactants

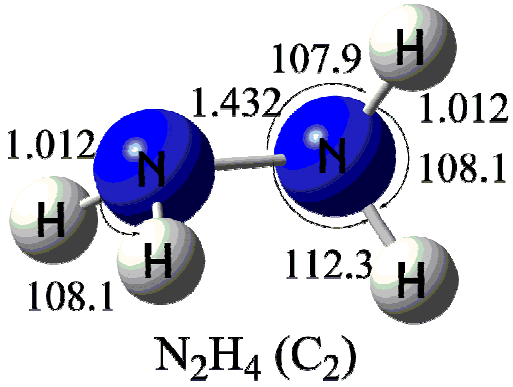

N_2H_4 (C_2)

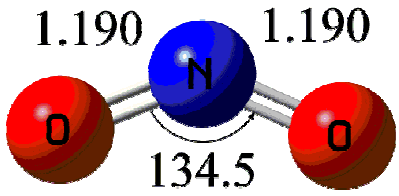

NO_2 (C_{2v})

(b) Intermediates

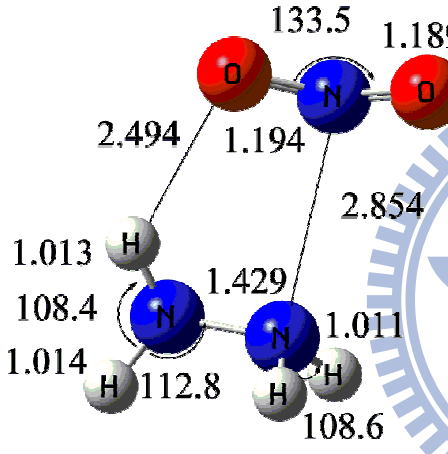

Complex1 (C_1)

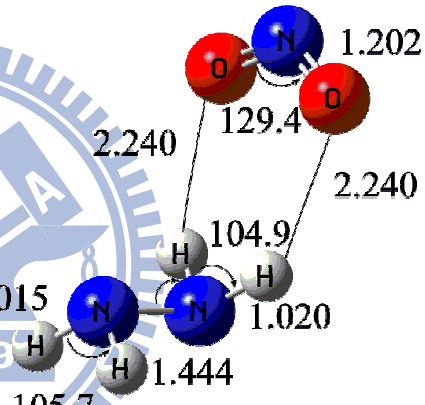

Complex2 (C_s)

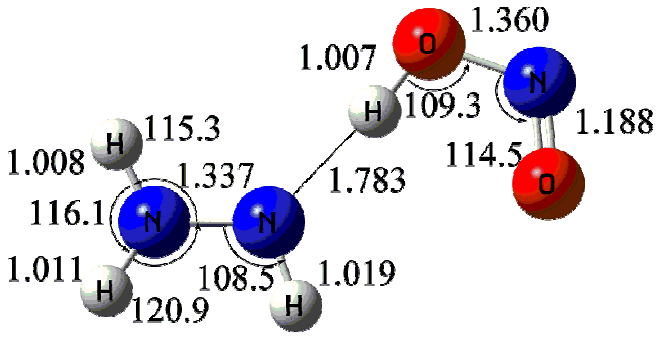

Complex3 (C_1)

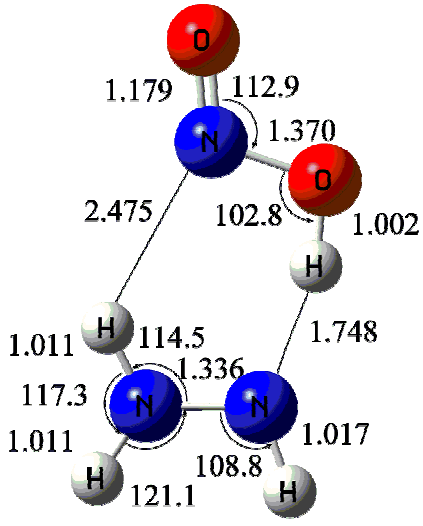

Complex4 (C_1)

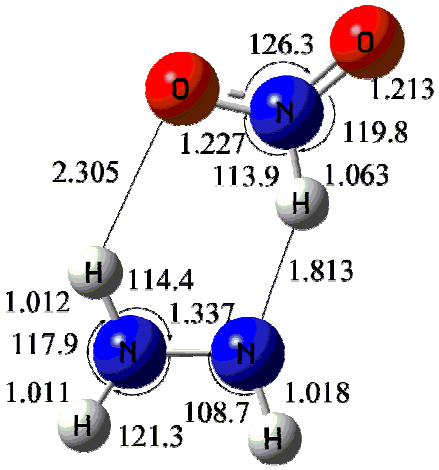

Complex5 (C_1)

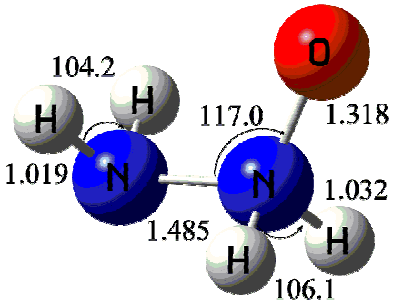

$H2NN(O)H_2$ (C_s)

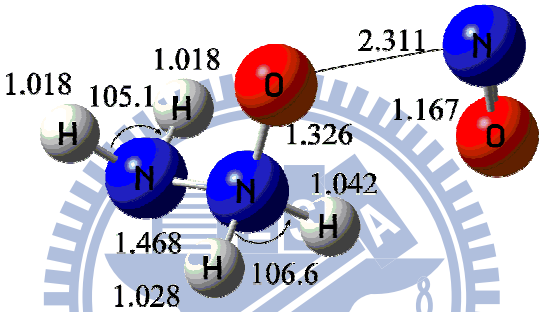

Complex6 (C_1)

(c) Transition States (TSs)

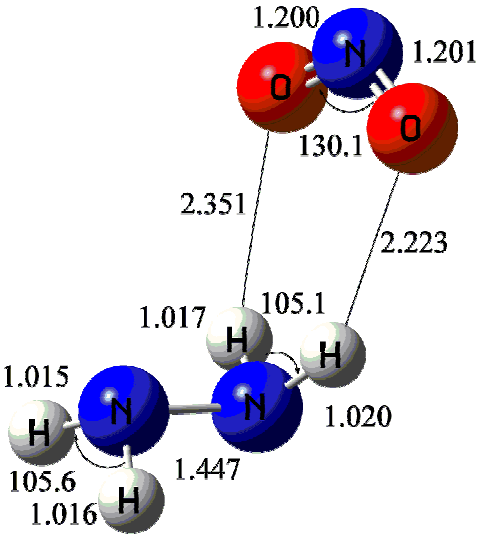

TS1 (C_1)

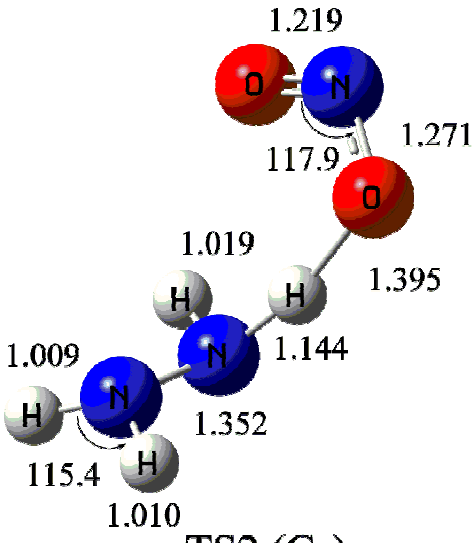

TS2 (C_1)

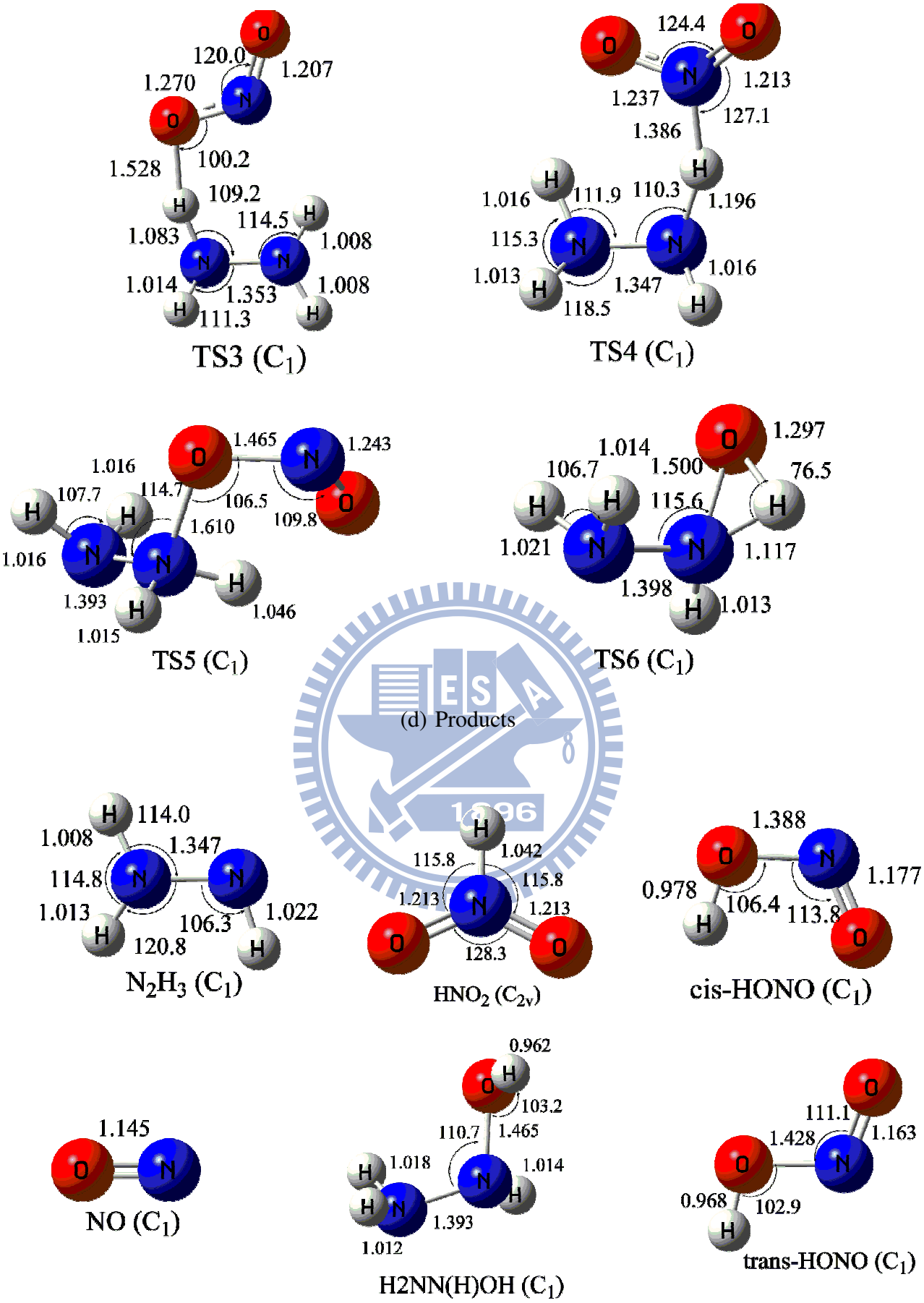

Fig3-1: The geometries in the PES are determined by B3LYP/6-311++G(3df,2p).

Table3-1: Moments of inertia (I_A, I_B, I_C) and vibration frequencies of the species computed at the B3LYP/6-311++G(3df,2p) level.

Species or Transition States	Moments of inertia I_i(a.u)	Vibrational Frequency υ_j (cm^{-1})
N_2H_4	12.4, 74.2, 74.3	439, 801, 974, 1114, 1294, 1323, 1674, 1686, 3462, 3471, 3562, 3568
NO_2	7.4, 137.6, 145.0	767, 1395, 1703
complex1	189.1, 757.8, 919.2	36, 77, 78, 723, 155, 174, 434, 763, 805, 970, 1115, 1297, 1321, 1383, 1668, 1680, 1702, 3464, 3470, 3556, 3567
complex2	189.8, 799.2, 898.3	60, 69, 93, 93, 131, 164, 200, 627, 914, 999, 1113, 1158, 1314, 1483, 1600, 1633, 1686, 3400, 3473, 3491, 3555
complex3	134.9, 992.7, 1126.8	39, 47, 124, 133, 202, 252, 487, 688, 703, 976, 992, 1142, 1293, 1453, 1490, 1662, 1673, 3063, 3473, 3513, 3650
complex4	144.2, 838.5, 981.5	92, 94, 158, 196, 232, 251, 485, 702, 728, 932, 980, 1149, 1297, 1470, 1534, 1653, 1653, 1740, 3112, 3487, 3499, 3630
complex5	151.3, 786.0, 936.4	68, 120, 165, 216, 244, 266, 481, 720, 787, 1149, 1191, 1374. 1470, 1564, 1634, 1660, 2866, 3480, 3493, 3626
complex6	178.8, 618.4, 717.8	73, 106, 161, 239, 318, 371, 489, 841, 998, 1049, 1191, 1297, 1443, 1458, 1647, 1678, 1810, 3124, 3320, 3456, 3530
N2H3	8.8, 58.6, 66.5	548, 696, 1136, 1238, 1479, 1658, 3425, 3488, 3632
trans-HONO	19.0, 143.1, 162.1	590, 621, 819, 1303, 1783, 3773
cis-HONO	21.1, 135.9, 157.0	635, 695, 876, 1342, 1716, 3597
HNO_2	16.7, 136.1, 152.8	796, 1060, 1410, 1514, 1650, 3173
H2NN(H)OH	41.4, 172.3, 194.6	290, 473, 793, 988, 1039, 1200, 1272, 1437, 1440, 1662, 1676, 3239, 3249, 3445, 3516
$H2NN(O)H_2$	41.1, 177.7, 199.6	319, 455, 492, 795, 853, 1044, 1184, 1265, 1389, 1511, 1688, 3436, 3506, 3567, 3822
NO	0, 34.9, 34.9	1979
TS1	191.8, 809.1, 906.6	114i, 51, 68, 96, 117, 141, 191, 634, 910, 996, 1106, 1173, 1317, 1470, 1615, 1636, 1688, 3402, 3472, 3512, 3557
TS2	169.0, 692.1, 769.7	657i, 81, 144, 180, 260, 287, 466, 619, 782, 934, 1123, 1177, 1269, 1439, 1458, 1573, 1653, 1745, 3491, 3536, 3660
TS3	147.0, 730.7, 870.7	622i, 91, 118, 168, 204, 259, 374, 595, 805, 978, 1068, 1137, 1273, 1492, 1524, 1621, 1673, 2225, 3536, 3543, 3686
TS4	160.0, 682.4, 827.1	1053i, 81, 99, 215, 284, 331, 510, 679, 760, 823, 1115, 1210, 1306, 1375, 1497, 1550, 1665, 1741, 3451, 3512, 3582
TS5	149.4, 532.8, 615.8	1032i, 104, 208, 270, 291, 387, 655, 747, 856, 941, 1127, 1185, 1225, 1382, 1470, 1627, 1696, 3008, 3474, 3530, 3561
TS6	40.9, 182.8, 205.2	1694i, 312, 423, 798, 835, 947, 1157, 1186, 1320, 1453, 1688, 2757, 3428, 3517, 3548

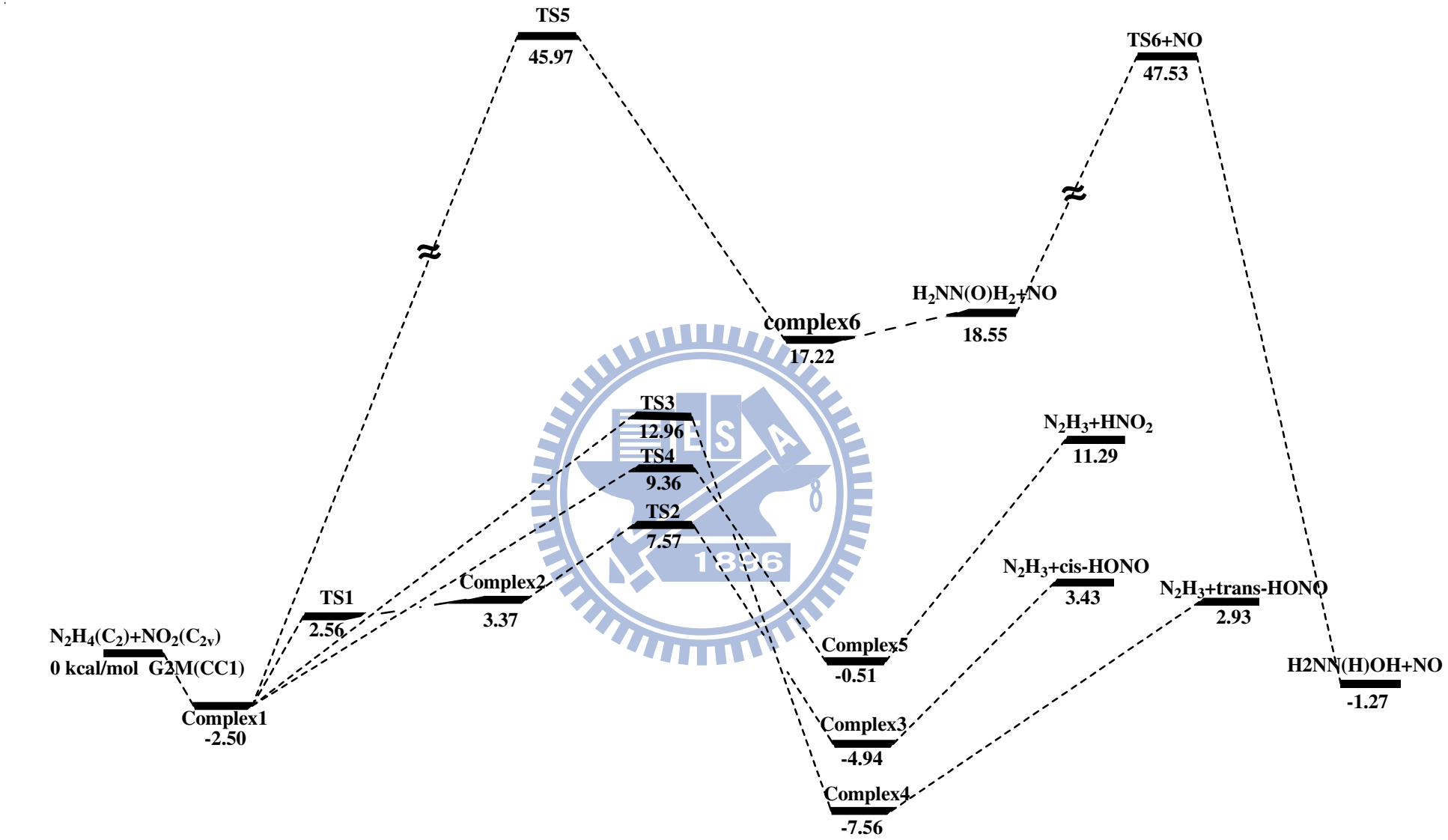

Fig 3-2: Potential Energy Surface of the N_2H_4+NO_2 reaction, whose energies are calculated by G2M(CC1)//B3LYP/6-311++G(3df,2p).

Table3-2: Relative energies of species predicted at various theoretical levels. [a]

	ZPE [b]	B3LYP/6-311++G(3df,2p)	CCSD(T)/6-311G(d,p)[c]	CCSD(T)/6-311G(3df,2p) [c]	G2M(CC1) [c]	G3B3 [c]	ΔH_f
$N_2H_4+NO_2$	38.93	-317.011335	-316.2485283	-316.4209306	-316.5287249	-316.7623438	
complex1	39.8	-1.21	-2.61	-3.6	-2.5	-1.64	
complex2	38.96	1.78	3.12	calculating	3.37	7.65	
complex3	38.67	-4.03	-4.88	-6.1	-4.94		
complex4	39.2	-6.18	-7.51	-8.26	-7.56	-6.95	
complex5	39.84	-0.24	1.16	-1.07	-0.51	0.05	
complex6	40.89	20.69	17.88	calculating	17.22	19.51	
cis-$HONO+N_2H_3$	37.4	3.96	3.63	3.44	3.43	4.42	3.76
trans-$HONO+N_2H_3$	37.44	3.42	4.04	3.93	2.93	3.76	3.25
$HNO_2+N_2H_3$	38.46	10.46	12.8	12.62	11.29	11.96	
$H_2NN(O)H_2+NO$	39.59	23.23	18.68	21.55	18.55	20.61	
$H_2NN(H)OH+NO$	39.04	3.61	-3.5	-1	-1.27	-0.30	
TS1	38.81	1.65	2.37	0.37	2.56	2.49	
TS2	36.99	2.38	8.81	7.72	7.57	7.33	
TS3	37.7	7.6	14.82	15.57	12.96	11.78	
TS4	36.86	4.75	11.06	10.36	9.36	9.89	
TS5	39.66	45.56	49.17	47.13	45.97	47.2	
TS6+NO	36.24	51.97	46.79	49.42	47.53	48.5	

a: The relative energy (kcal/mol) is taken the energy of $N_2H_4+NO_2$ as reference, whose energy unit is hartree/molecule.

b: The ZPE is determined by B3LYP/6-311++G(3df,2p) level, and the energy unit is kcal/mol for every specie.

c: The energies are including single-point energies, based on geometries of B3LYP/6-311++G(3df,2p), and ZPE. The G3B3 is represented in Table2-3.

Table3-3: Comparison of geometries (bond length in Å and bond angle in deg) of N_2H_4 by different computational methods and experimental results.

Method	r(N-N)	r(N-H_1)	R(N-H_0)	∠N-N-H_1	∠N-N-H_0	∠H_0-N-H_1	∠H_1-N-N-H_0
HF/cc-pVDZ [a]	1.412	1.007	1.004	112	107.8	107.3	88.3
HF/cc-pVTZ [a]	1.411	0.999	0.996	112.4	108.4	108.6	89.4
HF/cc-pVQZ [a]	1.408	0.998	0.995	112.6	108.7	108.8	89.7
B3LYP/cc-pVDZ [a]	1.436	1.027	1.022	111.6	106.7	105.8	87.9
B3LYP/cc-pVTZ [a]	1.436	1.015	1.011	112	107.4	108	90.2
B3LYP/cc-pVQZ [a]	1.433	1.014	1.01	112.2	107.7	108	90.2
B3LYP/cc-pV5Z [a]	1.432	1.014	1.01	112.3	107.9	108.2	90.2
B3LYP /6-311++G(3df,2p)	1.432	1.015	1.012	112.4	107.9	108.1	90.2
MP2/cc-pVDZ [a]	1.439	1.026	1.021	110.8	105.8	105.2	87.5
MP2/cc-pVTZ [a]	1.435	1.013	1.01	111.3	106.7	107	89.6
MP2/cc-pVQZ [a]	1.43	1.011	1.008	111.7	107.1	107.5	89.9
CCSD(T)/cc-pVDZ [a]	1.45	1.029	1.025	110.2	105.3	104.7	87.5
CCSD(T)/cc-pVTZ [a]	1.445	1.015	1.012	110.8	106.2	106.6	89.9
CCSD(T)/cc-pVQZ [a]	1.438	1.014	1.011	111.2	106.7	107.1	90
CCSD(T)/cc-pCVTZ [a]	1.445	1.015	1.012	110.8	106.2	106.6	89.9
CCSD(T)/cc-pCVTZ [a,g]	1.441	1.014	1.011	110.9	106.3	106.7	89.6
CCSD(T)/aVDZ [b]	1.4559	1.0252	1.0222	110.85	106.15	---	90.13
CCSD(T)/aVTZ [b]	1.4448	1.0162	1.013	111.13	106.63	---	89.73
Exp.[h] (MW)[c]	1.447(5)	1.008(8)	1.008(8)	109.2(8)	109.2(8)	113(3)	88.9(15)
Exp.[h] (IR) [d]	1.446	1.016	1.016	108.85	108.85	106	88.05
Exp.[h] (ED) [e]	1.449(4)	1.022(6)	1.022(6)	112(15)	112(15)	---	---
Exp.[h] (ED+MW) [f]	1.449(2)	1.021(3)	1.021(3)	112(2)	112(2)	106.6	91(2)

[a]: reference (1); [b]: reference (2); Microwave [c]: reference (3,4); Infrared [d]: reference (5); Electron diffraction [e]: reference (6); Electron diffraction plus microwave [f]: reference (7)

[g]: Correlating all electrons.

[h]: Uncertainties attached to the last significant digits are given in parentheses.

Table3-4: Calculated and Experimental Vibrational Frequencies (in cm^{-1}) of N_2H_4

Method	Vibrational Frequency Symmetry (a, a, b, a, b, a, b, a, b, a, a, b)
B3LYP/cc-pVDZ [a]	419, 828, 1027, 1125, 1302, 1340, 1661, 1675, 3382, 3399, 3499, 3508
B3LYP/cc-pVTZ [a]	436, 810, 999, 1112, 1301, 1333, 1676, 1687, 3444, 3455, 3552, 3558
B3LYP/cc-pVQZ [a]	438, 808, 989, 1113, 1299, 1329, 1675, 1686, 3452, 3461, 3554, 3559
B3LYP/cc-pV5Z [a]	441, 803, 977, 1111, 1297, 1326, 1674, 1686, 3457, 3466, 3558, 3564
B3LYP/6-311++G(3df,2p)	439, 801, 974, 1114, 1294, 1323, 1674, 1686, 3462, 3471, 3562, 3568
MP2/cc-pVDZ [a]	404, 885, 1077, 1154, 1326, 1370, 1677, 1690, 3469, 3479, 3591, 3597
MP2/cc-pVTZ [a]	421, 852, 1033, 1142, 1315, 1350, 1680, 1693, 3510, 3517, 3625, 1629
MP2/cc-pVQZ [a]	431, 843, 1013, 1142, 1310, 1346, 1679, 1691, 3522, 3525, 3633, 3637
CCSD(T)/cc-pVDZ [a]	382, 878, 1086, 1134, 1323, 1366, 1670, 1684, 3412, 3430, 3530, 3537
CCSD(T)/cc-pVTZ [a]	398, 858, 1047, 1126, 1314, 1347, 1676, 1690, 3465, 3477, 3572, 3578
CCSD(T)/cc-pCVTZ [a]	404, 858, 1045, 1130, 1316, 1350, 1679, 1693, 3471, 3482, 3577, 3582
CCSD(T)/aVDZ [b]	404.1, 841.7, 1026.6, 1104.6, 1292.7, 1332.3, 1651.2, 1665.3, 3426.0, 3436.8, 3535.8, 3538.6
CCSD(T)/aVTZ [b]	406.0, 804.7, 1020.0, 1114.0, 1302.7, 1338.7, 1674.0, 1685.2, 1460.0, 3469.0, 3563.8, 3569.0
Exp. [c,d,e]	376.7 [c], 780 [d], 966 [e], 1076 [d], 1275 [e], 1275 [d], 1628 [e], 1642 [d], 3314 [e], 3329 [d], 3398 [d], 3350 [e]
Exp. [f]	377, 780, 966, 875, 933, 1098, 1275, 1312, 3280, 3261, 3350, 3330
Exp. [g]	377, 780, 937, 1098, 1283, 1324, 1587, 1628, 3297, ---, ---, 3390
Exp. [h]	(627), 871 (884), 1042 (1066), 1098 (1126), 1324 (1350), 1283 (1304), 1608 (1655), 1806 (1603), 3332 (3310), 3189(3200), 3332 (3310), 3332 (3310)
Exp. [i]	394, 832, 982, 1087, 1265, 1312, ---, ---, 3297 (3280), (3261), 3390 (3350), 3356 (3330)
Exp. [j]	---, 780 (800), [966, 933] [k] (1038), (873), 1275 (1280), 1098, [1587, 1628], 1493, [3314, 3280] (3338), ---, 3325, 3350 (3338)

[a]: reference (1); [b]: reference (2); [c]: reference (8); [d] reference (9) ; [e] reference (10); [f] reference (11), which complied from different experimental source.; [g] reference (12), which complied from different experimental source.; [h] reference (13), which was infrared liquid and solid (in parentheses); [i] reference (14), which was infrared and Raman (in parentheses); [j] reference (15), which was infrared gas and liquid (in parentheses); [k]: double peaks [in square brackets].

Table3-5: Calculated and Experimental bond lengths (in Å), bond angles (in deg), and vibrational Frequencies (in cm^{-1}) of NO_2.

Method	r(N-O)	∠O-N-O	ω_1	ω_2	ω_3
MP2/6-31G(d) [a]	1.217	133.7	2271	1380	752
B3LYP/6-31G(d) [a]	1.203	133.8	1717	1402	749
B3LYP/6-311++G(3df,2p)	1.19	134.5	1703	1395	767
CASSCF/cc-pVDZ [b]	1.209	133.8	1640	1328	751
CASSCF/cc-pVTZ [b]	1.205	133.9	1626	1319	757
CCSD(T)/cc-pVDZ [b]	1.207	134.1	1759	1370	725
CCSD(T)/aug-cc-pVDZ [b]	1.21	134	1751	1367	693
CCSD(T)/cc-pVTZ [b]	1.199	134.2	1668	1348	658
Exp. [c]	1.194	133.8	1671	1353	760
Exp. [d,e]	1.1939 [d]	133.5 [d]	1655.5 [e]	1357.8 [e]	756.8 [e]

[a]: reference (16); [b]: reference (17); [c]: reference (18); [d]: reference (19); [e]: reference (20)

Table3-6: Fitting expressions for the rate constants of the N_2H_4+NO_2 reactions employing transition-state theory. (in Units of cm^3/(molecule · Sec))

Reaction Channel	300K	100K ≦ T ≦ 4000K
k_1: product [cis-HONO+N_2H_3] via TS2	1.88×10^{-18}	$3.20\times10^{-25}T^{3.74}\exp(-1662.5/T)$
k_2: product [trans-HONO+N_2H_3] via TS3	9.44×10^{-23}	$2.88\times10^{-26}T^{4.09}\exp(-4395.2/T)$
k_3: product [HNO_2+N_2H_3] via TS4	1.82×10^{-22}	$1.40\times10^{-23}T^{3.27}\exp(-4880.3/T)$

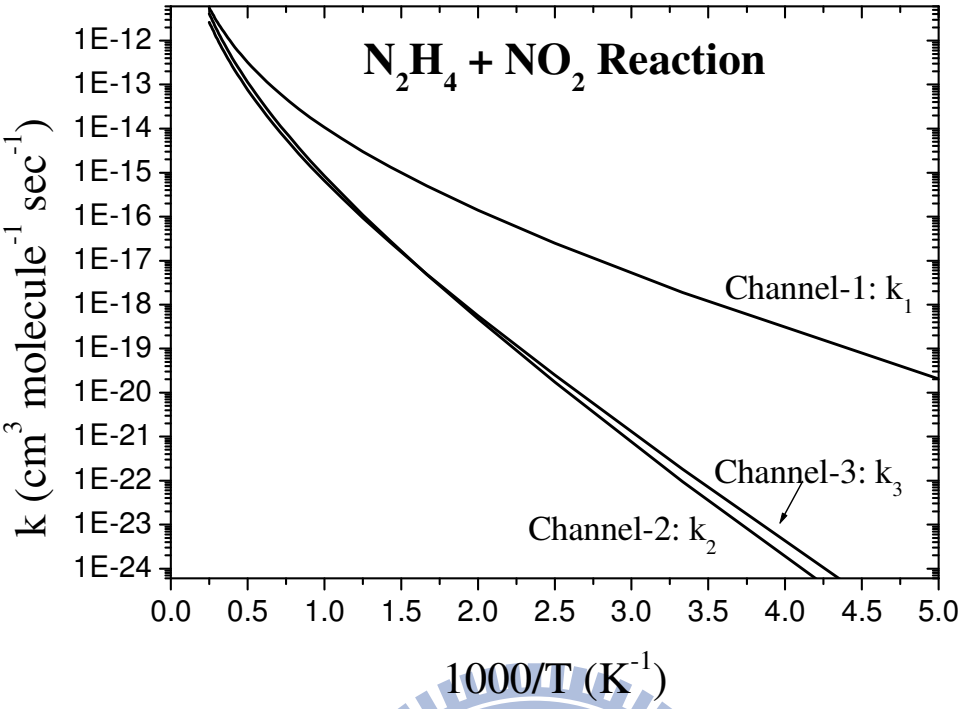

Fig3-3: Arrhenius plots of the calculated rate constants for various channels of the N_2H_4+NO_2 reaction.

3.2 N_2O_4 isomerization reaction

The isomerization reaction of dinitrogen tetroxide is still unknown, since the isomers are mostly too unstable to study the properties in experiments, including structures, vibrational frequencies, dipole moments, and other physical parameters. Some computational works predict the geometries of isomers as discussed in section1.3, and we studied the geometries of trans-$ONONO_2$ and cis-$ONONO_2$. The geometries of the N_2O_4 isomers and the transition states between these isomers are determined at the B3LYP/6-311++G(3df,2p), PW91PW91/6-311++G(3df,2p), BHandHLYP/6-311++G(3df,2p), and CCSD/6-311+G(d,p) levels, as shown in Fig.3-4; the moments of inertia and vibrational frequencies are listed in Table3-7. The potential energy surface (PES) of the isomerization reaction is presented in Fig.3-5; the energies of species and TSs are determined by G2M(CC1) single-point calculations. Moreover, we use the notations of i-complexes and i-TSs in the PES for clarity.The energies from other calculations, such as the CCSD(T) method, and the heat of dissociation for $N_2O_4(D_{2h})$ to $2NO_2$ with different basis sets are listed in Table3-8 and Table.3-10, respectively.

3.2.1 The geometries of N_2O_4 isomers

The N_2O_4 (D_{2h}) molecule is the most stable structure of all isomers. The weak N-N bond, which is 1.756 Å, connects two NO_2 to form this well-studied molecule. Comparison of the computational and experimental results for the bond lengths, the bond angles, and the vibrational frequencies are presented in Table3-10 and Table3-11. The MP2, B3LYP, and CASSCF methods have larger errors than the CCSD(T) in the prediction of the N-N bond, which is overpredicted by 0.05Å on average, whereas B3LYP and CCSD(T) methods

performs well in the prediction of the N-O bond and O-N-O angle. The PW91PW91 predicted a longer N-N bond, which is higher than experimental data by 0.1 Å, and the BHandHLYP has an inverse prediction, in which the N-N bond is shorter than experimental results by 0.07 Å. Moreover, the CCSD/6-311+G(d,p) also has underpredicted the N-N bond. Therefore, among the DFT methods in our calculations, the B3LYP provides the best prediction for the N-N bond of N_2O_4. Furthermore, the errors of frequencies determined by the DFT and CCSD(T) are low, with 26 and 24 cm^{-1} by B3LYP/6-311++G(3df,2p) and CCSD(T)/cc-pVTZ, respectively. Therefore, the DFT (we use B3LYP) calculation can predict the geometry and frequencies of the N_2O_4 to be as good as those by the CCSD(T) method; the B3LYP method has the advantage of saving computational resources.

The trans-$ONONO_2$ and cis-$ONONO_2$ molecules have been detected experimentally in several studies which employed infrared and Raman spectra. However, the geometries are still unknown in experiment. St. Louis and Crawford, [37] suggested that the two structures were planar with a C_s symmetry after calculating the relationship with the vibrational frequencies and molecule structures. In addition, St. Louis and Crawford noted that these two molecules can undergo cis-trans isomerization without specifying which is cis or trans. McKee[16] firstly predicted the geometries of N_2O_4 isomers by ab-initio calculations, and Wang, Qin, and Fan[36] also calculated them later and obtained a different prediction for cis-$ONONO_2$ geometry. Moreover, Dyshlovoi's group[40] provided another cis-$ONONO_2$ structure. The geometries of cis-$ONONO_2$, cis-$ONONO_2$_2, and cis-$ONONO_2$_3 originate from Dyshlovoi[40], Wang[36], and McKee[16], respectively; we optimize these three structures at the B3LYP/6-311++G(3df,2p), PW91PW91/6-311++G(3df,2p), BHandHLYP/ 6-311++G(3df,2p), and CCSD/6-311+G(d,p) levels as presented in Fig.3-4, respectively. First, cis-$ONONO_2$ calculated at B3LYP is a non-planar structure with C_s symmetry, and the ONO-NO_2 bond is the longest bond, 1.640Å. The cis-$ONONO_2$ optimized by BHandHLYP

and CCSD methods have similar structure, whereas the ON-ONO_2 bond is longer than ONO-NO_2 bond by 0.02 and 0.07 Å for BHandHLYP and CCSD method, respectively. Due to the small bond differences, we suggest the difference of cis-$ONONO_2$ optimized by B3LYP, BHandHLYP, and CCSD is simply due to the calculation methods, and these results point to the same stationary point. On the other hand, the longest bond in cis-$ONONO_2$_2 and cis-$ONONO_2$_3 computed at B3LYP is the ON-ONO_2 bond, which is 1.685 and 1.751Å, respectively. cis-$ONONO_2$_2 is non-planar with C_1 symmetry, and the structure is just like the trans-$ONONO_2$ after rotating the ON group. The cis-$ONONO_2$_2 predicted by PW91PW91 has the same prediction as B3LYP. The cis-$ONONO_2$_3 optimized by B3LYP, PW91PW91, BHandHLYP, and CCSD are planar with C_s symmetry, which fits the suggestion of St. Louis and Crawford. However, as shown in Table3-12, cis-$ONONO_2$_3 computed by different methods have a small imaginary frequency, which means that it may be a saddle point on the PES. Compared with the experimental result, the errors in frequencies are 20.6 and 37.5 for cis-$ONONO_2$ and cis-$ONONO_2$_2 geometries predicted at the B3LYP/6-311++G(3df,2p) level, respectively. In the experimental literature, Jones[41] and Givan[42] proposed that the autoionization, which is a formation of ionic nitrosonium nitrate ($NO^+NO_3^-$), originates from the D' isomer (Jones named it as II-$ONONO_2$ whose frequencies are 1961 and 1578 cm^{-1} etc.)). The peaks of D isomer (otherwise known as I-$ONONO_2$ whose frequencies are 1840 and 1625 cm^{-1} etc.)) were stable, whereas the peaks of D' are annihilated as the enhanced peaks of $NO^+NO_3^-$. Moreover, St. Louis and Crawford suggest that the D' form might be more stable in thermodynamic. According to this experimental evidence, we suggest that the D isomer is cis-$ONONO_2$. The longest bond of cis-$ONONO_2$_2 is ON-ONO_2, and this may provide a possibility for the occurrence of autoionization as the temperature increases. The cis-$ONONO_2$_3 is thermodynamically unstable and is s saddle point, since every computation indicates that there is one small imaginary frequency. The existence of cis-$ONONO_2$_3 seems

less reasonable than cis-$ONONO_2$ and cis-$ONONO_2$_2, even though cis-$ONONO_2$ is not a planar structure, its C_s symmetry provides the correct relationship in vibrational frequencies. Therefore, we conclude that the frequencies of D and D' in the research of St. Louis and Crawford belong to a cis- and a trans-$ONONO_2$ structure, respectively. This assignment of the vibrational frequencies is contrary to Wang's work[36]. Fortunately the energies of these three cis-$ONONO_2$ structures are very close, as shown in Table3-8, and the difference between them is smaller than 0.2 kcal/mol at the B3LYP/6-311++G(3df,2p) level of theory. The comparison of vibrational frequencies is listed in Table3-12, 3-13, and 3-14. The calculated results compare with those optimized by B3LYP/6-311++G(3df,2p) in Table3-12, and the frequencies of cis-$ONONO_2$ are much closer to the experimental result than those of cis-$ONONO_2$_2. Precisely, the deviations comparing with experimental data are -20.6 and 37.5 cm^{-1} for cis-$ONONO_2$ and cis-$ONONO_2$_2 computed at B3LYP, respectively. Moreover, the B3LYP method provides better predictions than the MP2 method does for cis-$ONONO_2$_2. The three types of cis-$ONONO_2$ geometries optimized by B3LYP, PW91PW91, BHandHLYP, CCSD methods are compared in Table3-13 and Table3-14. It is worthy to note is that the error of cis-$ONONO_2$_2 predicted by PW91PW91 is 21.4 cm^{-1}, which is close to the error of cis-$ONONO_2$. Therefore, the geometries of cis-$ONONO_2$ and cis-$ONONO_2$_2 are acceptable.

Even though there is no complete experimental result to describe on these isomers, the geometries of trans-$ONONO_2$ predicted in different computational works are similar. In Table3-15, the ON-ONO_2 bond is the longest, 1.685, 1.634, 1.514, 1.550, 1.654, and 1.657Å computed at the B3LYP/6-311++G(3df,2p), PW91PW91/6-311++G(3df,2p), BHandHLYP/ 6-311++G(3df,2p), CCSD/6-311+G(d,p), MP2/6-31G(d)[16], and MP2/6-311G*[36] levels, respectively, for the trans-$ONONO_2$ molecule. All of the trans-$ONONO_2$ geometries are almost planar and C_s symmetry except that the one calculated by CCSD, and there is no other trans-isomer structure found in our calculations. These predictions of a long bond length may

help explain the appearance of the autoionization producing $NO^+NO_3^-$ complex. The vibrational frequencies are listed in Table3-15, and the errors in frequencies obtained by B3LYP, PW91PW91, and CCSD are 22.5, 13.1, 27.1 cm^{-1} on average, respectively. The trans-$ONONO_2$_BHandHLYP has a small imaginary frequency. Basically the trans-$ONONO_2$ structure has consistent results among different methods. These three N_2O_4 isomers determined here will be used as the reactants to react with N_2H_4.

3.2.2 PES of N_2O_4 isomerization

Due to its low dissociation energy, at room temperature, the N_2O_4 (D_{2h}) molecule also contains a small amount of NO_2 monomers. The equilibrium concentration of the N_2O_4 increases as the temperature decreases. The N-N bond is 1.776 Å by experiment, and this weak bond is also evidenced by the low values of the enthalpies of reaction at 0K, 12.7-12.9 kcal/mol, and at 298K, 13.1-13.7 kcal/mol.[27,28] The rate constant of the dissociation reaction is 4.5×10^6 L mol^{-1} sec^{-1} and 1.7×10^5 sec^{-1} in the low-pressure (k_1) and the high-pressure (k_∞) regions, respectively.[43] Shock waves measurements of the dissociation in the temperature range of 253-301K show activation energies varying from 11.0±0.6 kcal/mol (1 atm) to 13.0 kcal/mol (high pressure).[44] In Table3-9, the CCSD(T)/6-311++G(3df,2p) method shows a better prediction of the reaction enthalpy at 0K. However, other methods, even CCSD(T)/cc-pVTZ and G2M(CC1) methods, have poor performances. i-TS1 is a very high barrier from N_2O_4 (D_{2h}) to trans-$ONONO_2$, as shown in Fig.3-5. It is easier to form cis-$ONONO_2$ via i-TS2. Although the reaction coordinate of i-TS1 and i-TS2 is similar, which breaks the N-N bond and creates a new O-N bond, their energies are highly different, as presented in Fig3-5. According to the discussion in Section 3.2.1, cis-$ONONO_2$ and cis-$ONONO_2$_2 optimized by B3LYP/6-311++G(3df,2p) can possibly exist, and we consider them in the N_2O_4 isomerization reactrion. The two NO_2 group in cis-$ONONO_2$ is

perpendicular, and the cis-$ONONO_2$_2 is similar to trans-$ONONO_2$, which has long ON-ONO_2 bond as shown in Fig.3-4. The cis-$ONONO_2$ structure cannot directly transform to trans-$ONONO_2$; the cis-$ONONO_2$ first transforms to cis-$ONONO_2$_2 via i-TS3, which corresponds to the rotation of the ONO group. Since the cis-$ONONO_2$_2 and trans-$ONONO_2$ both have the long ON-ONO_2 bond, the i-TS4, which corresponds to the rotation of the ON group connect between cis-$ONONO_2$_2 and trans-$ONONO_2$ molecules. Since i-TS3 and i-TS4 are the transition state of the internal rotations, the activation energy of cis-trans isomerization is very small, their imaginary frequencies are 42 and 188 cm^{-1} for i-TS3 and i-TS4. The energy barrier of i-TS4 for the cis-to-trans direction is only 1.71 kcal/mol at the G2M(CC1) level. However, that of i-TS3 is lower than cis-$ONONO_2$ and cis-$ONONO_2$_2 by 1.5 and 0.23 kcal/mol, respectively. It may be due to a computational error, since the energy difference is less than 0.02 kcal/mol by B3LYP/6-311++G(3df,2p). The calculated energies of species and transition states at the G2M(CC1) level are very close to those by CCSD(T) /6-311++G(3df,2p), as shown Table3-8. Since the activation energy for trans-$ONONO_2$ formation from N_2O_4 is higher than that for cis-$ONONO_2$ by 32 and 32.3 kcal/mol at G2M(CC1) and CCSD(T)/6-311++G(3df,2p), respectively, the possible channel is that N_2O_4 transforms to cis-$ONONO_2$ first and later trans-$ONONO_2$ forms. This lowest-energy channel is consistent with the phenomenon observed by St. Louis and Crawford.

The rate constants with Eckart's tunneling correction of isomerizations are calculated by TST using the energy barrier predicted by G2M(CC1) values are shown in Table3-7. We consider the reactions between the two isomers, including N_2O_4 to trans-$ONONO_2$ via i-TS1, N_2O_4 to cis-$ONONO_2$ via i-TS2, and both directions of cis-$ONONO_2$ to trans-$ONONO_2$ via i-TS3, and the Arrhenius plots and the three-parameters fitting the expressions for the rate constants are shown in Fig:3-6. According to the kinetic calculations at temperatures varying from 100 to 1000K, we confirm that the formation of trans-$ONONO_2$ accounts for N_2O_4

isomerization to cis-$ONONO_2$ via i-TS2 followed by cis-trans isomerization via i-TS3 and i-TS4 with very high rate constant.

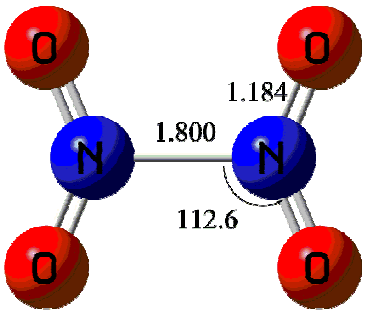

N_2O_4 (D_{2h}, planar)

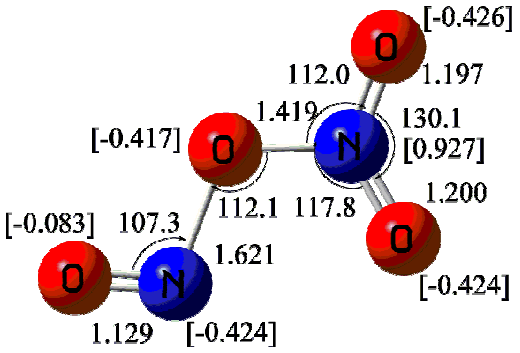

trans-$ONONO_2$ (C_s, close to planar)

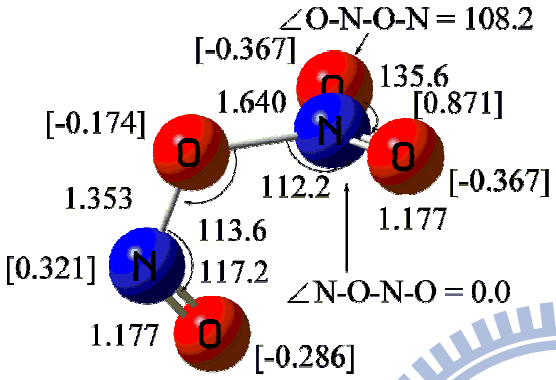

cis-$ONONO_2$ (C_s, non-planar)

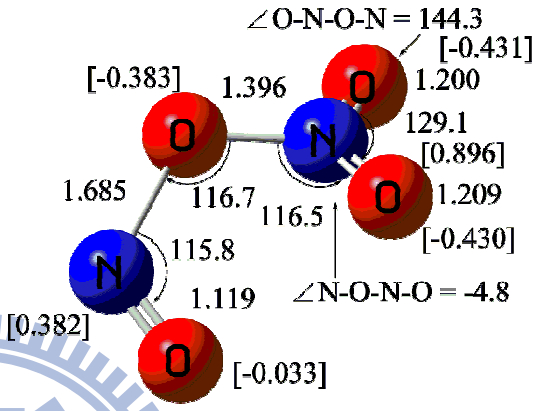

cis-$ONONO_2$_2 (C_1, non-planar)

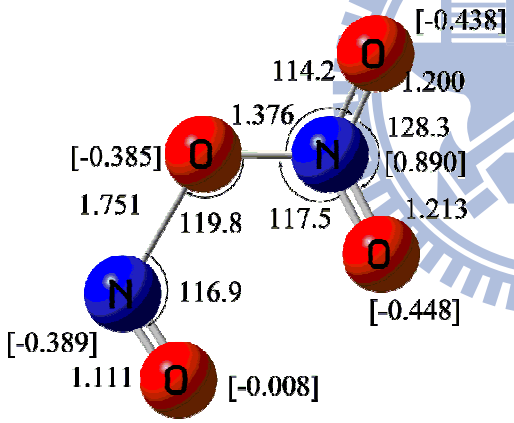

cis-$ONONO_2$_3 (C_s, planar)

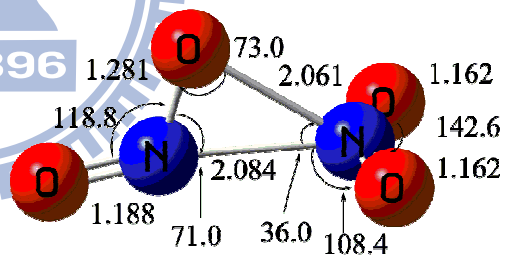

i-TS1 (C_s)

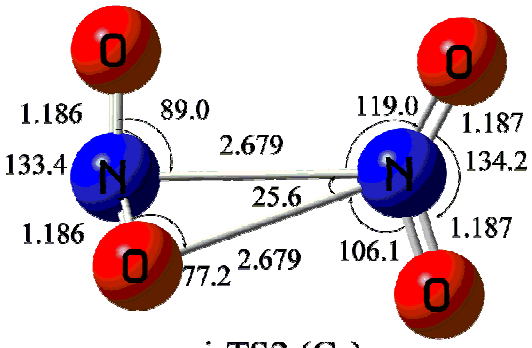

i-TS2 (C_1)

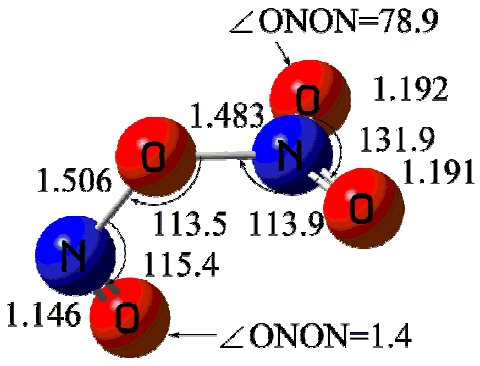

i-TS3 (C_1)

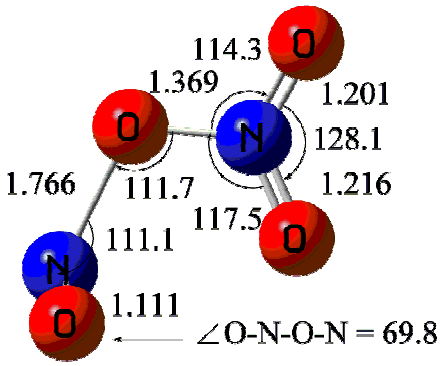

i-TS4 (C_1)

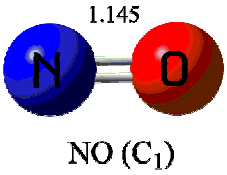

NO (C_1)

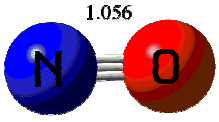

NO^+ (C_1)

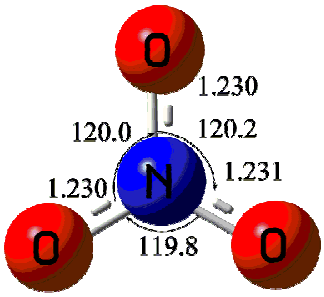

NO_3 (C_{3h})

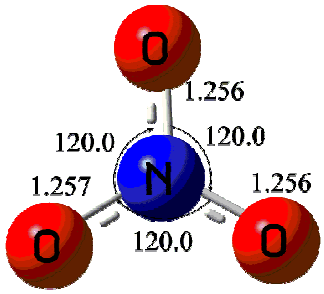

NO_3^- (C_{3h})

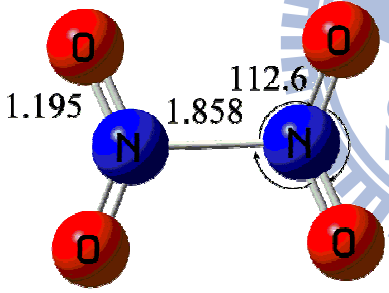

N_2O_4_PW91PW91 (D_{2h})

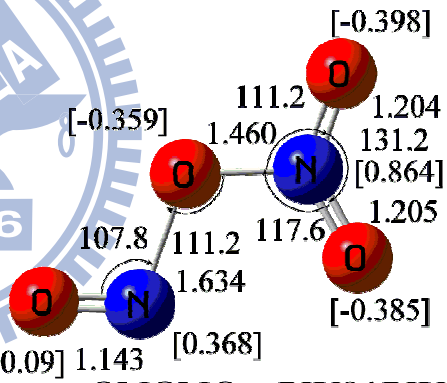

trans-$ONONO_2$_PW91PW91
(C_s, close to planar)

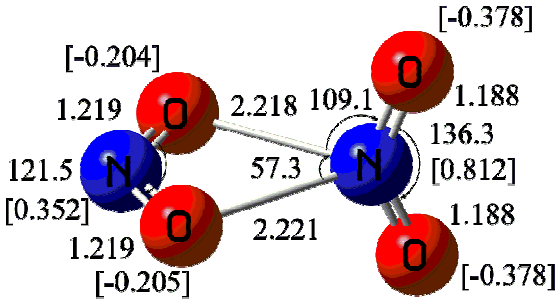

cis-$ONONO_2$_PW91PW91
(C_1, non-planar)

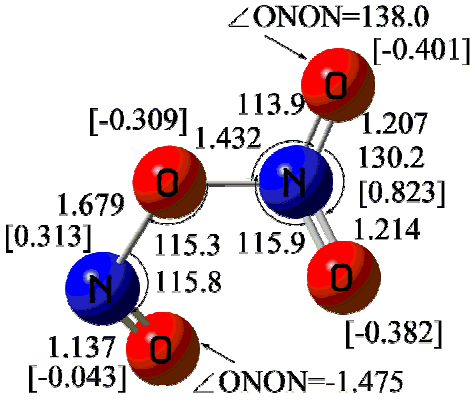

cis-$ONONO_2$_2_PW91PW91
(C_1, non-planar)

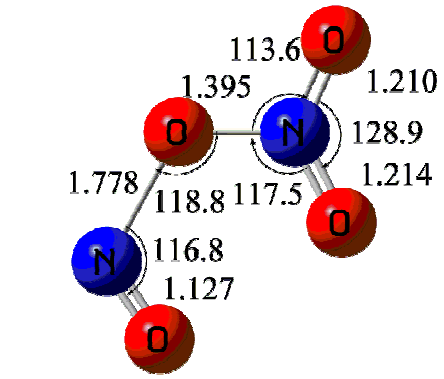

cis-$ONONO_2$_3_PW91PW91
(C_s, planaer)

(b)

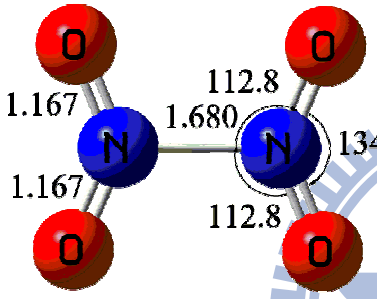

N_2O_4_BHandHLYP
(D_{2h}, planar)

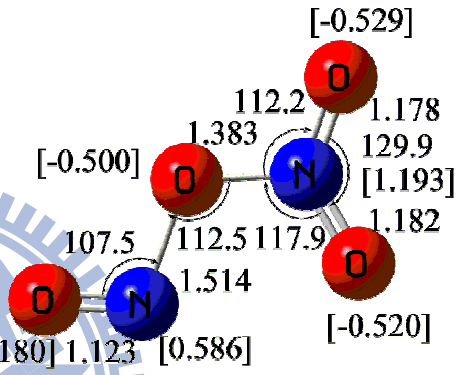

trans-$ONONO_2$_BHandHLYP
(Cs, close to planar)

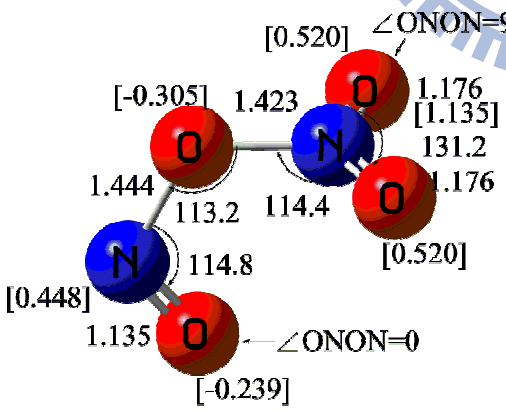

cis-$ONONO_2$_BHandHLYP
(C_1, non-planar)

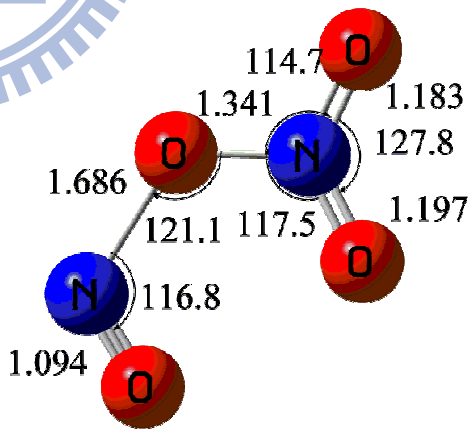

cis-$ONONO_2$_3_BHandHLYP
(C_s, planar)

(c)

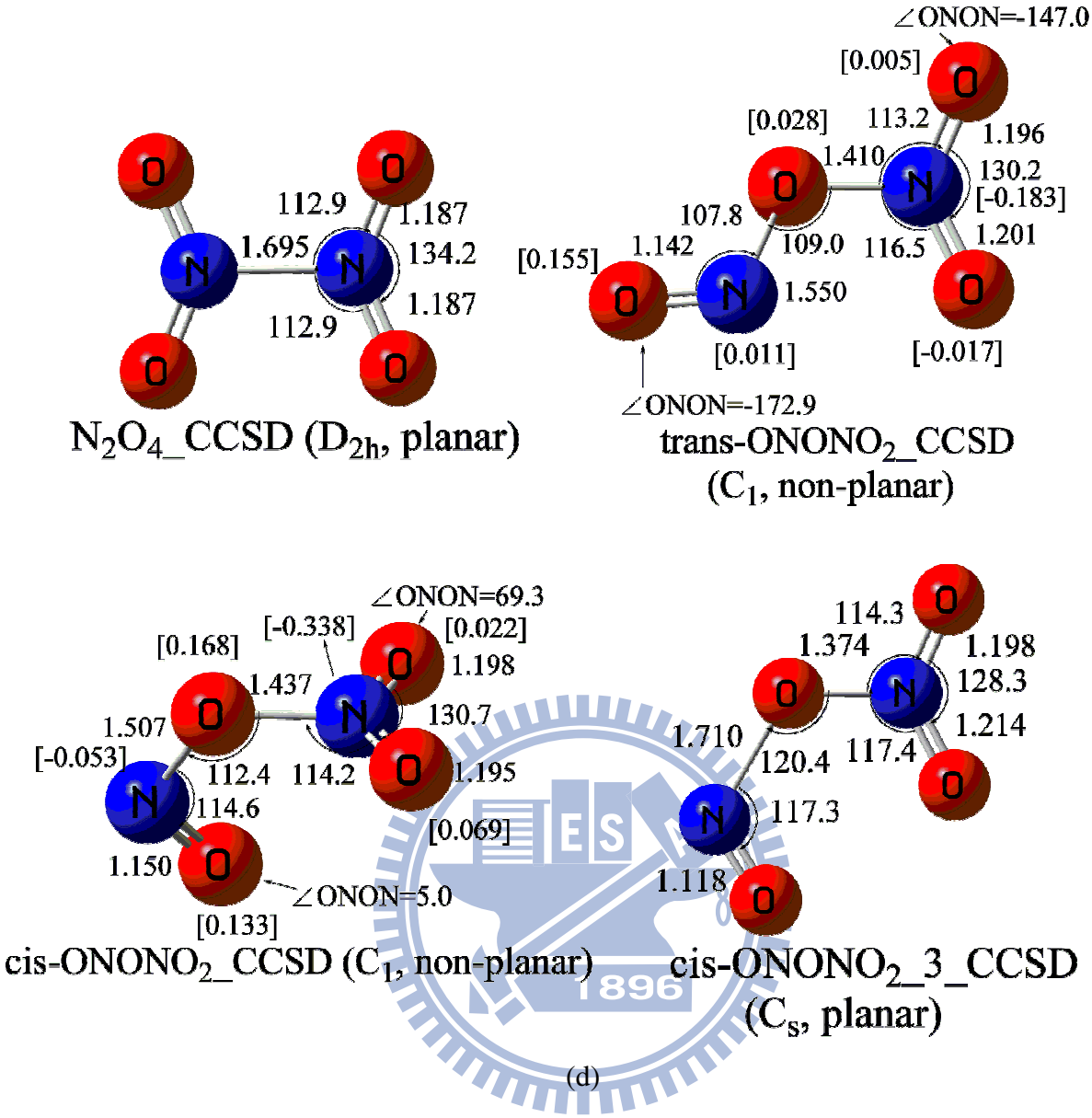

(d)

Fig3-4: (a) The geometries in the PES of N_2O_4 isomerization are determined at B3LYP/ 6-311++G(3df,2p) level, (b) PW91PW91/6-311++G(3df,2p) level, (c) BHandHLYP/ 6-311++G(3df,2p) level, and (d) CCSD/6-311+G(d,p) The value in parentheses is noted for Mulliken charge.

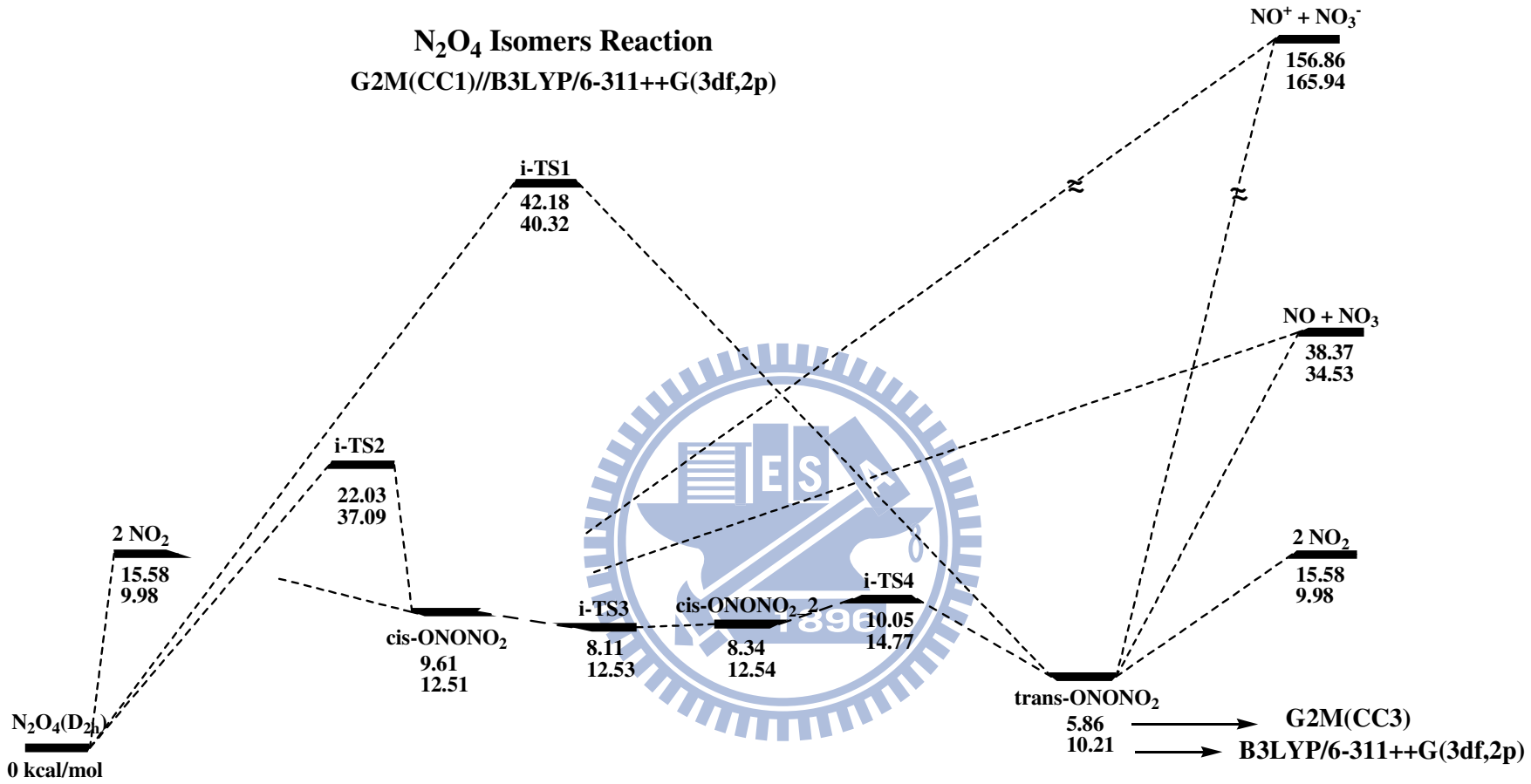

Fig3-5: The PES of N_2O_4 isomerization, whose energies are calculated by G2M(CC1)//B3LYP/6-311++G(3df,2p).

Table3-7: Moments of inertia (I_A, I_B, I_C) and vibration frequencies of the species in N_2O_4 isomerization computed at B3LYP/6-311++G(3df,2p).

Species or Transition States	Moments of inertia I_i(a.u)	Vibrational Frequency u_j (cm^{-1})
$N_2O_4(D_{2h})$	273.2, 500.4, 773.7	87, 222, 293, 446, 490, 704, 760, 850, 1307, 1450, 1787, 1826
trans-$ONONO_2$ (C_s)	151.2, 773.8, 925.0	9, 131, 209, 294, 486, 647, 786, 801, 945, 1330, 1709, 1934
cis-$ONONO_2$ (C_s, non-planar)	244.9, 605.7, 632.1	73, 135, 179, 285, 542, 564, 693, 862, 909, 1360, 1683, 1845
cis-$ONONO_2$_2 (C_1, non-planar)	195.3, 634.6, 770.1	39, 188, 205, 294, 601, 623, 748, 823, 876, 1312, 1667, 1989
cis-$ONONO_2$_3 (C_s, planar)	171.0, 673.2, 844.2	34i, 168, 202, 278, 590, 654, 761, 798, 892, 1310, 1649, 2038
i-TS1 (C_s)	216.1, 716.5, 777.2	638i, 125, 250, 273, 375, 426, 714, 751, 1178, 1332, 1634, 1952
i-TS2 (C_1)	277.2, 730.3, 967.5	454i, 55, 116, 133, 149, 259, 633, 789, 1254, 1406, 1716, 1756
i-TS3 (C_1)	241.6, 595.4, 636.9	42i, 152, 178, 259, 549, 591, 700, 841, 893, 1336, 1753, 1829
i-TS4 (C_1)	173.6, 687.8, 807.7	188i, 77, 181, 288, 616, 666, 707, 791, 910, 1304, 1643, 2034
$NO_2(C_{2v})$	7.4, 137.6, 145.0	767, 1395, 1703
$NO(C_1)$	0.0, 34.9, 34.9	1979
$NO_3(C_{3h})$	129.4, 130.0, 259.4	220, 248, 810, 1103, 1121, 1137
$NO^+(C_1)$	0.0, 29.8, 29.8	2487
$NO_3^-(C_{3h})$	135.1, 135.3, 270.5	710, 711, 849, 1072, 1379, 1381

Table3-8: Relative energies of species in N_2O_4 isomerization reaction at various theoretical levels. [a]

Species or Transition States	ZPE [b]	B3LYP /6-311++G(3df,2p)	CCSD(T) /6-311+G(d,p) [c]	CCSD(T) /6-311++G(3df,2p) [c]	G2M(CC1) [c]	ΔH_0^o
$N_2O_4(D_{2h})$	14.61	-410.308886	-409.3648607	-409.6067069	-409.7113339	
trans-$ONONO_2$ (C_s)	13.27	10.21	6.1	6.19	5.86	
cis-$ONONO_2$ (C_s, non-planar)	13.05	12.51	9.63	9.72	9.61	
cis-$ONONO_2$_2 (C_1, non-planar)	13.39	12.54	8.48	8.69	8.34	
i-TS1 (C_s)	12.88	40.32	42.48	42.86	42.18	
i-TS2 (C1)	11.82	37.09	19.15	23.2	22.03	
i-TS3 (C1)	12.98	12.54	8.33		8.11	
i-TS4 (C1)	13.18	14.77	10.27	10.59	10.05	
2 NO_2 (C_{2v})	11.05	9.98	9.01	11.86	15.58	12.7, 12.9
NO + NO_3	9.46	34.53	31.71	35.25	38.37	
$NO^+ + NO_3^-$	12.28	165.92	153.97	157.33	156.86	

[a]: The relative energy (kcal/mol) is taken the energy of N_2O_4 (D_{2h}) as reference, whose energy unit is hartree/molecule.

[b]: The ZPE is determined by B3LYP/6-311++G(3df,2p) level, and the energy unit is kcal/mol for every specie.

[c]: The energies are including single-point energies, based on geometries of B3LYP/6-311++G(3df,2p), and ZPE.

Table3-9: The heat of dissociation for N_2O_4 to $2NO_2$ at 0K and one atmosphere.

	CCSD(T) /cc-pVDZ [a]	CCSD(T) /aug-cc-pVDZ [a]	CCSD(T) /cc-pVTZ [a]	CCSD(T) /6-311+G(d,p) [b]	CCSD(T) /6-311++G(3df,3p) [b]	G2M(CC1) [b]	Exp.
ΔH_0^o	8.7	11.39	14.61	9.01	11.86	15.58	12.7 [c], 12.9 [d]

[a]: reference (17); [b]: this work, the methods are single-point calculation based on B3LYP/6-311++G(3df,2p) level.

[c]: reference (27); [d]: reference (28)

Table3-10: Comparison of geometries (bond length in Å and bond angle in deg) of N_2O_4 by different computational methods and experimental results.

Method	r(N-N)	r(N-O)	∠(O-N-O)
MP2/6-31G(d) [a]	1.824	1.214	135.2
B3LYP/6-31G(d) [a]	1.783	1.196	134.6
B3LYP/6-311++G(3df,2p) [b]	1.8	1.184	134.8
B3LYP/6-311++G(d,p) [c]	1.81	1.188	134.8
B3PW91/6-311++G(d,p) [c]	1.783	1.183	134.8
B3P86/6-311++G(d,p) [c]	1.773	1.183	134.8
B1PB95/6-311++G(d,p) [c]	1.775	1.181	134.9
B1LYP/6-311++G(d,p) [c]	1.793	1.186	134.7
MPW1PW91/6-311++G(d,p) [c]	1.757	1.18	134.7
PBE1PBE/6-311++G(d,p) [c]	1.754	1.18	134.8
PW91PW91/6-311++G(3df,2p) [b]	1.858	1.195	134.8
BHandHLYP/6-311++G(3df,2p) [b]	1.68	1.167	134.4
QCISD/6-311++G(d,p) [c]	1.701	1.19	134.2
CASSCF/cc-pVDZ [d]	1.806	1.171	134.4
CASSCF/cc-pVTZ [d]	1.806	1.168	134.1
CASSCF/QT [e]	1.803	1.167	134
CASPT2/QT [e]	1.794	1.191	134.8
CCSD/6-311+G(d,p) [b]	1.695	1.187	134.2
CCSD(T)/TZP2f [d]	1.752	1.195	134.7
CCSD(T)/cc-pVDZ [d]	1.776	1.2	135.2
CCSD(T)/aug-cc-pVDZ [d]	1.78	1.204	134.7
CCSD(T)/cc-pVTZ [d]	1.774	1.194	134.8
Exp. [f]	1.756	1.19	134.4
Exp. (ED) [h]	1.776(4)	1.191(4)	134.6(5)
Exp. (XRD) [i]	1.712(17)	1.189(12)	134.8(15)
Exp. (ND) [j]	1.7561(9)	1.1893(5)	134.40(7)
Exp. (IRR) [k]	1.756(10)	1.196(5)	133.7(5)

[a]: reference (16); [b]: this work; [c]: reference (29); [d]: reference (17); [e]: cc-PVQZ for nitrogen and cc-PVTZ for oxygen, reference(30); [f]: reference (18); [g]: Uncertainties attached to the last significant digits are given in parentheses.; [h]: Electron diffraction in gas phase at T=294K, reference (31); [i]:X-ray diffraction in solid state at T=25K, reference (32); [j]: Neutron diffraction at T=20K, reference (33); [g]: Infrared roationally resolved measurement at T≒50K, reference (34)

Table3-11: Calculated and Experimental Vibrational Frequencies (in cm^{-1}) of N_2O_4

Method	ω_1 (a_u)	ω_2 (b_{2u})	ω_3 (a_g)	ω_4 (b_{3u})	ω_5 (b_{3g})	ω_6 (b_{2g})	ω_7 (b_{1u})	ω_8 (a_g)	ω_9 (b_{1u})	ω_{10} (a_g)	ω_{11} (b_{3g})	ω_{12} (b_{2u})
B3LYP/6-311++G(3df,2p) [a]	87	222	293	446	490	704	760	850	1307	1450	1787	1826
B3LYP/6-311++G(d,p) [b]	83	225	292	436	492	673	762	849	1306	1448	1794	1828
B3PW91/6-311++G(d,p) [b]	83	236	304	449	508	693	775	859	1336	1474	1844	1878
B3P86/6-311++G(d,p) [b]	84	239	310	450	512	695	776	861	1339	1475	1848	1882
B1PB95/6-311++G(d,p) [b]	86	256	318	452	512	696	776	861	1345	1483	1859	1894
B1LYP/6-311++G(d,p) [b]	83	235	301	447	502	687	770	855	1316	1456	1805	1839
MPW1PW91/6-311++G(d,p) [b]	83	249	319	463	524	711	786	858	1356	1489	1870	1904
PBE1PBE/6-311++G(d,p) [b]	84	252	322	464	527	714	787	869	1361	1492	1878	1913
PW91PW91/6-311++G(3df,2p) [a]	86	190	264	401	449	641	727	821	1264	1407	1738	1773
BHandHLYP/6-311++G(3df,2p) [a]	85	292	366	526	569	820	823	899	1410	1524	1897	1940
QCISD/6-311++G(d,p) [b]	53	282	352	474	540	684	783	858	1328	1428	1791	1818
CASSCF/cc-pVDZ [c]	98	210	221	430	482	682	826	877	1457	1558	2043	2067
CASSCF/cc-pVTZ [c]	93	230	246	454	502	716	831	884	1439	1598	2013	5035
CCSD/6-311+G(d,p) [a]	49	288	353	480	548	631	793	862	1347	1445	1837	1871
CCSD(T)/cc-pVDZ [c]	95	232	278	434	495	677	759	820	1301	1414	1803	1834
CCSD(T)/aug-cc-pVDZ [c]	80	222	273	429	463	677	737	804	1273	1389	1741	1788
CCSD(T)/cc-pVTZ [c]	92	249	302	454	512	711	763	829	1288	1398	1782	1813
Exp. [d]				441	484	707	776	826	1294	1413	1777	1818
Exp. [e]	82	265	282	428	480	676	751	812	1261	1383	1724	1757

[a]: this work; [b]: reference (29); [c]: reference (17); [d]: Harmonic frequencies, reference (35); [e]: Fundamental frequencies, reference (35)

Table3-12: Calculated (B3LYP) and Experimental Vibrational Frequencies (in cm^{-1}) of cis-$ONONO_2$.

	cis-$ONONO_2$	cis-$ONONO_2$_2			cis-$ONONO_2$_3			
	B3LYP/ 6-311++G(3df,2p)[a]	B3LYP/ 6-311++G(3df,2p) [a]	MP2/ 6-31G* [b]	MP2/ 6-311G* [b]	B3LYP/ 6-311++G(3df,2p) [a]	B3LYP/ 6-31G(d) [c]	MP2/ 6-31G(d) [c]	Exp. [d]
NO_2 torsion	73	39	52.6	48.4	34i	55i	90i	
NO torsion	135	188	176.7	174.5	168	169	145	
NO_2 rock	179	205	221.3	216.5	202	206	250	
O-N(O) str	285	294	337.2	336.1	278	270	286	304
N-O-N bend	542	601	604.9	616.9	590	588	674	488
NO_2 wag	564	623	638.2	662.1	654	620	802	641
O=N-O bend	693	748	729.2	745.4	761	769	902	
NO_2 bend	862	823	785	799	798	791	965	783
O-N(O_2) str	909	876	871	888.5	892	872	1055	905
NO_2 s-str	1360	1312	1298.1	1301.9	1310	1338	1568	1290
NO_2 a-str	1683	1667	1832.5	1826.8	1649	1722	1950	1645
NO str [e]	1845	1989	1919.3	1959.8	2038	1986	2165	1829

[a]: this work; [b]: reference (36); [c]: reference (16); [d]: reference (37); [e]: the assignment of frequencies is from reference (36)

Table3-13: Calculated Vibrational Frequencies (in cm^{-1}) of the cis-$ONONO_2$ and cis-$ONONO_2$_2 structures.

	cis-$ONONO_2$				cis-$ONONO_2$_2		
	B3LYP/ 6-311++G(3df,2p)	PW91PW91/ 6-311++G(3df,2p)	BHandHLYP/ 6-311++G(3df,2p)	CCSD/ 6-311+G(d,p)	B3LYP/ 6-311++G(3df,2p)	PW91PW91/ 6-311++G(3df,2p)	Exp. [a]
NO_2 torsion	73	48	36	43	39	39	
NO torsion	135	159	212	218	188	175	
NO_2 rock	179	179	270	236	205	220	
O-N(O) str	285	205	375	343	294	280	304
N-O-N bend	542	404	637	601	601	537	488
NO_2 wag	564	475	647	625	623	579	641
O=N-O bend	693	747	794	759	748	700	
NO_2 bend	862	817	926	883	823	789	783
O-N(O_2) str	909	1249	987	917	876	813	905
NO_2 s-str	1360	1359	1445	1373	1312	1265	1290
NO_2 a-str	1683	1519	1855	1779	1667	1637	1645
NO str [e]	1845	1792	1930	1853	1989	1878	1829

[a]: reference (37)

Table3-14: Calculated Vibrational Frequencies (in cm^{-1}) of the cis-$ONONO_2$_3 structures.

	cis-$ONONO_2$_3			
	B3LYP/ 6-311++G(3df,2p)	PW91PW91/ 6-311++G(3df,2p)	BHandHLYP/ 6-311++G(3df,2p)	CCSD/ 6-311+G(d,p)
NO_2 torsion	34i	32i	52i	71i
NO torsion	168	181	152	126
NO_2 rock	202	186	228	222
O-N(O) str	278	266	268	263
N-O-N bend	590	562	633	608
NO_2 wag	654	590	738	699
O=N-O bend	761	717	836	787
NO_2 bend	798	762	864	794
O-N(O_2) str	892	832	1001	929
NO_2 s-str	1310	1258	1425	1358
NO_2 a-str	1649	1600	1758	1708
NO str [e]	2038	1943	2163	2023

Table3-15: Computational and Experimental Vibrational Frequencies (in cm^{-1}) of trans-$ONONO_2$.[g]

	B3LYP/ 6-311++G(3df,2p) [a]	PW91PW91/ 6-311++G(3df,2p) [a]	BHandHLYP/ 6-311++G(3df,2p) [a]	CCSD/ 6-311+G(d,p) [a]	MP2/ 6-31G* [b]	MP2/ 6-311G* [b]	B3LYP/ 6-31G(d) [c]	MP2/ 6-31G(d) [c]	Exp. [d]	Exp. [d]	Exp. [e]
NO_2 torsion	88	26	32i	84	43.6	64.4	29	31i			
NO torsion	131	135	144	130	116.3	113	140	123			
NO_2 rock	209	191	252	252	215.1	220.6	214	205			
O-N(O) str	294	289	320	349	316.1	319.4	322	310	304		310
N-O-N bend	486	424	552	545	497.1	517.6	477	489	524	564	489
O=N-O bend	647	582	745	683	633.4	653.8	636	636	660	679	636
NO_2 wag	786	746	849	774	745.3	761.4	760	751	794	782	778
NO_2 bend	801	766	863	847	783	810.6	797	778			
O-N(O_2) str	945	895	1054	990	925	933.8	954	926	916	882	926
NO_2 s-str	1330	1287	1444	1377	1312.8	1313.7	1353	1315	1290	1280	1315
NO_2 a-str	1709	1686	1827	1765	1845.5	1863.9	1769	1839	1584	1576	1839
NO str [f]	1934	1850	2002	1898	1868.8	1895.5	1906	1871	1899-1889	1961	1871

[a]: this work; [b]: reference (36); [c]: reference (16); [d]: reference (37); [e]: bands observed at liquid-helium temperature in oxygen matrix, reference (38); [e]: reference (39); [f]: the assignment of frequencies is from reference (36); [g]: the trans-$ONONO_2$ geometries of different are different, which depend on the optimized methods.

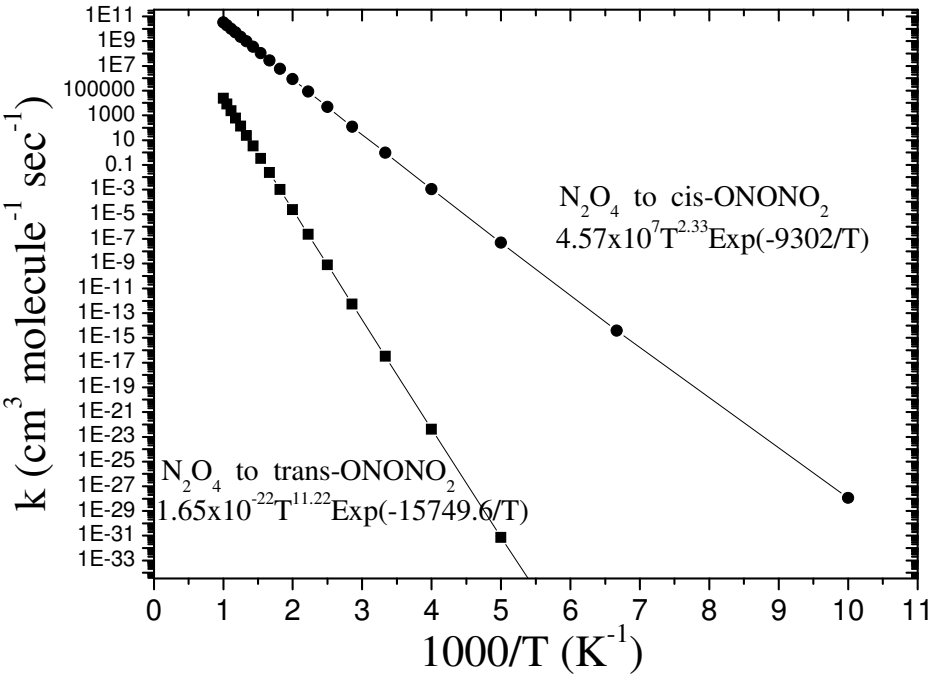

Fig3-6: Arrhenius plots and three-parameters fitting expressions for the rate constants. (a) The faster reaction is N_2O_4 to cis-$ONONO_2$ via i-TS2, and the lower one is N_2O_4 to trans-$ONONO_2$ via i-TS1.

3.3 N_2H_4+N_2O_4 reaction

In the 3.2 section, we have discussed the properties of the three isomers, including $N_2O_4(D_{2h})$, trans-$ONONO_2(C_s)$, and cis-$ONONO_2(C_s)$ molecules. Since under real experimental conditions the combustion reaction may produce these molecules to react with the N_2H_4 molecule, the PES of N_2H_4+trans-$ONONO_2$, N_2H_4+cis-$ONONO_2$, and N_2H_4+$N_2O_4(D_{2h})$ reactions should be considered. Even though these reactions are complex, which contain four nitrogen atoms, four oxygen atoms, and four hydrogen atoms, fortunately, all of the dimer reactions are on their singlet surface without spin-contamination problems unlike the monomer reaction, N_2H_4+NO_2.

3.3.1 N_2H_4 + trans-$ONONO_2$ reaction and N_2H_4 + cis-$ONONO_2$ reaction

In this section, we consider the reaction of N_2H_4 + trans-$ONONO_2$ and cis-$ONONO_2$ molecules. The geometries of stationary points, such as reactants, intermediates, transition states, and products, in the reactions are computed by the B3LYP/ 6-311++G(3df,2p) method, as shown in Fig3-7. The single-point energies for the full potential energy surface, as presented in Fig.3-8, are calculated by G2M(CC3) instead of G2M(CC1) due to the larger number of atoms in this system. Since the trans-$ONONO_2$ and cis-$ONONO_2$ are of C_s symmetry, we make the notations of C_s-Complexes and C_s-TSs in the PES for clarity. Moreover, in order to compare the PES of N_2H_4 + $N_2O_4(D_{2h})$ reaction more easily, the energy of the most stable reactants, N_2H_4 + $N_2O_4(D_{2h})$, is taken as the reference energy in these reactions. The moments of inertia and vibrational frequencies are listed in Table3-16, and the energies of all species obtained by different computational methods are shown in Table3-17.

The N_2H_4 + trans-$ONONO_2$ reaction provides the lowest-energy path in all of N_2H_4+N_2O_4 reactions. In the beginning, trans-$ONONO_2$ forms an intermediate, C_s-complex1,

with N_2H_4 molecule, as shown in Fig3-7. In order to form hydrogen bonds and decrease the energy, the N-N bond of N_2H_4 twists to make two hydrogen atoms upward to terminal oxygen atom of trans-$ONONO_2$. Furthermore, as we discussed the trans-$ONONO_2$ molecule in the previous section, the bond length of ON-ONO_2 is 1.621Å, and the ON group has a positive charge distribution, whereas the ONO_2 group has a negative electron distribution. These special properties make the ON-ONO_2 bond in C_s-complex1 to be much longer than the individual molecule by 0.661Å, but the ON group still connects with the ONO_2 group. On the other hand, the attraction of ONO_2 makes the N-H bond longer than that in N_2H_4 by 0.06Å. Therefore, C_s-Complex1 has a lower energy than the reactants, N_2H_4 + trans-$ONONO_2$. C_s-TS1 is a six-member ring structure, and the ring is composed of the N-O-N-O atoms of trans-$ONONO_2$, (in which the first N belongs to the NO group,) and the N-H atoms of N_2H_4. The major motion of TS is that the ON group breaks the connection with ONO_2 and forms an N-N bond with N_2H_3, and the bonding hydrogen atom transfers to ONO_2 group to form a stable nitric acid. The two doublet radicals, N_2H_3 and NO, are unstable, and the unpair electrons would prefer to decrease energy by forming the $H_2NN(H)NO$ molecule, which is stable and the process is exothermic. This molecule may decompose into many small reactive molecules, and we will discuss this decomposition reaction in the next section. Moreover, it is well-known that nitric acid, $HONO_2$, may decompose into NO_2 gas at high temperature, and the products from the decomposition of nitric acid, OH+NO_2, may react further and release more energy. The dihedral angle [O-N-O-N]O_2 is 160.1° and 154.8° for C_s-Complex1 and C_s-TS1, respectively, and the other angles and dihedral angles are similar. However, it is unreasonable that the energy of C_s-Complex1 is higher than C_s-TS1 by 1.17, 2.89, and 2.66 kcal/mol by the B3LYP/6-311++G(3dr,2p), CCSD(T)/6-311+G(3df,2p), G2M(CC3) methods, respectively, as shown in Table3-17. However, the electronic energy of C_s-complex1 is lower than C_s-TS1 by 0.17 kcal/mol, and the result of IRC calculation also confirms that the energy

difference is only 0.00027 hartrees, as shown in Fig3-9. The zero-point energy (ZPE) of the C_s-complex1 is higher than that of the C_s-TS1 by 1.30 kcal/mol; therefore, we believe that the fact that the energy of the C_s-complex1 is higher than that of the C_sTS1 arises from the zero-point energy correction and computational errors. In addition, the free energy with ZPE correlation of the C_s-complex1 is higher than that of C_s-TS1 by 0.78 kcal/mol computed at B3LYP/6-311++G(3df,2p). Since the DFT calculations may have larger error in the geometry predictions than CCSD(T), the single-point calculation error would be increased based on the DFT geometries. Moreover, these structures on the major channel can be reoptimized by PW91PW91/6-311++G(3df,2p), and the geometries are similar with the results optimized by B3LYP, as presented in Fig.3-7. The moments of inertia and the frequencies are shown in Table3-18, and the relative energies are listed in Table3-19. The PW91PW91 results in energy have the same trend as these by B3LYP calculation, in which the electronic energy with ZPE correction of the C_s-TS1 is lower than that of C_s-Complex1 by 1.11 kcal/mol. However, the zero-point energy of the C_s-complex1 is higher than that of the C_s-TS1 by 2.4 kcal/mol optimized by PW91PW91/6-311++G(3df,2p). Therefore, this phenomenon arises from the zero-point energy correction and computational errors similar to those computed by B3LYP. The PESs of major channel in the trans-$ONONO_2$ + N_2H_4 reaction optimized by B3LYP/6-311++G(3df,2p) and PW91PW91/ 6-311++G(3df,2p) are shown in the Fig. 3-9. After all, the reaction of the major channel starts from the formation of C_s-complex1, and the barrierless hydrogen transfer via C_s-TS1 will react very fast kinetically. In order to get the correct relative energy, it may need a higher level of theory to optimize the geometries, such as the CCSD method.

In the N_2H_4 + cis-$ONONO_2$ reaction, there is one similar reaction path as N_2H_4 + trans-$ONONO_2$ reaction. The physical attraction and hydrogen bonding make N_2H_4 and cis-$ONONO_2$ form an intermediate, C_s-Complex3, and the structures of two molecules do not

change much comparing with the structures of individual molecules, as shown in Fig3-7. The longest and weakest ONO-NO_2 bond only elongates 0.02Å, and the nearest distance between two molecules is 2.97Å for the bonding oxygen atom to the bonding hydrogen atom. That means the interaction between them is smaller than the situation in C_s-Complex1, and the energy of C_s-Complex3 is lower than N_2H_4+cis-$ONONO_2$ by 3.85 kcal/mol at the G2M(CC3) level. C_s-TS2 is a four-member ring structure, as shown in Fig. 3-7. In C_s-TS2, the N_2H_4 structure is similar to that in the C_s-Complex1 and C_s-TS1, and it rotates along the N-N bond to make two hydrogen atoms upward to the oxygen atom of NO_2. After moving over C_s-TS2, the ONO-NO_2 bond breaks and one hydrogen atom transfer from N_2H_4 to the oxygen atom of the ONO group. This exothermic reaction produces the $H_2NN(H)NO_2$ molecule and nitrous acid, trans-HONO, which is the same products in the N_2H_4+NO_2 reaction. However, the energy barrier of four-member ring, C_s-TS2, is as high as 20.07 and 14.4 kcal/mol with respect to reference point and C_s-Complex3. Therefore, it is kinetically more difficult to react, comparing with the lowest-energy channel of N_2H_4 + trans-$ONONO_2$ reaction. For hydrogen transfer reactions involving cis-$ONONO_2$ and trans-$ONONO_2$, we notice that the weakest bond breaks as the reaction occurs. If we choose cis-$ONONO_2$_2 as the cis-reactant, then it would have similar transition states and products as those in the trans-$ONONO_2$+N_2H_4 reaction. Therefore, it is reasonable to not consider the other two possible structures in cis-isomer reacting with N_2H_4. On the other hand, the imaginary frequencies of the two hydrogen transfer reaction are very small comparing the simple conventional hydrogen transfer reaction, whose value is around 1200 to 1500 1/cm, and it might be affected by other bonding or breaking motions in the ring of transition states. The effect of hydrogen bond is another important factor that affects the motion on the coordinate of reaction path.

The other two reaction channels of the N_2H_4 + cis-$ONONO_2$ reaction have similar reaction mechanisms, but the cis-$ONONO_2$ is in a different position related to the N_2H_4

molecule in the C_s-TS3 and C_s-TS5. These two reactions are originated from the C_s-Complex3, and they break the O-N bond to form the C_s-Complex5 and C_s-Complex7 via the C_s-TS3 and C_s-TS5, respectively. The C_s-TS3 and C_s-TS5 geometries show that the NO group of cis-$ONONO_2$ is on the top of the N_2H_4 molecule, and the ONO_2 group is in the middle of the N_2H_4 molecule and the NO group, which is like a sandwich structure, as shown in Fig3-7. The NO_2 group is tilted in both structures of C_s-TS3 and C_s-TS5, and the lower position of oxygen atom is on the inner side and outer side of N_2H_4 for C_s-TS3 and C_s-TS5, respectively. The N_2H_4 molecules in the C_s-TS3 and C_s-TS5 have the similar geometries as those in C_s-TS1 and C_s-TS2, where the two hydrogen atoms of N_2H_4 turn upward to form the hydrogen bonds and thus decrease the system energy. In section3.1, the highest-energy path of the N_2H_4+NO_2 reaction has the same mechanism as the reaction channels through C_s-TS3 and C_s-TS5, and all of them have very high energy barriers. The NO_2 group is near and far away from the oxygen atom of $H_2NN(O)H_2$ in C_s-Complex5 and C_s-Complex7, respectively, due to the origins from the different geometries of transition states. Therefore, the C_s-Complex5 undergoes the hydrogen transfer reaction via C_s-TS4, which abstracts one hydrogen from the nitrogen connecting with oxygen in the $H_2NN(O)H_2$ moiety, giving C_s-Complex6 which is composed of trans-HONO and $H_2NN(H)ONO$ molecules. On the other hand, the NO_2 group of C_s-Complex7 can also undergo a hydrogen transfer reaction from the nitrogen atom, which does not connect with oxygen in $H_2NN(O)H_2$ molecule, to produce trans-HONO + $H_2NN(H)ONO$. Finally, the C_s-Complex8, including a trans-HONO, a cis-HONO, and a cis-N_2H_2 molecule, form through C_s-TS6. However, even these two paths produces many exothermic products, but the mechanism, breaking N-O bond of NO_2 and forming N-O bond to N_2H_4 without hydrogen transfer, seems very difficult to occur comparing with other hydrogen-transfer channel, and it has the consistent results in both monomer and dimer reactions.

In Table3-17, comparing with the single-point energies between CCSD(T)/6-311+G(d,p) and G2M(CC3) methods, it is apparent that most of the energies calculated by G2M(CC3) is lower than those by the CCSD(T) method, but they have the similar energy differences between the intermediates and transition states in the same reaction channels. Such as the channel of hydrogen transfer in the N_2H_4+cis-$ONONO_2$, the energy barrier is 24.32 and 24.6 kcal/mol predicted by G2M(CC3) and CCSD(T)/6-311+G(d,p) methods, respectively. According to the heat of reaction, which is calculated by the heat of formation in experimental data[23], the value of G2M(CC3) is very close to the experimental result similar to the monomer reaction. However, the difference between CCSD(T)/ 6-311+G(d,p) and experimental value is 2.46 kcal/mol, which means that the smaller basis set in CCSD(T) calculations may be incorrect and unreliable.

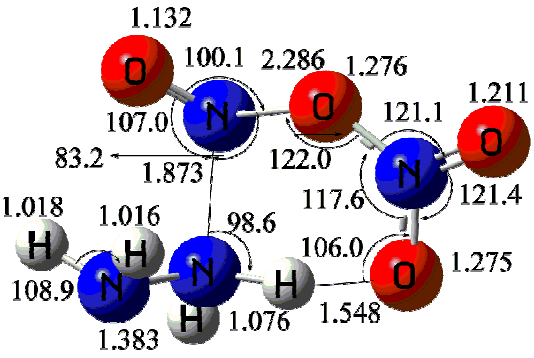

C_s-Complex1 (C_1)

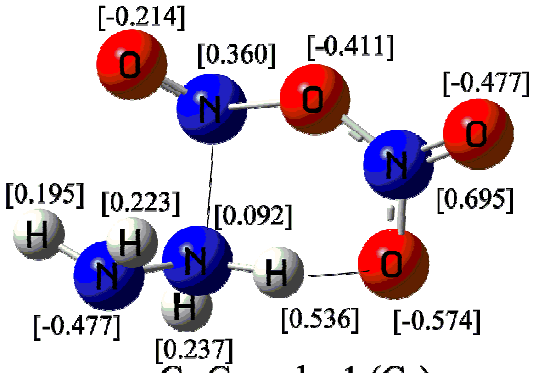

C_s-Complex1 (C_1)

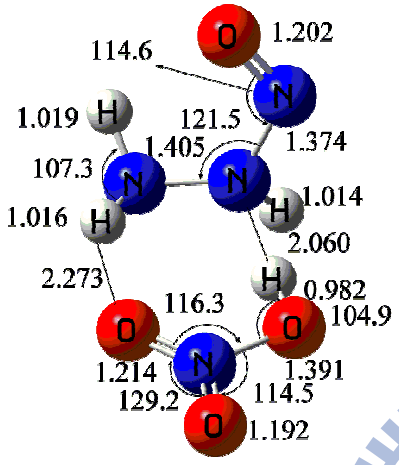

C_s-Complex2 (C_1)

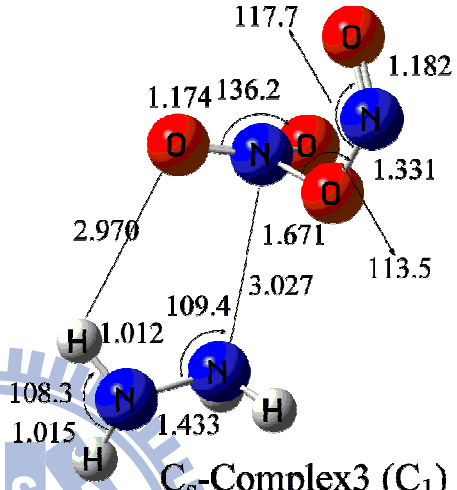

C_s-Complex3 (C_1)

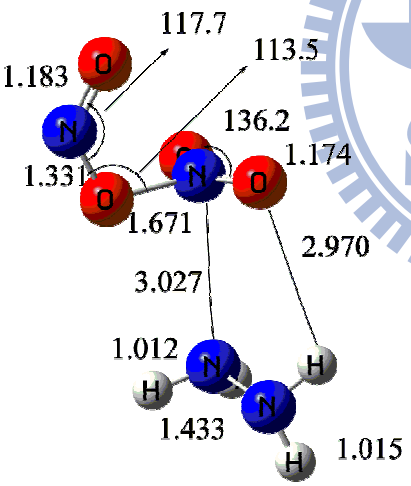

Cs-Complex3 (C_1)

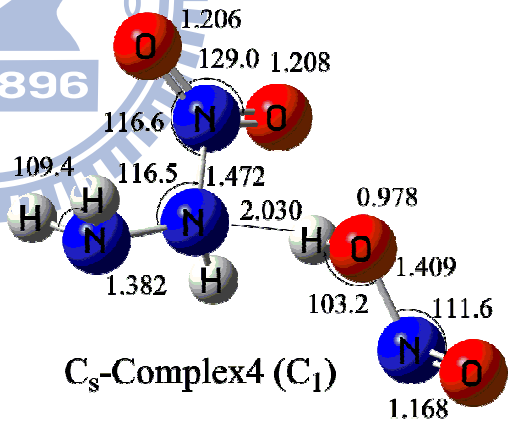

C_s-Complex4 (C_1)

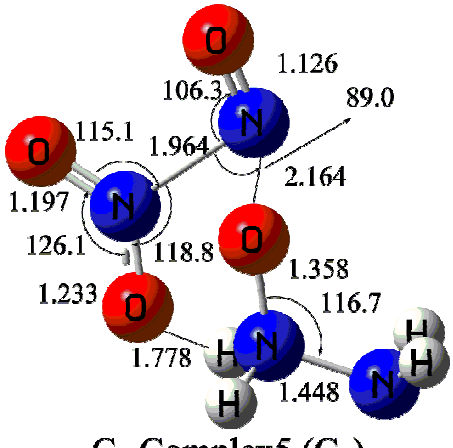

C_s-Complex5 (C_1)

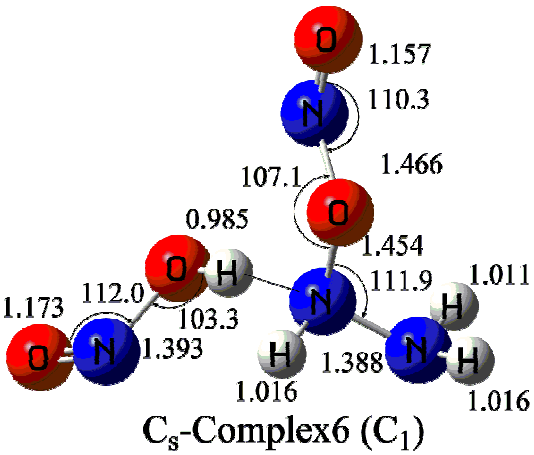

C_s-Complex6 (C_1)

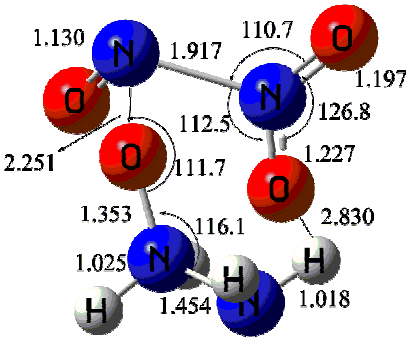

C_s-Complex7 (C_1)

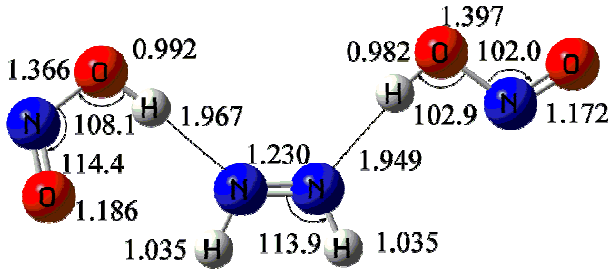

C_s-Complex8 (C_1)

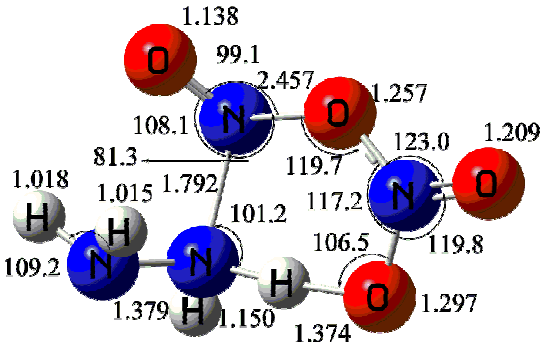

C_s-TS1 (C_1)

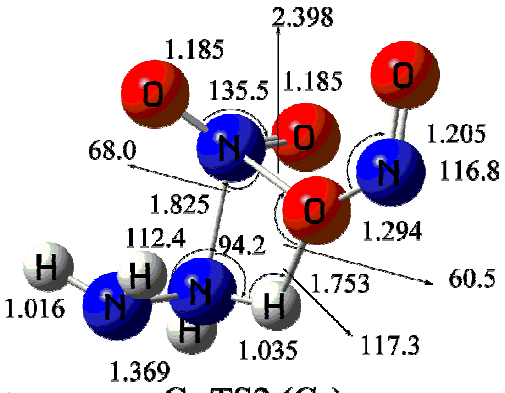

C_s-TS2 (C_1)

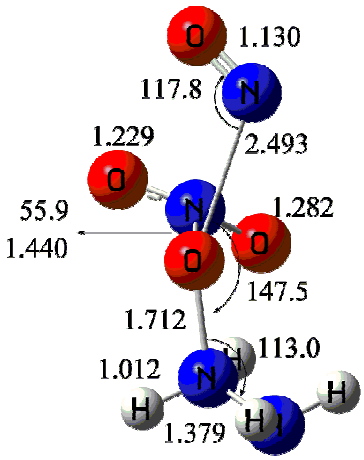

C_s-TS3 (C_1)

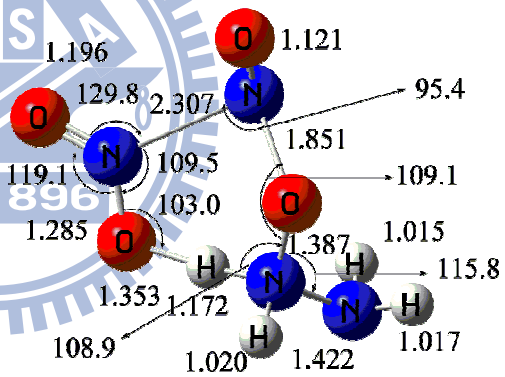

C_s-TS4 (C_1)

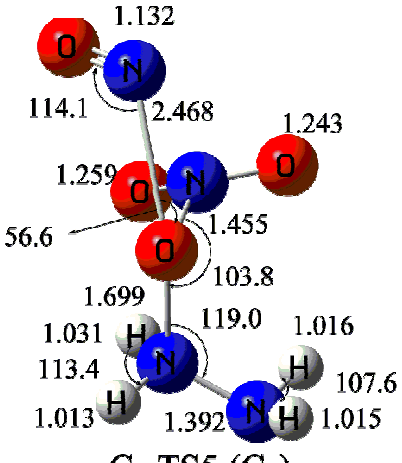

C_s-TS5 (C_1)

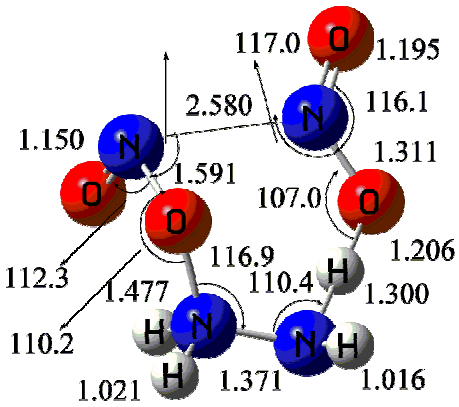

C_s-TS6 (C_1)

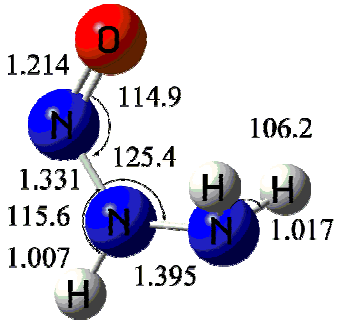

$H_2NN(H)NO$ (C_s)

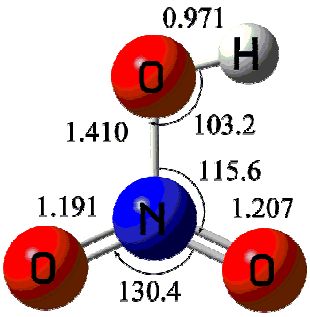

$HONO_2$ (C_s)

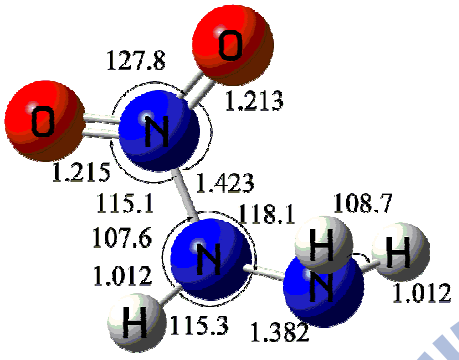

$H_2NN(H)NO_2$ (C_1)

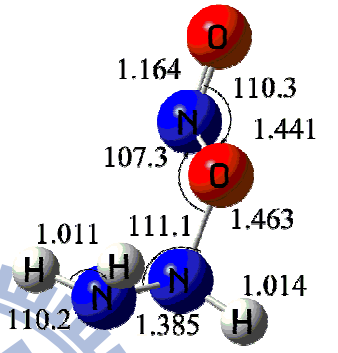

$H_2NN(H)ONO$ (C_1)

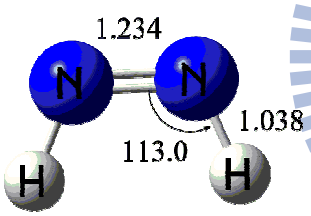

cis-N_2H_2 (C_{2v})

(a)

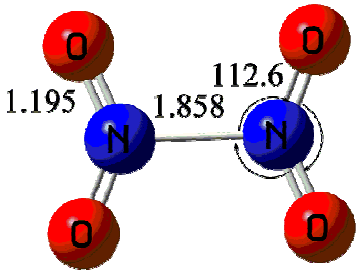

N_2O_4_PW91PW91 (D_{2h})

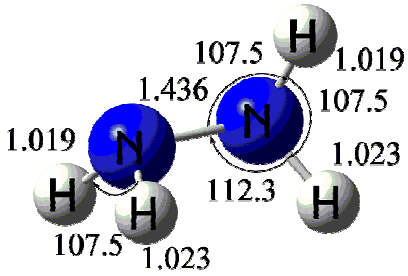

N_2H_4_PW91PW91 (C_2)

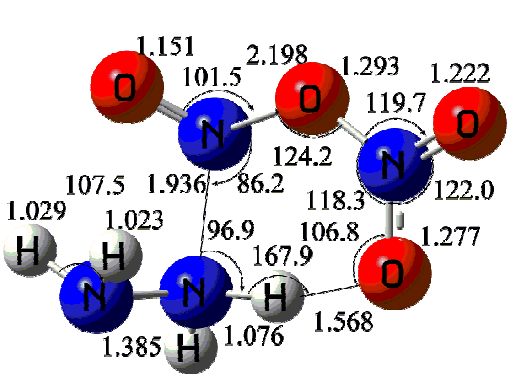

Cs-Complex1_PW91PW91 (C_1)

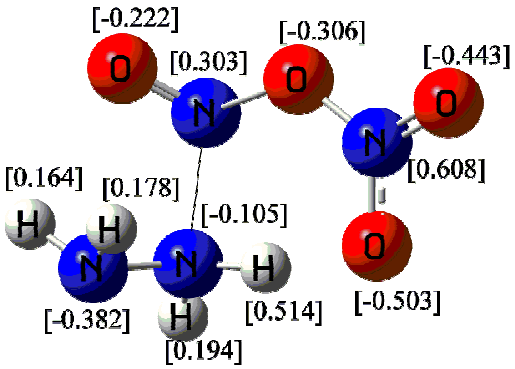

C_s-Complex1_PW91PW91 (C_1)

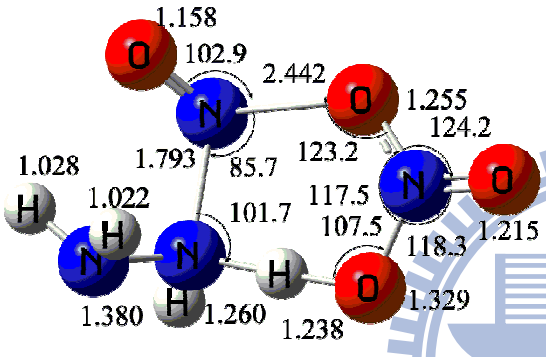

C_s-TS1_PW91PW91 (C_1)

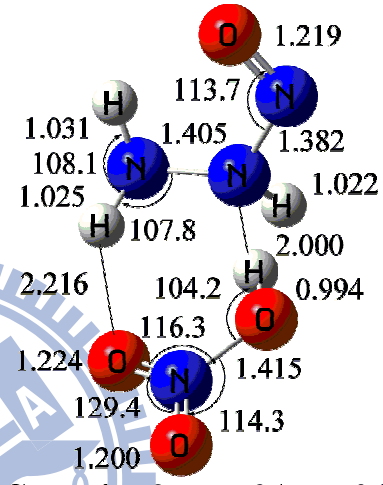

C_s-Complex2_PW91PW91 (C_1)

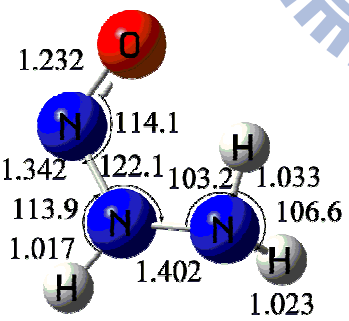

$H_2NN(H)NO$_PW91PW91 (C_1)

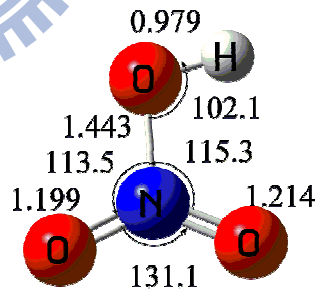

$HONO_2$_PW91PW91 (C_1)

(b)

Fig3-7: (a) The stationary points in the PES of trans-$ONONO_2$ + N_2H_4 reaction and cis-$ONONO_2$ + N_2H_4 reaction are optimized by B3LYP/6-311++G(3df,2p), and (b) the stationary points on the major channel of trans-$ONONO_2$ + N_2H_4 reaction optimized by PW91PW91 /6-311++G(3df,2p).

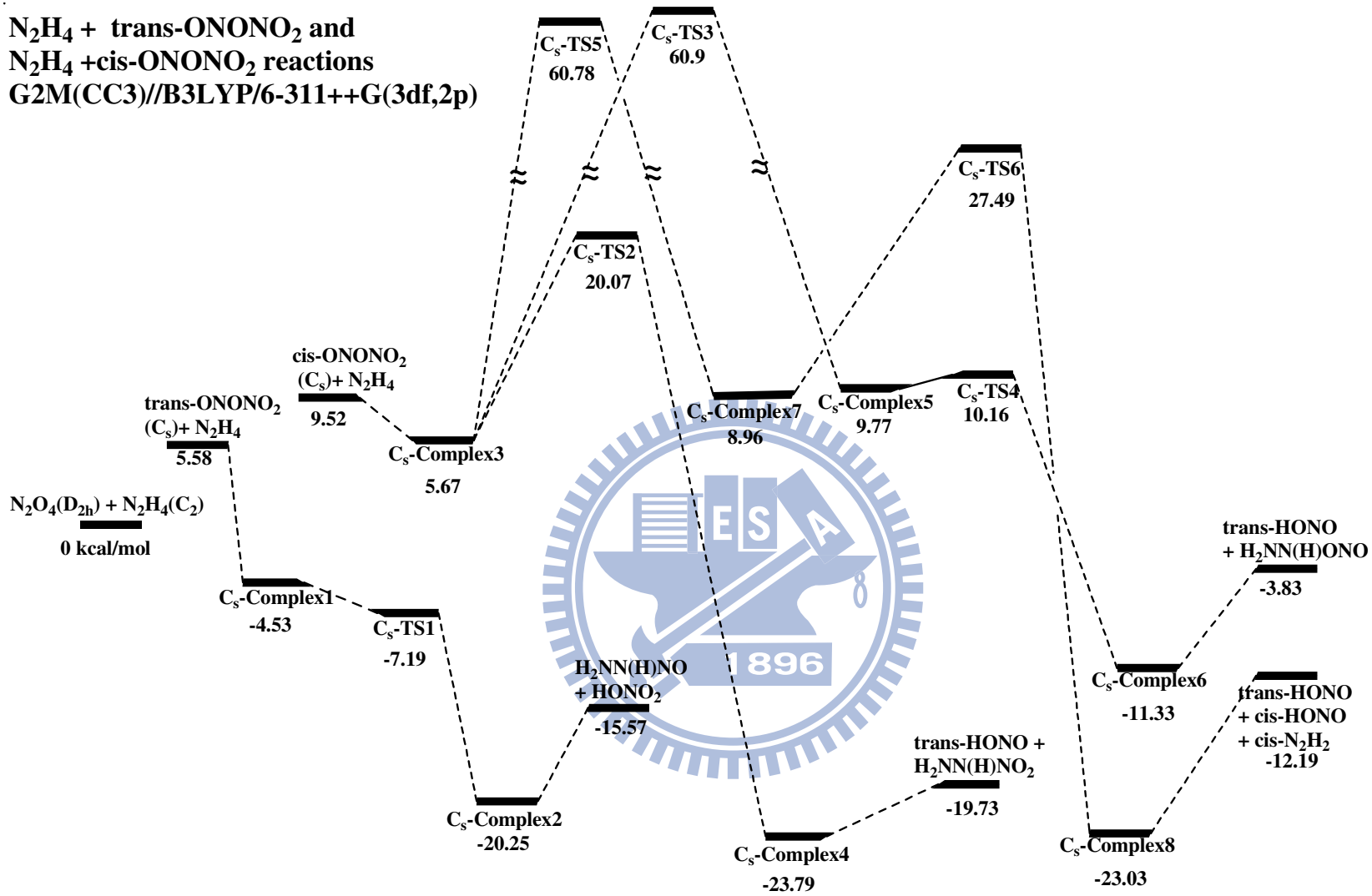

Fig3-8: Potential Energy Surface of trans-$ONONO_2$ + N_2H_4 reaction and cis-$ONONO_2$ + N_2H_4 reactions, whose energies are calculated by G2M(CC3) // B3LYP/6-311++G(3df,2p).

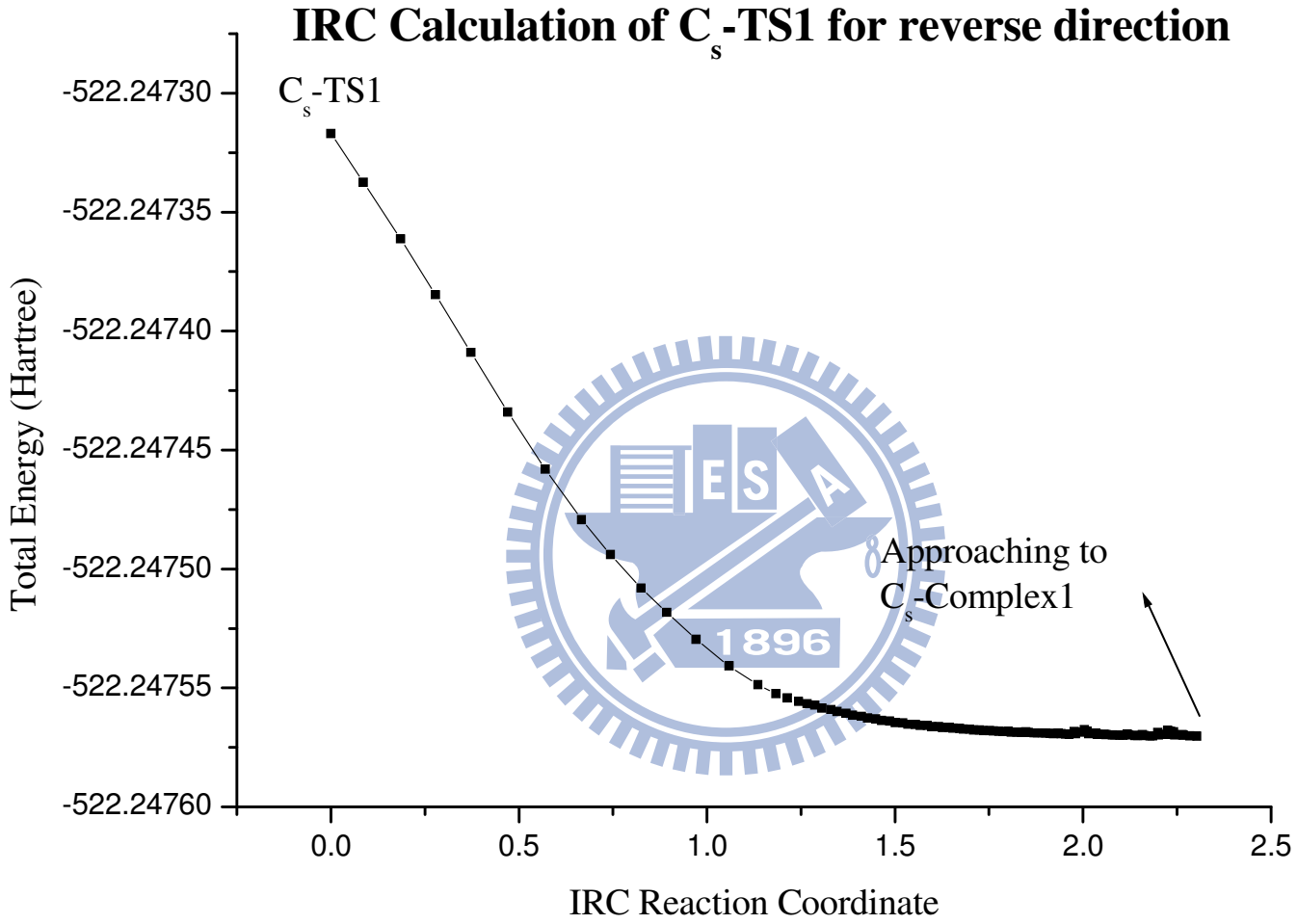

Fig3-9: The IRC calculation of C_s-TS1 is determined by B3LYP/6-311++G(3df,2p) for reverse direction. The highest point is the position of C_s-TS1, and the lowest point is approaching to the C_s-Complex1. The energy difference is 0.00027 Hartree (0.17 kcal/mol).

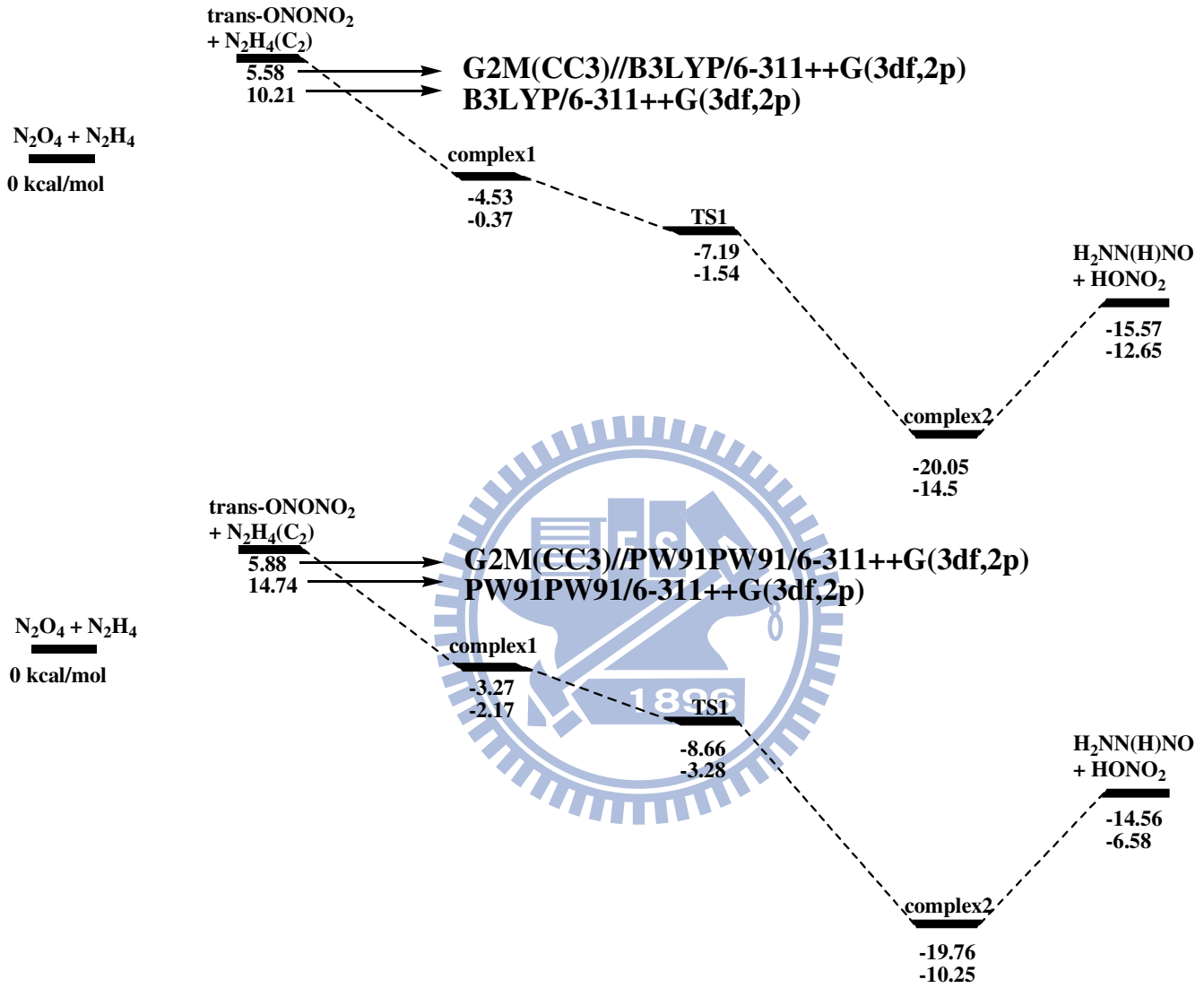

Fig3-10: The comparison for the major channel of trans-$ONONO_2$ + N_2H_4 reaction optimized by B3LYP/6-311++G(3df,2p) and PW91PW91/ 6-311++G(3df,2p).

Table3-16: Moments of inertia (I_A, I_B, I_C) and vibration frequencies of the species in trans-$ONONO_2$ + N_2H_4 and cis-$ONONO_2$ + N_2H_4 reactions computed at B3LYP/6-311++G(3df,2p).

Species or Transition States	Moments of inertia I_i(a.u)	Vibrational Frequency υ_j (cm^{-1})
N_2O_4	273.2, 500.4, 773.7	87, 222, 293, 446, 490, 704, 760, 850, 1307, 1450, 1787, 1826
trans-$ONONO_2$	151.2, 773.8, 925.0	9, 131, 209, 294, 486, 647, 786, 801, 945, 1330, 1709, 1934
cis-$ONONO_2$	244.9, 605.7, 632.1	73, 135, 179, 285, 542, 564, 693, 862, 909, 1360, 1683, 1845
N_2H_4	12.4, 74.2, 74.3	439, 801, 974, 1114, 1294, 1323, 1674, 1686, 3462, 3471, 3562, 3568
C_s-Complex1	508.6, 1412.0, 1695.8	48, 64, 101, 135, 205, 240, 262, 301, 324, 405, 665, 712, 727, 822, 833, 899, 1057, 1153, 1190, 1242, 1299, 1455, 1544, 1660, 1707, 1886, 2481, 3445, 3510, 3551
C_s-Complex2	439.1, 2040.2, 2195.3	22, 41, 85, 106, 110, 134, 204, 345, 455, 584, 616, 675, 794, 853, 909, 928, 988, 1196, 1333, 1351, 1397, 1411, 1617, 1690, 1746, 3449, 3494, 3523, 3539
C_s-Complex3	484.4, 1854.4, 1965.1	24, 39, 43, 64, 92, 120, 130, 172, 246, 283, 450, 538, 551, 714, 814, 878, 912, 989, 1115, 1297, 1327, 1364, 1656, 1675, 1687, 1867, 3458, 3472, 3557, 3568
C_s-Complex4	485.2, 2398.5, 2638.5	17, 29, 49, 71, 109, 137, 216, 319, 354, 482, 613, 663, 776, 800, 805, 834, 857, 988, 1223, 1311, 1365, 1399, 1441, 1694, 1705, 1763, 3481, 3518, 3559, 3588
C_s-Complex5	615.6, 1318.9, 1727.1	51, 62, 103, 142, 169, 186, 214, 285, 302, 385, 465, 507, 622, 823, 876, 1005, 1019, 1169, 1309, 1338, 1451, 1489, 1619, 1669, 1688, 1931, 3035, 3376, 3465, 3543
C_s-Complex6	666.8, 1856.0, 2280.3	35, 56, 74, 94, 152, 164, 166, 201, 342, 427, 506, 540, 635, 698, 825, 864, 892, 964, 1069, 1188, 1348, 1461, 1497, 1687, 1749, 1797, 3415, 3468, 3509, 3578
C_s-Complex7	722.8, 1126.3, 1485.2	21, 47, 76, 117, 158, 211, 241, 260, 307, 330, 474, 490, 651, 824, 866, 998, 1010, 1175, 1304, 1342, 1446, 1487, 1602, 1651, 1681, 1902, 3173, 3360, 3460, 3538
C_s-Complex8	299.3, 4559.1, 4857.4	10, 18, 20, 54, 61, 71, 134, 138, 180, 186, 542, 297, 684, 685, 862, 873, 908, 949,

		1277, 1350, 1427, 1444, 1546, 1680, 1682, 1753, 3199, 3260, 3340, 3494
C_s-TS1	492.1, 1449.5, 1727.3	224i, 38, 67, 140, 173, 239, 257, 288, 319, 440, 681, 712, 730, 830, 838, 882, 995, 1087, 1188, 1231, 1409, 1497, 1569, 1606, 1696, 1736, 1872, 3452, 3490, 3557
C_s-TS2	660.0, 1301.4, 1608.6	184i, 29, 59, 94, 121, 200, 233, 241, 278, 382, 454, 521, 766, 817, 854, 900, 1031, 1124, 1194, 1237, 1309, 1469, 1533, 1559, 1676, 1794, 3178, 3449, 3504, 3556
C_s-TS3	434.3, 1522.1, 1651.2	773i, 69, 83, 99, 183, 202, 236, 261, 283, 310, 512, 590, 644, 741, 774, 843, 908, 1012, 1124, 1207, 1216, 1408, 1466, 1635, 1695, 1928, 3013, 3478, 3561, 3576
C_s-TS4	791.8, 1144.0, 1804.4	427i, 58, 81, 145, 158, 195, 232, 250, 293, 358, 451, 498, 620, 787, 843, 899, 990, 1097, 1175, 1283, 1375, 1475, 1592, 1672, 1687, 1750, 1957, 3435, 3471, 3556
C_s-TS5	422.1, 1464.3, 1550.0	779i, 43, 66, 105, 159, 177, 233, 247, 301, 344, 496, 539, 637, 738, 757, 868, 923, 1063, 1149, 1172, 1197, 1389, 1469, 1624, 1701, 1918, 3274, 3482, 3557, 3576
C_s-TS6	681.6, 1171.9, 1623.1	1061i, 59, 92, 120, 135, 193, 240, 281, 324, 417, 459, 521, 652, 711, 796, 863, 1020, 1079, 1153, 1293, 1387, 1417, 1541, 1600, 1634, 1728, 1783, 3319, 3427, 3506
$HONO_2$	137.8, 149.0, 286.8	493, 589, 655, 787, 904, 1325, 1350, 1756, 3734
$H_2NN(H)NO$	79.4, 271.1, 340.5	151, 212, 332, 583, 674, 901, 978, 1168, 1285, 1433, 1630, 1672, 3504, 3567, 3600
$H_2NN(H)NO_2$	155.4, 34.6, 534.8	173, 313, 330, 499, 591, 790, 795, 852, 976, 1236, 1315, 1367, 1430, 1663, 1705, 3471, 3562, 3576
$H_2NN(H)ONO$	80.4, 672.2, 687.1	96, 187, 323, 438, 501, 555, 612, 832, 967, 1042, 1189, 1335, 1504, 1687, 1766, 3453, 3515, 3584
cis-N_2H_2	6.1, 45.6, 51.8	1281, 1361, 1555, 1651, 3102, 3195
trans-HONO	19.0, 143.1, 162.1	590, 621, 819, 1303, 1783, 3773
cis-HONO	21.1, 135.9, 157.0	635, 695, 876, 1342, 1716, 3597

Table3-17: Relative energies of species in trans-$ONONO_2$ + N_2H_4 reaction and cis-$ONONO_2$ + N_2H_4 reaction predicted at various theoretical levels. [a]

	ZPE [b]	B3LYP/ 6-311++G(3df,2p) [c]	CCSD(T)/ 6-311+G(d,p) [c]	G2M(CC3)
N_2O_4 + N_2H_4	48.02	-522.173728	-520.93814	-521.3804132
trans-$ONONO_2$ + N_2H_4	46.67	10.21	6.1	5.85
cis-$ONONO_2$ + N_2H_4	46.46	12.51	9.63	9.52
complex1	48.45	-0.37	-3.07	-4.53
complex2	49.09	-14.5	-18.75	-20.25
complex3	47.28	10.9	5.3	5.67
complex4	48.84	-17.24	-23.89	-23.79
complex5	49.03	13.11	9.51	9.77
complex6	47.75	-1.98	-13.27	-11.33
complex7	48.9	16.93	11.8	8.96
complex8	45.5	-13.72	-25.96	-23.03
H2NN(H)NO + $HONO_2$	47.88	-12.65	-13.95	-15.57
H2NN(H)NO_2 + trans-HONO	47.93	-15.26	-19	-19.73
H_2NN(H)-ONO + trans-HONO	46.42	3.31	-5.39	-3.83
trans-HONO + cis-HONO + cis-N2H2	42.73	-4.5	-14.72	-12.19 (-12.26) [d]
TS1	47.12	-1.54	-5.96	-7.19
TS2	47.98	21.52	21.25	20.07
TS3	47.26	66.98	62.27	60.9
TS4	46.29	13.15	9.02	10.16
TS5	47.47	67.26	64.06	60.78
TS6	45.39	33.33	28.36	27.49

[a]: The relative energy (kcal/mol) is calculated with the energy of N_2O_4 (D_{2h})+N_2H_4 as reference, whose total energy unit is hartree/molecule.

[b]: The ZPE is determined by B3LYP/6-311++G(3df,2p) level, and the energy unit is kcal/mol for every species.

[c]: The energies are including single-point energies, based on geometries of B3LYP/6-311++G(3df,2p), and ZPE.

[d]:The heat of reaction in the experimental result is calculated by species of the reactants and products, whose heat of formation are from the reference (23).

Table3-18: Moments of inertia (I_A, I_B, I_C) and vibration frequencies of the species in the major channel of trans-$ONONO_2$ + N_2H_4 reaction computed at PW91PW91/6-311++G(3df,2p).

Species or Transition States	Moments of inertia I_i(a.u)	Vibrational Frequency $_j$ (cm^{-1})
N_2H_4_PW91PW91	12.6, 74.6, 74.7	434, 766, 958, 1097, 1260, 1290, 1626, 1639, 3367, 3379, 3474, 3480
N_2O_4_PW91PW91	278.4, 526.5, 804.9	86, 190, 264, 401, 449, 641, 727, 851, 1264, 1407, 1738, 1773
trans-$ONONO_2$_PW91PW91	157.8, 792.9, 947.7	26, 13, 191, 289, 424, 582, 746, 766, 895, 1287, 1686, 1850
C_s-TS1_PW91PW91	495.2, 1481.3, 1811.2	607i, 34, 67, 135, 149, 222, 239, 271, 332, 414, 497, 680, 702, 743, 783, 850, 869, 1002, 1153, 1205, 1325, 1390, 1475, 1516, 1609, 1639, 1753, 3337, 3408, 3469
C_s-omplex1_PW91PW91	521.3, 1411.3, 1713.4	41, 68, 123, 149, 203, 232, 264, 295, 354, 396, 623, 682, 698, 756, 790, 901, 1004, 1107, 1160, 1181, 1208, 1408, 1483, 1614, 1655, 1781, 2536, 3329, 3450, 3465
C_s-Complex2-_PW91PW91	425.4, 2021.8, 2257.7	28, 44, 83, 104, 115, 134, 299, 359, 474, 570, 594, 632, 746, 748, 830, 868, 887, 943, 1160, 1278, 1291, 1342, 1367, 1513, 1612, 1694, 3311, 3317, 3415, 3455
$H_2NN(H)NO$_PW91PW91	87.0, 246.5, 327.0	223, 343, 399, 579, 844, 902, 998, 1165, 1277, 1368, 1488, 1618, 3294, 3417, 3521
$HONO_2$_PW91PW91	140.5, 153.4, 293.9	482, 554, 600, 750, 844, 1267, 1302, 1717, 3629

Table3-19: Relative energies of species in the major channel of the trans-$ONONO_2$ + N_2H_4 reaction at various theoretical levels. [a]

	ZPE [b]	PW91PW91 /6-311++G(3df,2p)	CCSD(T) /6-311+G(d,p) [c]	G2M(CC3) [c]
N_2O_4+N_2H_4	46.51	-522.0717000000	-520.9408055	-521.3819786
trans-$ONONO_2$+N_2H_4	45.23	14.74	6.18	5.88
C_s-Complex1_PW91PW91	47.11	-2.17	-1.48	-3.27
C_s-Complex2_PW91PW91	47.51	-10.25	-17.61	-19.76
C_s-TS1-new_PW91PW91	44.71	-3.28	-7.44	-8.66
$H_2NN(H)NO$+$HONO_2$	46.57	-6.58	-12.37	-14.56

[a]: The relative energy (kcal/mol) is calculated with the energy of N_2O_4 (D_{2h})+N_2H_4 as reference, whose total energy unit is hartree/molecule.

[b]: The ZPE is determined by PW91PW91/6-311++G(3df,2p) level, and the energy unit is kcal/mol for every species.

[c]: The energies are including single-point energies, based on geometries of PW91PW91/6-311++G(3df,2p), and ZPE.

3.3.2 Decomposition of $H_2NN(H)NO$ molecule

The $H_2NN(H)NO$ molecule is the product of the lowest-energy path in the N_2H_4 + isomeric N_2O_4 reactions, as discussed in the previous section. This molecule can be formed the combination of NO and N_2H_3 radicals, and we want to know whether there is another lower-energy path to produce highly reactive products in the decomposition reaction. The optimized geometries of stationary points, such as intermediates, transition states, and product molecules, in the reaction are determined at the B3LYP/ 6-311++G(3df,2p) level, as shown in Fig3-11. Further, the full potential energy surface of decomposition reaction is represented in Fig.3-12, and the energies of species are predicted by the G2M(CC1) single-point calculation. Since this is the decomposition reaction of $H_2NN(H)NO$, we add a notation d in front of the complexes and TSs for easy recognition. The moments of inertia and vibrational frequencies of all species are listed in Table3-20, and the energies by G2M(CC1), CCSD(T)/6-311+G(d,p), and CCSD(T)/6-311++G(3df,2p) are shown in Table3-21.

The $H_2NN(H)NO$ molecule is a stable structure, and we separate $H_2NN(H)NO$ into three groups, including NH_2, NH, and NO for conveniently explaining geometries. Since the two hydrogen atoms of NH_2 turn upward to NO tail, the hydrogen bonding makes molecule more stable. However, if the molecule undergoes a dissociation reaction to produce the N_2H_3+NO radicals, the hydrogen bonding will retard this reaction. Therefore, the possible path to dissociate into two radicals may be that $H_2NN(H)NO$ molecule first undergoes NH_2 rotation, to form d-Complex1 via d-TS1, turning the two H atoms into the opposite direction, and the energy of d-Complex1 raises as the hydrogen bonding disappears. Furthermore, d-Complex1 undergoes the dissociation reaction producing N_2H_3 and NO. The energy barrier of d-TS1 is 6.28 kcal/mol, which is the same as d-Complex1 at the G2M(CC1) level. At

CCSD(T)/6-311++G(3df,2p), it is 6.82 kcal/mol which is higher than d-Complex1 by 0.54 kcal/mol. Moreover, the dissociation from d-Complex1 to N_2H_3+NO radicals needs 21.55 and 24.06 kcal/mol by G2M(CC1) and CCSD(T), respectively. Comparing the other channels in the $H_2NN(H)NO$ molecule decomposition, the channel producing the N_2H_3+NO radicals is most likely with the lowest-energy path.

Another path is the hydrogen transfer from NH_2 group to the oxygen atom of the NO group in the $H_2NN(H)NO$ molecule via d-TS2; the energy barrier is only 18.75 and 19.17 kcal/mol with G2M(CC1) and CCSD(T)/6-311++G(3df,2p) methods, respectively. The d-TS2 has a five-member ring structure for hydrogen transfer, which is the major motion in this path, and the imaginary frequency is 1395 cm^{-1} as shown in Table3-20. However, the N-N bond between the NO and NH group is as short as 1.279Å with an N=N double bond character; the dissociation of d-Complex2 to HON+cis-N_2H_2 requires very high energy, 62.45 kcal/mol above d-Complex2. In addition, the unstable HON molecule raises the system energy. Therefore, the formation of d-Complex2 does not lead to another lower-energy path for the decomposition of $H_2NN(H)NO$. Even though the energy of initial hydrogen transfer is low, the high dissociation energy makes this reaction channel be very hard to occur kinetically. On the other hand, the d-Complex2 may undergo a hydrogen transfer reaction via d-TS6, and the d-complex6 dissociates to highly active products, N_3H_2 + OH radicals, without a barrier. However, the energy barrier of the hydrogen transfer via d-TS6 is 37.6 kcal/mol computed at G2M(CC1) level. Since the N_3H_2 radical is highly unstable, the dissociation energy from d-Complex5 to N_3H_2 + OH is 58.3 kcal/mol. Therefore this channel seems to be difficult to occur kinetically.

The third reaction is also the hydrogen transfer via d-TS3, whose energy barrier is as high as 43.79 and 44.18 kcal/mol at the G2M(CC3) and CCSD(T)/6-311++G(3df,2p) levels, respectively, and the hydrogen atom is from nitrogen atom of the NH group to that of NO group to form d-Complex3. The d-Complex3 is as stable as the $H_2NN(H)NO$ molecule, since this complex also obeys by the Octet rule. However, it needs very high energy to dissociate the d-Complex3 into HNO and H_2NN molecules, similar to d-Complex2. The dissociation energy is 53.01 kcal/mol with respect of the d-Complex3, and it is too high to happen. The product, H_2NN, is an unstable molecule, which increases the system energy, therefore, we seek another reaction channel from d-Complex3 to produce the N_2H_2 and HNO. However, in order to form the d-Complex4, it should overcome d-TS4, whose energy barrier is 63.16 kcal/mol at the G2M(CC1) level. Even though d-TS5 is only higher than d-Complex4 by 8.32 kcal/mol, the final products HNO+trans-N_2H_2 are still controlled by the high barrier of d-TS4. In conclusion, these decomposition reaction channels cannot compete with the dissociation to NO+N_2H_3 radicals kinetically.

In the present case, the CCSD(T)/6-311++G(3df,2p) method has been used for comparison with the values of G2M(CC1), since the total number of atom is only seven. The energy differences between CCSD(T)/6-311++G(3df,2p) and G2M(CC1) methods are smaller than 1 kcal/mol for all species except for NO+N_2H_3, whose G2M value is lower than CCSD(T) by 2.55 kcal/mol. The reason causing the larger energy difference for NO+N_2H_3 may be the spin contamination on the doublet molecules, since the G2M method use the projection method of MPn and higher level corrections to correct the problem of spin contamination. The other species in this decomposition reaction are all singlet, so the spin-contamination does not affect the energies of G2M and CCSD(T) methods. Therefore, the G2M(CC1) can generally provide good predictions as CCSD(T)/6-311++G(3df,2p) does, and it can also save the

computational resource. On the other hand, comparing with the CCSD(T)/6-311++G(3df,2p) and G2M(CC1) methods, the CCSD(T)/6-311+G(d,p) method underpredicts the energies of product molecules, and there is no systematic correlation for complexes and transition states.

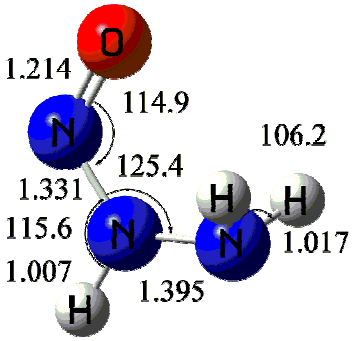

$H_2NN(H)NO$ (C_s)

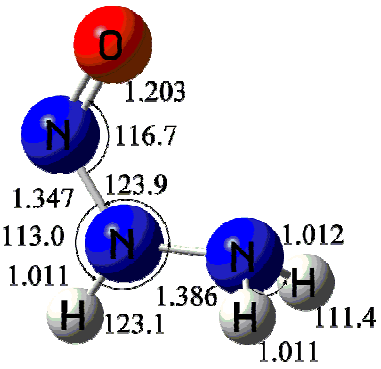

d-Complex1 (C_s)

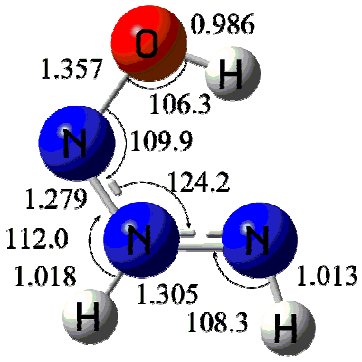

d-Complex2 (C_s)

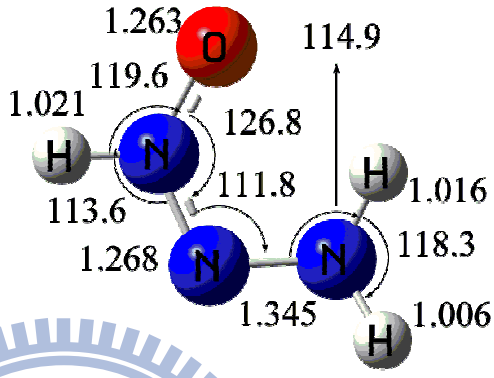

d-Complex3 (C_1)

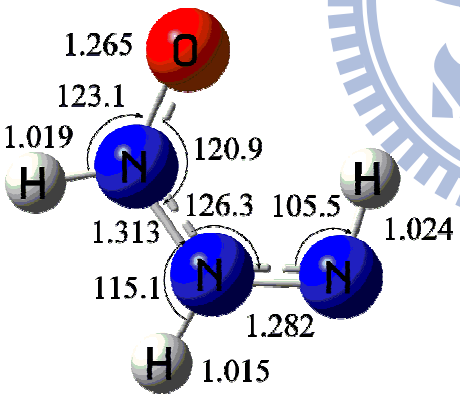

d-Complex4 (C_s)

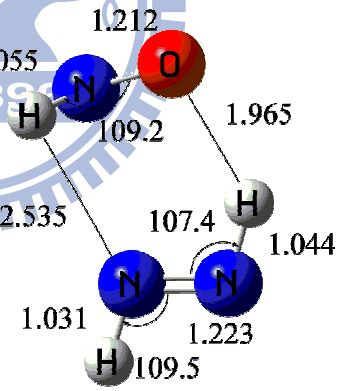

d-Complex5 (C_1)

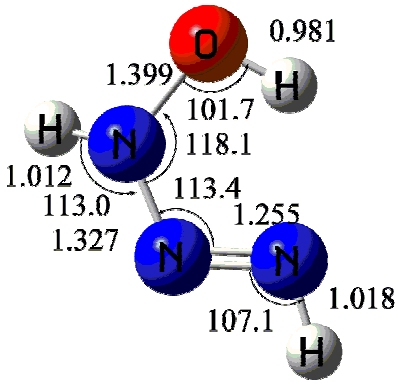

d-Complex6 (C_1)

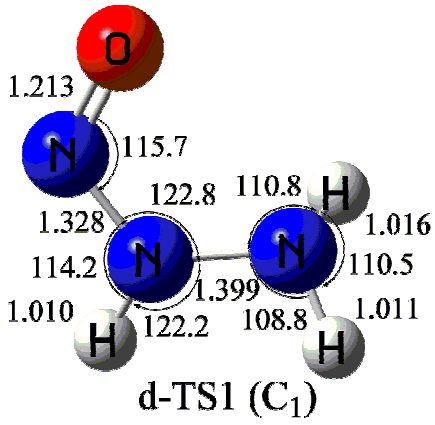

d-TS1 (C_1)

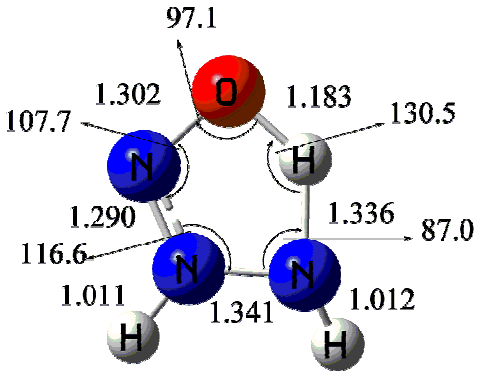

d-TS2 (C_1)

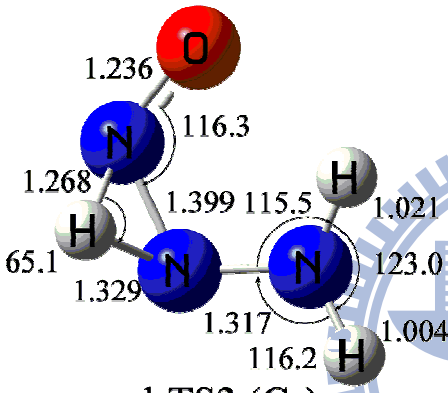

d-TS3 (C_1)

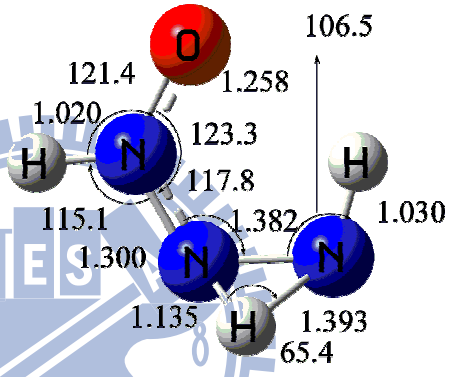

d-TS4 (C_1)

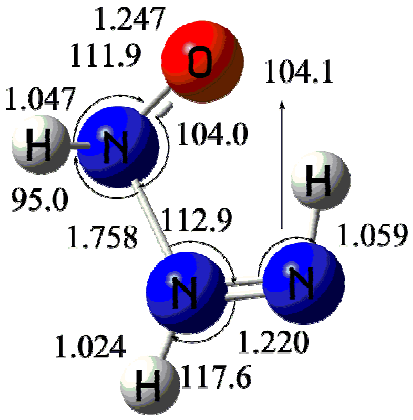

d-TS5 (C_1)

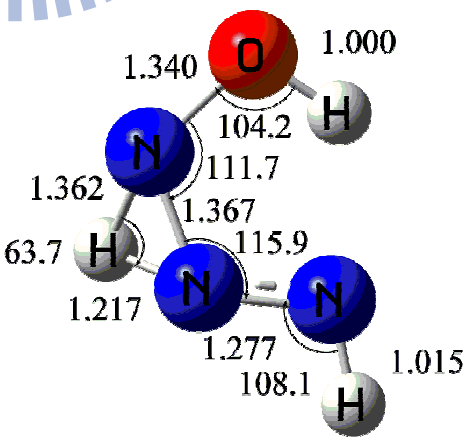

d-TS6 (C_1)

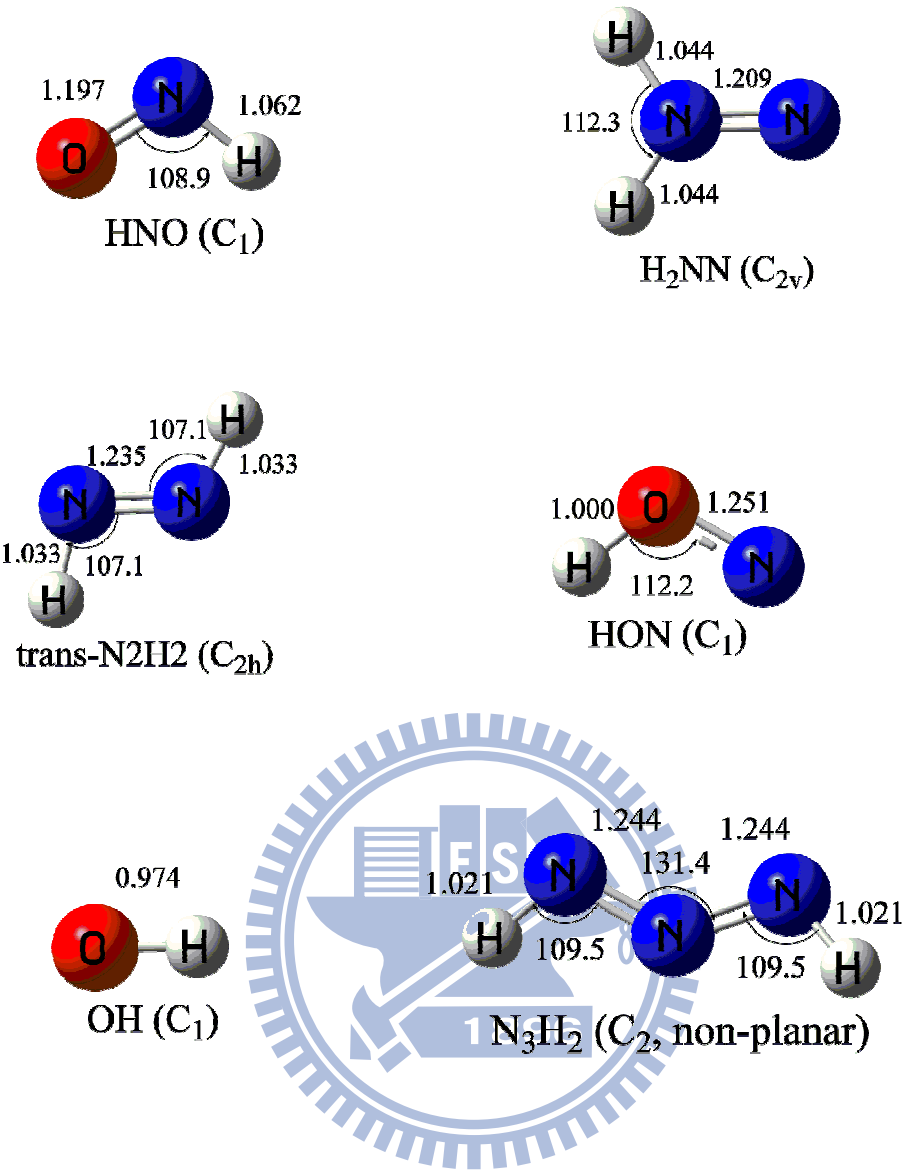

Fig3-11: The stationary points in the PES of $H_2NN(H)NO$ decomposition are optimized by B3LYP/6-311++G(3df,2p)

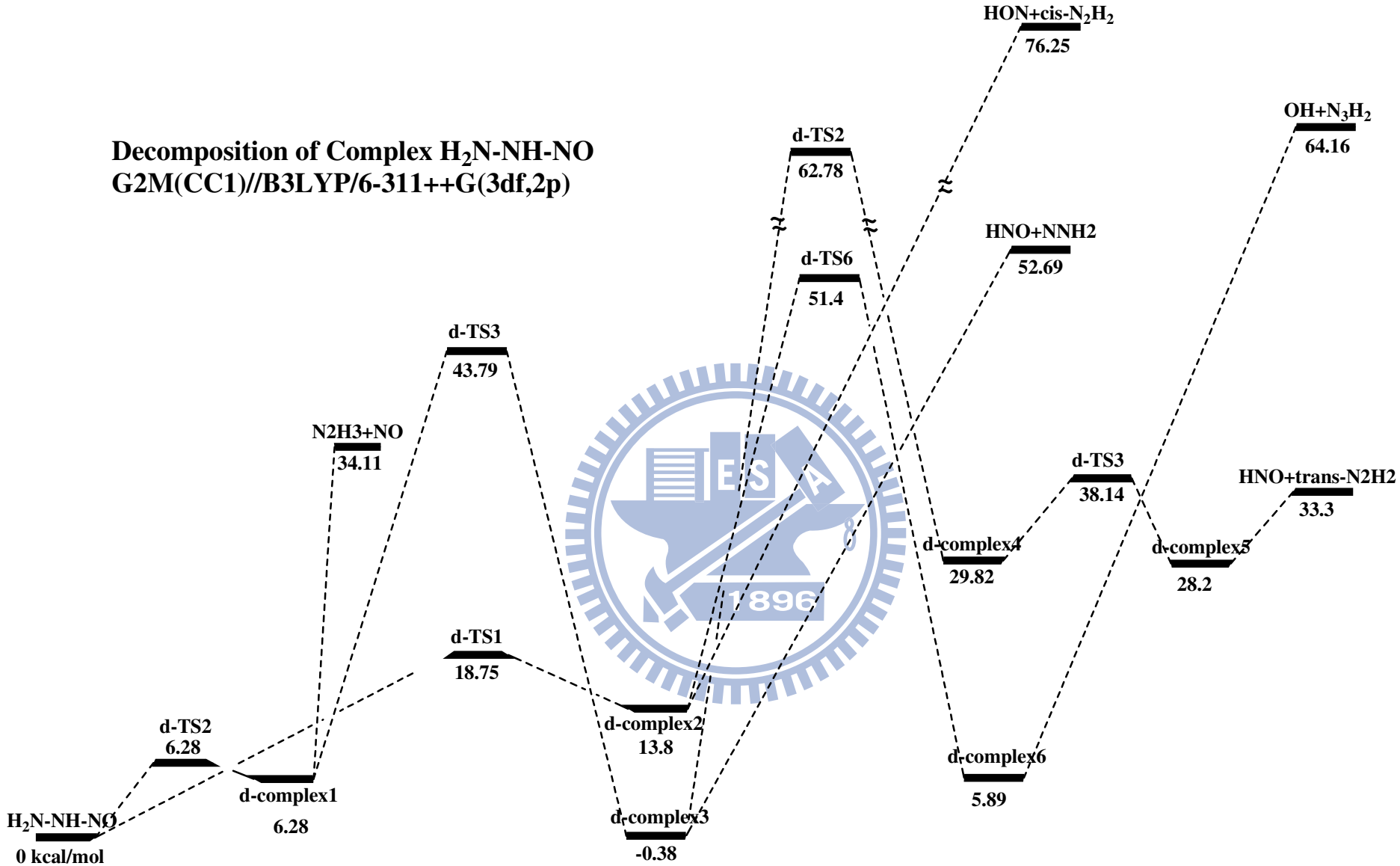

Fig3-12: Potential Energy Surface of $H_2NN(H)NO$ decomposition, whose energies are calculated by G2M(CC1) // B3LYP/6-311++G(3df,2p).

Table3-20: Moments of inertia (I_A, I_B, I_C) and vibration frequencies of the species in $H_2NN(H)NO$ decomposition computed at B3LYP/6-311++G(3df,2p).

Species or Transition States	Moments of inertia I_i(a.u)	Vibrational Frequency υ_j (cm^{-1})
$H_2NN(H)NO$	85.7, 251.3, 327.5	38, 288, 324, 589, 871, 901, 1042, 1219, 1330, 1411, 1585, 1695, 3454, 3515, 3634
d-complex1	79.4, 271.1, 340.5	151, 212, 332, 583, 674, 901, 978, 1168, 1285, 1433, 1630, 1672, 3504, 3567, 3600
d-complex2	86.3, 228.8, 315.1	378, 444, 586, 667, 815, 871, 1037, 1169, 1317, 1430, 1522, 1620, 3421, 3485, 3547
d-complex3	82.4, 236.4, 317.5	366, 496, 580, 627, 798, 858, 1128, 1247, 1325, 1493, 1562, 1617, 3439, 3471, 3672
d-complex4	79.7, 251.6, 331.3	178, 316, 515, 651, 847, 852, 1084, 1228, 1376, 1502, 1541, 1592, 3420, 3530
d-complex5	907, 386.8, 470.9	129, 161, 224, 360, 368, 565, 1305, 1307, 1534, 1572, 1582, 1686, 2960 3120, 3284
d-complex6	86.1, 236.9, 320.3	353, 416, 545, 574, 813, 911, 1031, 1130, 1342, 1469, 1507, 1565, 3470, 3503, 3580
d-TS1	81.5, 259.2, 334.4	205, 177, 340, 538, 766, 923, 967, 1178, 1314, 1436, 1586, 1648, 3469, 3585, 3609
d-TS2	91.9, 201.7, 291.8	1395i, 479, 573, 693, 796, 935, 1098, 1160, 1177, 1266, 1373, 1546, 2125, 3564, 3583
d-TS3	85.6, 231.8, 310.4	1570i, 374, 393, 598, 654, 786, 890, 1087, 1268, 1299, 1403, 1545, 2012, 3399, 3690
d-TS4	84.1, 244.2, 323.0	1700i, 335, 503, 624, 681, 853, 914, 1095, 1252, 1382, 1435, 1520, 2614, 3331, 3455
d-TS5	89.2, 266.3, 349.4	375i, 265, 392, 555, 726, 1069, 1152, 1184, 1346, 1434, 1529, 1637, 2965, 3042, 3397
d-TS6	88.1, 225.5, 307.6	1607i, 354, 605, 700, 773, 876, 926, 1061, 1138, 1356, 1428, 1527, 2165, 3183, 3516
N_2H_3	8.8, 58.6, 66.5	548, 696, 1136, 1238, 1479, 1658, 3425, 3488, 3632
NO	0, 34.9, 34.9	1979
HON	2.8, 45.2, 48.0	1282, 1489, 3107
HNO	3.2, 41.9, 45.1	1562, 1672, 2876
H_2NN	5.4,46.0, 51.4	100.8, 1329, 1612, 1733, 2998, 3036
trans-N_2H_2	5.9, 45.4, 51.3	1341, 1351, 1588, 1652, 3235, 3036

cis-N_2H_2	6.1, 45.6, 51.8	1281, 1361, 1555, 1651, 3102, 3195
N_3H_2	11.2, 153.1, 163.1	556, 642, 725, 1197, 1249, 1356, 1660, 3439, 3445
OH	0.0, 3.2, 3.2	3722

Table3-21: Relative energies of species in $H_2NN(H)NO$ decomposition computed at various theoretical levels. [a]

	ZPE [b]	B3LYP /6-311++G(3df,2p) [c]	CCSD(T) /6-311+G(d,p) [c]	CCSD(T) /6-311++G(3df,2p) [c]	G2M(CC1) [c]
$H_2NN(H)NO$	31.3	-151368.1213	-150999.8933	-151090.8409	-151137.0469
d-complex1	31.01	5.57	6.02	6.32	6.28
d-complex2	31.89	14.85	16.05	14.22	13.8
d-complex3	32.42	-1.09	1.45	0.06	-0.37
d-complex4	31.57	28.16	34.29	30.64	29.82
d-complex5	28.82	25.51	25.13	28.29	28.01
d-complex6	31.7	5.74	5.88	6.02	5.89
N_2H_3+NO	27.56	31.07	26.48	30.38	27.83
HON+cis-N_2H_2	25.76	78.02	73.68	76.19	76.25
HNO+H_2NN	25.79	53.27	49.31	52.76	52.69
HNO+trans-N_2H_2	26.51	32.83	29.37	33.43	33.31
N_3H_2+OH	25.72	53.62	56.52	60.49	64.16
d-TS1	30.79	5.96	6.9	6.86	6.28
d-TS2	29.12	18.76	20.05	19.17	18.75

d-TS3	27.73	44.18	45.11	44.18	43.79
d-TS4	28.58	66.61	68.04	66.15	65.33
d-TS5	29.58	36.17	38.56	38.75	38.15
d-TS6	28.03	52.02	52.24	51.88	51.4

[a]: The relative energy (kcal/mol) is based on the energy of N_2O_4 (D_{2h})+N_2H_4 as reference, whose energy unit is hartree/molecule.

[b]: The ZPE is determined by B3LYP/6-311++G(3df,2p) level, and the energy unit is kcal/mol for every species.

[c]: The energies are including single-point energies, based on geometries of B3LYP/6-311++G(3df,2p), and ZPE.

3.3.3 N_2H_4+N_2O_4 (D_{2h}) reaction

We consider the reaction of N_2O_4(D_{2h}) and N_2H_4 in this section. Since high-symmetry N_2O_4 (D_{2h}) molecule is less reactive than the monomer NO_2, the reaction channels in N_2H_4+N_2O_4 (D_{2h}) are not as many intuitively. The products are the same as those in the previous reactions, such as $H_2NN(H)NO_2$, $H_2NN(H)ONO$, NO_2, trans-HONO, cis-HONO, and N_2H_3 radical. All geometries of species in this potential energy surface are optimized at the B3LYP/6-311++G(3df,2p) level, and the details of bond lengths and angles are shown in Fig3-13. The potential energy surface is based on the single-point energies determined by G2M(CC3) in Fig3-14. It is easier to recognize the species in PES from other reactions, if we add a notation D_{2h} in front of the complexes and TSs. The information, including the moments of inertia and vibrational frequencies, are listed in Table3-22; moreover, the energies by different computational methods with the zero-point energy (ZPE) of B3LYP/6-311++G(3df,2p) are compared in Table3-23

The N_2O_4(D_{2h}) and N_2H_4 form an intermediate, D_{2h}-Complex1, due to the physical attraction and hydrogen bonding, and the energy is lower than the reactants by 6.98 kcal/mol at the G2M(CC3) level. Basically the N_2O_4 and N_2H_4 molecules in the D_{2h}-Complex1 have the same geometries as those in the individual molecules, the nearest distance between these two molecules is 2.662Å. There are three channels starting from D_{2h}-Complex1 in the PES, and the lowest-energy path is to produce the $H_2NN(H)NO_2$ and trans-HONO molecules via D_{2h}-TS1. The structure of five-member ring in D_{2h}-TS1 connects the two nitrogen and one oxygen atoms of N_2O_4 with one nitrogen atom and one hydrogen atom of N_2H_4, as in Fig.3-13. The N-N bond of N_2O_4 twists to make the planes of two NO_2 group be perpendicular, and the nitrogen atom of the NO_2 group connects with the one of nitrogen atoms of the N_2H_4 molecule as the two oxygen atoms is parallel with the N-N bond of N_2H_4 upwardly. The

structure of N_2H_4 in the D_{2h}-TS1 makes two hydrogen atoms point upward to one oxygen atom, and it forms the hydrogen bonds and reduces the system energy as in C_s-TS1 and C_s-TS2. The major motion of D_{2h}-TS1 is the hydrogen transfer to form the trans-HONO with the concerted formation of $H_2NN(H)NO_2$. The energy barrier is 14.16 and 21.14 kcal/mol above the reactants and D_{2h}-Complex1 at the G2M(CC3) level. The products $H_2NN(H)NO_2$ and trans-HONO, from D_{2h}-Complex2, have appeared in the N_2H_4+cis-$ONONO_2$ reaction; therefore, we will discuss further about the decomposition reaction of $H_2NN(H)NO_2$ molecule in the next section. The D_{2h}-TS4 has the a six-member ring structure, as shown in Fig.3-13. The hydrogen transfer reaction from N_2H_4 to one of the NO_2 groups is accompanied by the formation N-O bond between N_2H_4 and the other NO_2 group, and the breaking of the N-N bond of N_2O_4, producing trans-HONO and $H_2NN(H)ONO$. However, the energy barrier is higher than D_{2h}-TS1 by 6.7 kcal/mol. Comparing with the structure between two transition states, it is apparent that the D_{2h}-TS1 has tight connection with each element in the ring, whereas the ring structure of D_{2h}-TS4 is relatively loose. The N-N bond length of the N_2O_4 molecule is 2.257 and 2.672 Å in D_{2h}-TS1 and D_{2h}-TS4, respectively. The motion of breaking the N-N bond in D_{2h}-TS1 is more drastic than that in D_{2h}-TS4, which means that it needs to elongate the N-N bond before reaching the D_{2h}-TS4. Therefore, the barrier of D_{2h}-TS3 is higher than the D_{2h}-TS1. On the other hand, the products of the D_{2h}-TS4 are $H_2NN(H)ONO$ and trans-HONO molecules, dissociated from D_{2h}-Complex5, have also appeared in the cis-$ONONO_2$+N_2H_4 reaction, we will not discuss the decomposition of the $H_2NN(H)ONO$ molecule due to the higher energy for its formation.

D_{2h}-TS3 is the transition state which is not originated from the D_{2h}-Complex1 but directly from the reactants, N_2H_4 and N_2O_4, attributable to the unique structure of the D_{2h}-TS3, which is the ball-like geometries with C_2 symmetry, and it is difficult to achieve this structure from other intermediates. Every oxygen atoms of N_2O_4 molecule connects with the hydrogen

atoms of N_2H_4 molecule without repetition, and the dihedral angle of four nitrogen atoms is 4^o, which means nearly on one plane. Due to the C_2 symmetry, the distances between hydrogen atom and oxygen atom on the diagonal position are the same. One pair of N-O distance is short as 1.836Å, whereas the other pair of N-O distance is long as 2.406Å. This structure indicates that the two hydrogen transfer reaction occur concurrently in the D_{2h}-TS3 with the breaking N-N bond of the N_2O_4 molecule, and its energy barrier is 21.37 and 25.07 kcal/mol obtained at G2M(CC3) and CCSD(T)/6-311+G(d,p) levels. The reaction via the D_{2h}-TS3 produces the D_{2h}-Complex4, including two cis-HONO and one trans-N_2H_2 molecules, with 11.8 kcal/mol exothermally.

The last reaction channel in the N_2H_4+N_2O_4(D_{2h}) reaction is the transfer of only one hydrogen atom to an oxygen atom of N_2O_4 via D_{2h}-TS2, whose geometry is shown in Fig3-13. The seven-member ring is constructed by the H-N-N-N atoms of N_2H_4 and the O_2N group of N_2O_4 molecule; D_{2h}-TS2 has the C_1 symmetry. The distance between oxygen and hydrogen atoms on the side not being transferred is 2.255 Å, and the connection is built up by the hydrogen bond. On the other side of the seven-member ring, the hydrogen atom is 1.515Å far from the nitrogen atom of N_2H_4 and much closer to the oxygen atom of N_2O_4, 1.062 Å. The position of hydrogen atom in D_{2h}-TS2 is different comparing with the other transition states of hydrogen transfer, which is much closer to the bonding N atom of N_2H_4 and far away from the N or O atoms of N_2O_4 isomers. Therefore, it is believed that the high energy barrier predicted by B3LYP/6-311++G(3df,2p) is reasonable, since the hydrogen atom needs to elongate the N-H bond by raising energy. However, the prediction of CCSD(T)/6-311+G(d,p) and G2M(CC3) methods are very low, which is the contrary result to that of B3LYP, as shown in Table3-23. The IRC calculation confirms the large difference of energy between D_{2h}-Complex1 and D_{2h}-TS2. Therefore, we assume the strange results in CCSD(T) and G2M(CC3) single-point energy calculations are caused by the incorrect prediction in the

electronic energy instead the geometry optimized by B3LYP/6-311++G(3df,2p). Since the G2M methods are based on the correction with CCSD(T)/6-311G(d,p), it is understandable that the G2M and CCSD(T) have problems at the same time. On the other hand, the D_{2h}-Complex3, composed of a N_2H_3 radical and cis-HONO molecule, forms with the breaking N-N bond of N_2O_4 after passing over the D_{2h}-TS2. The total energy of D_{2h}-Complex3 and NO_2 should be lower than that of D_{2h}-TS2, therefore, it is another proof that the single-point energies of CCSD(T) and G2M are incorrect.

In Table3-23, comparing with the energies determined by CCSD(T)/6-311+G(d,p) and G2M(CC3), it is difficult to summarize a systematic relationship. Most of the energies at CCSD(T)/6-311+G(d,p) level is lower than those at G2M(CC3), but it has a opposite relationship in transition states. Therefore, the difference of intermediate and transition states at CCSD(T) is larger than those at G2M. This is not consistent with the relationship in section3.3.1. Moreover, if we compare the heat of reaction with experimental results, it is apparent that the G2M(CC3) performs well for the production of cis-N_2H_2+ 2 cis-HONO only, whereas the CCSD(T)/6-311+G(d,p) performs bad at both cases. Therefore, it is very important to decide which lower single-point energy computation can perform well for this larger system, and we will discuss this topic in section 3.3.5.

Observing the full PES of N_2H_4 with N_2O_4 isomers, it is consistent that all of the complexes passing over the TSs, including Cs-Complex2, 4, 6, 8 and D_{2h}-Complex2, 3, 4, 5, still need high energy to separate the product molecules. The dissociation energy of these complexes are 3~8 kcal/mol for two-molecular cases and 11~14 kcal/mol for three-molecular cases at the G2M(CC3) level. This phenomenon of high complexation energies is caused by the strong hydrogen bonds as appears in the NO_2 reaction, discussed in section 3.1. Even though these dissociation energies from complexes to molecules are high, most of the energies of final products are lower than the reactants, N_2H_4+N_2O_4; they are all formed exothermically.

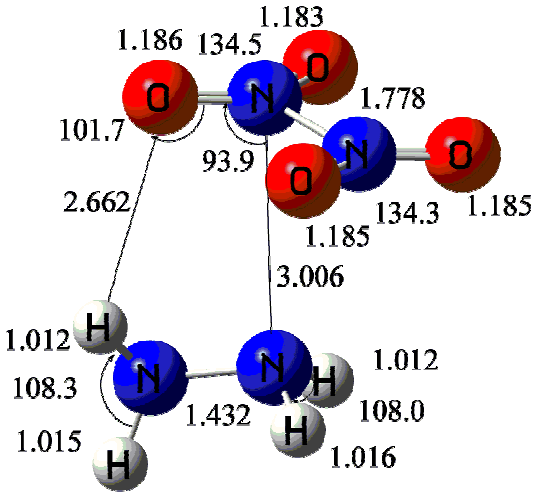

D_{2h}-Complex1 (C_1)

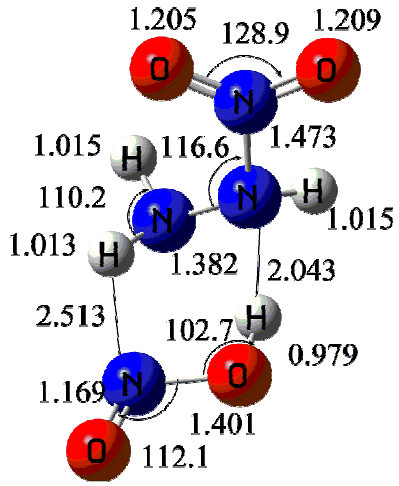

D_{2h}-Complex2 (C_1)

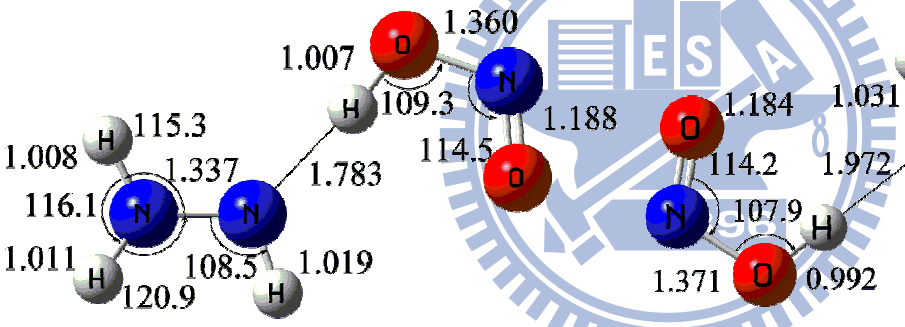

Complex3 (C_1)

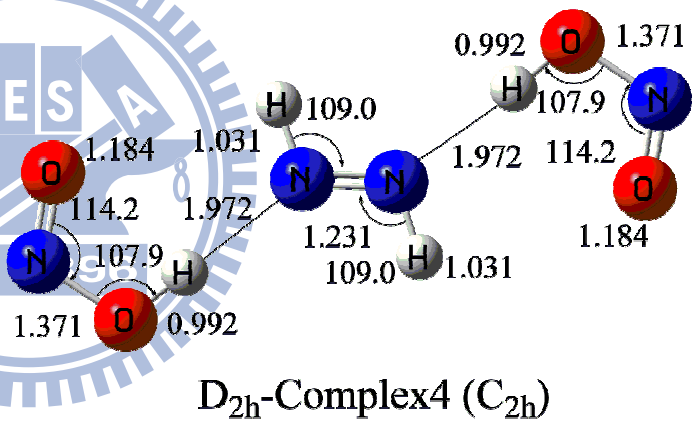

D_{2h}-Complex4 (C_{2h})

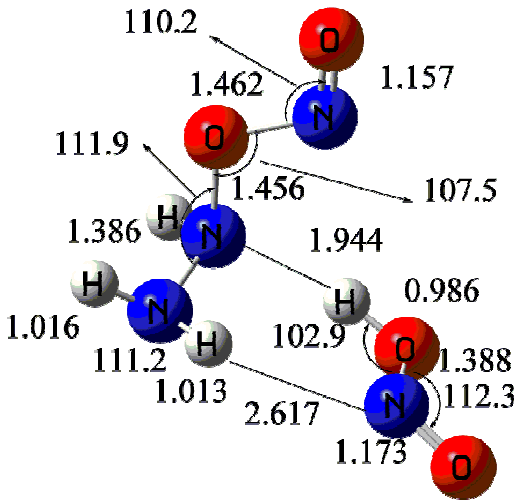

D_{2h}-Complex5 (C_1)

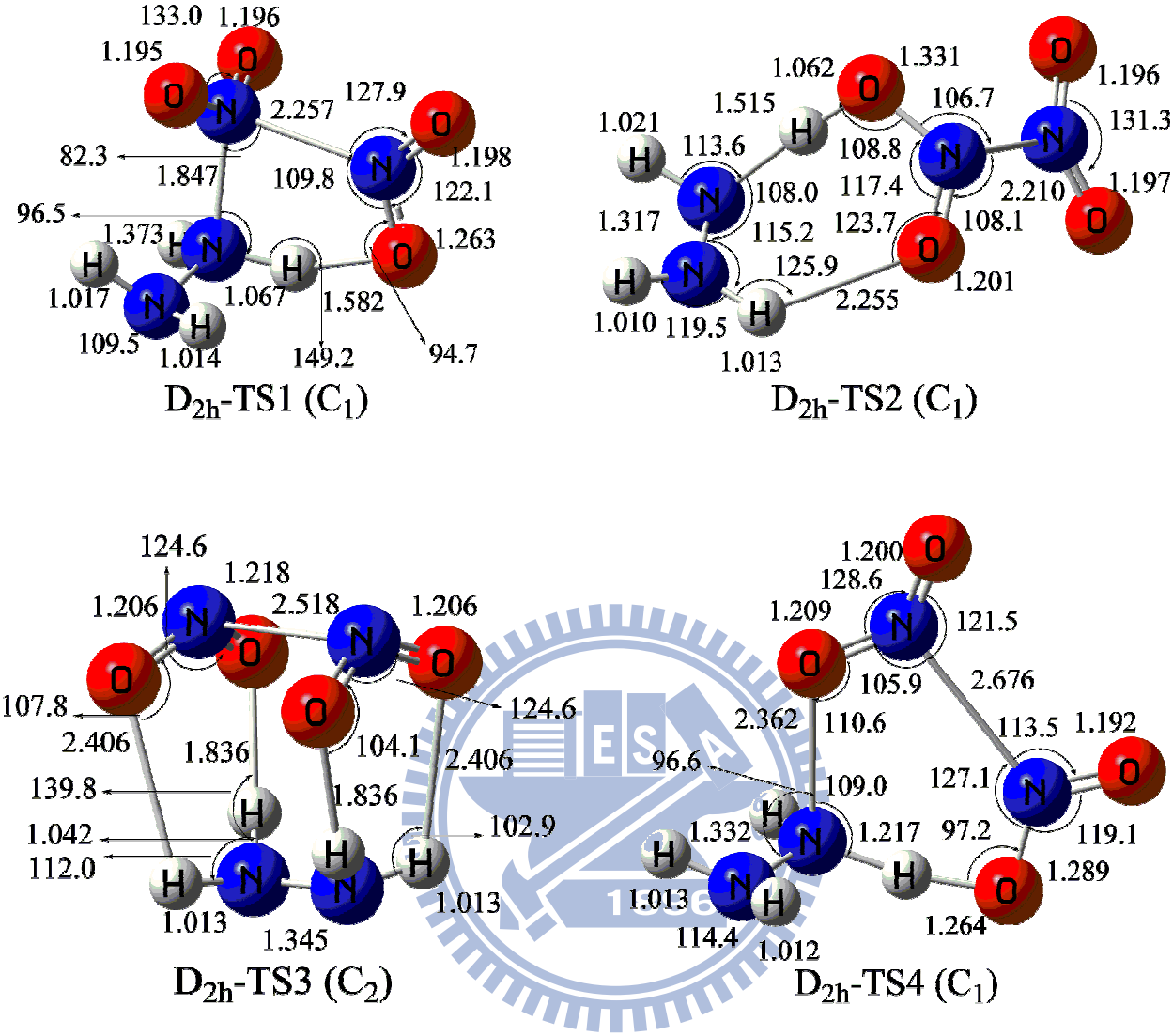

Fig3-13: The stationary points in the PES of N_2O_4 (D_{2h}) + N_2H_4 reaction are optimized by B3LYP/6-311++G(3df,2p)

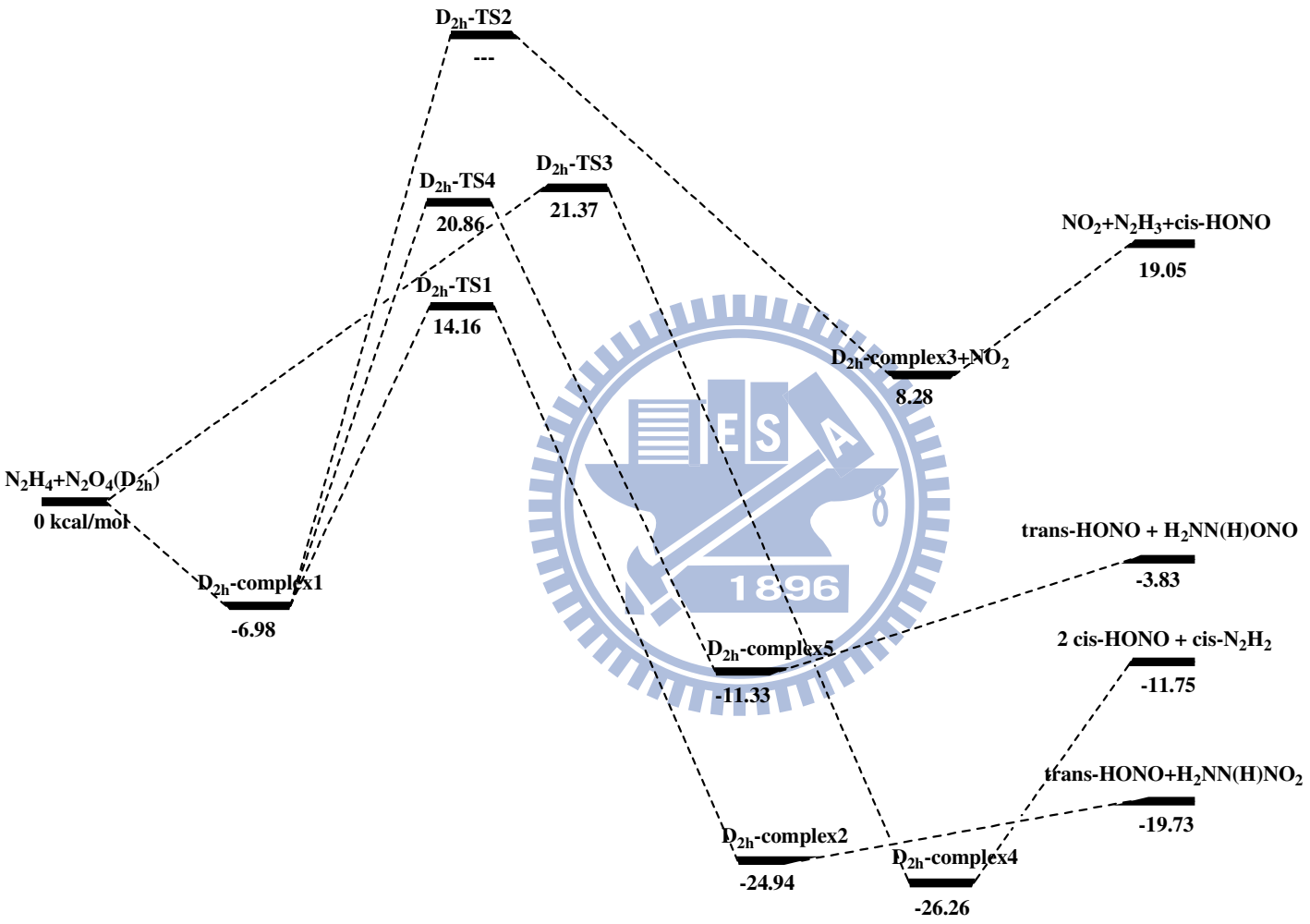

Fig3-14: Potential Energy Surface of the N_2O_4 (D_{2h}) + N_2H_4 reaction, whose energies are calculated by G2M(CC3) // B3LYP/6-311++G(3df,2p).

Table3-22: Moments of inertia (I_A, I_B, I_C) and vibration frequencies of the species in the N_2O_4 (D_{2h}) + N_2H_4 reaction computed at B3LYP/6-311++G(3df,2p).

Species or Transition States	Moments of inertia I_i(a.u)	Vibrational Frequency υ_j (cm^{-1})
N_2H_4	12.4, 74.2, 74.3	439, 801, 974, 1114, 1294, 1323, 1674, 1686, 3462, 3471, 3562, 3568
N_2O_4	273.2, 500.4, 773.7	87, 222, 293, 446, 490, 704, 760, 850, 1307, 1450, 1787, 1826
D_{2h}-Complex1	776.6, 1229.5, 1435.3	30, 53, 61, 74, 107, 115, 164, 234, 302, 451, 463, 505, 701, 767, 822, 853, 995, 1116, 1295, 1311, 1331, 1448, 1673, 1686, 1787, 1823, 3455, 3471, 3555, 3564
D_{2h}-Complex2	516.9, 2021.0, 2135.4	38, 57, 64, 92, 135, 163, 221, 318, 381, 482, 607, 673, 767, 801, 815, 841, 869, 989, 1223, 1320, 1368, 1412, 1439, 1693, 1703, 1763, 3477, 3520, 3549, 3573
D_{2h}-Complex3	190.8, 649.9, 839.4	82, 149, 191, 206, 256, 268, 496, 717, 735, 1032, 1056, 1146, 1308, 1468, 1504, 1623, 1663, 2802, 3488, 3494, 3625
D_{2h}-Complex4	267.9, 4696.8, 4964.6	9, 21, 33, 40, 40, 87, 121, 150, 179, 181, 255, 315, 678, 896, 902, 936, 937, 1332, 1346, 1427, 1432, 1579, 1677, 1687, 1690, 3284, 3313, 3330, 3354
D_{2h}-Complex5	666.4, 1857.8, 2282.0	35, 55, 74, 94, 152, 164, 166, 201, 342, 427, 506, 540, 635, 698, 825, 865, 892, 964, 1069, 1188, 1349, 1461, 1497, 1687, 1749, 1797, 3415, 3468, 3509, 3578
D_{2h}-TS1	717.6, 1072.4, 1381.5	223i, 48, 126, 144, 205, 213, 255, 287, 354, 388, 488, 551, 769, 814, 867, 883, 1134, 1196, 1231, 1275, 1309, 1437, 1596, 1626, 1695, 1712, 2613, 3466, 3515, 3569
D_{2h}-TS2	503.1, 1969.7, 2073.4	246i, 28, 34, 79, 88, 143, 163, 205, 236, 270, 315, 427, 498, 720, 766, 828, 886, 1099, 1144, 1249, 1346, 1457, 1479, 1588, 1652, 1677, 1987, 3457, 3490, 3694
D_{2h}-TS3	840.0, 981.8, 1277.8	198i, 101, 111, 140, 151, 158, 191, 194, 254, 260, 323, 467, 473, 716, 795, 815, 905, 1142, 1227, 1253, 1351, 1450, 1533, 1565, 1642, 1678, 3055, 3094, 3573, 3586
D_{2h}-TS4	1051,6, 1084.9, 2055.5	1332i, 31, 54, 79, 108, 123, 154, 189, 222, 244, 268, 299, 538, 633, 710, 740, 849,

		1129, 1204, 1224, 1325, 1416, 1546, 1599, 1613, 1659, 1678, 3493, 3554, 3618
H2NN(H)NO2	155.4, 34.6, 534.8	173, 313, 330, 499, 591, 790, 795, 852, 976, 1236, 1315, 1367, 1430, 1663, 1705, 3471, 3562, 3576
H2NN(H)ONO	80.4, 672.2, 687.1	96, 187, 323, 438, 501, 555, 612, 832, 967, 1042, 1189, 1335, 1504, 1687, 1766, 3453, 3515, 3584
trans-HONO	19.0, 143.1, 162.1	590, 621, 819, 1303, 1783, 3773
cis-N2H2	6.1, 45.6, 51.8	1281, 1361, 1555, 1651, 3102, 3195
NO2	7.4, 137.6, 145.0	767, 1395, 1703
N2H3	8.8, 58.6, 66.5	548, 696, 1136, 1238, 1479, 1658, 3425, 3488, 3632

Table3-23: Relative energies of species in N_2O_4 (D_{2h}) + N_2H_4 reaction computed at various theoretical levels. [a]

	ZPE [b]	B3LYP/ 6-311++G(3df,2p)	CCSD(T)/ 6-311+G(d,p) [c]	G2M(CC3) [c]	ΔH_{Exp} [d]
N_2O_4+N_2H_4	48.02	-522.173728	-520.938139	-521.3804132	
D_{2h}-Complex1	48.91	-3.03	-7.34	-6.98	
D_{2h}-Complex2	49.11	-17.74	-24.86	-24.94	
D_{2h}-Complex3 + NO_2	39.04	3.73	2.18	8.28	
D_{2h}-Complex4	45.62	-16.87	-29.36	-26.26	
D_{2h}-Complex5	47.75	-1.98	-13.27	-11.33	
$H_2NN(H)NO_2$+trans-HONO	47.93	-15.26	-19	-19.73	
cis-N_2H_2+ 2 cis-HONO	42.69	-3.96	-13.66	-11.75	-11.75
$H_2NN(H)ONO$+trans-HONO	46.42	3.31	-5.39	-3.83	
trans-HONO+N_2H_3+NO_2	42.92	13.94	12.64	19.05	15.94
D_{2h}-TS1	48.27	12.82	16.25	14.16	
D_{2h}-TS2	44.24	38.18	-9.27	1.16	
D_{2h}-TS3	45.98	23.67	25.07	21.37	
D_{2h}-TS4	43.32	36.57	19.94	20.86	

[a]: The relative energy (kcal/mol) is taken the energy of N_2O_4 (D_{2h})+N_2H_4 as reference, whose energy unit is hartree/molecule.

[b]: The ZPE is determined by B3LYP/6-311++G(3df,2p) level, and the energy unit is kcal/mol for every specie.

[c]: The energies are including single-point energies, based on geometries of B3LYP/6-311++G(3df,2p), and ZPE.

[d]:The heat of reaction in the experimental result is calculated by species of the reactants and products, whose heat of formation are from the reference (23).

3.3.4 Decomposition of $H_2NN(H)NO_2$ molecule

The $H_2NN(H)NO_2$ molecule is the product of lowest-energy path via D_{2h}-TS1 in the N_2H_4+$N_2O_4(D_{2h})$ reaction; it also appears in the lowest-energy path via C_s-TS2 in the N_2H_4+cis-$ONONO_2$ (C_s) reaction. In this section, we denote this molecule separately into three groups, including NH_2, NH, and NO_2, for describing the geometries in the PES conveniently. This molecule can be formed by the combination of NO_2 and N_2H_3 radicals. The products $H_2NN(H)NO_2$ + trans-HONO are energetically more stable than that of $H_2NN(H)NO$ + $HONO_2$. However, the oxygen atoms of NO_2 group may provide more possibilities to generate the active and exothermic products in different channels of the decomposition reaction. All geometries of the optimized species, such as intermediates, transition states, and products, are shown in Fig3-15. To distinguish the complexes and TSs in this reaction, we make a notation "d2" in front of them. The PES represents all decomposition channels in Fig.3-16, and the relative energies of the species are determined by G2M(CC1) method. Moreover, the moments of inertia and vibrational frequencies of the species are listed in Table3-24, and the energies calculated by different methods as shown in Table3-25.

Since $H_2NN(H)NO_2$ is the most stable configuration on the PES, all of reaction channels start from this molecule, and there is no other configurations of the molecule appearing in the PES. The first decomposition path is to form the NO_2 and N_2H_3 radicals directly, with this dissociation energy of 38.23 kcal/mol at the G2M(CC1) level. Unlike the decomposition reaction of $H_2NN(H)NO$, whose dissociation energy is 27.86 kcal/mol, the high decomposition energy for NO_2 and N_2H_3 provides the possibility of another reaction channels to occur. The lowest-energy path is to form the trans-HONO and trans-N_2H_2 via d2-TS1, with a five-member ring structure. The ring connects the three nitrogen atoms, one oxygen atom, and one hydrogen atom of the NH_2 group, and the motion along the reaction

coordinate is one hydrogen transfer reaction by breaking the N-N bond connecting NO_2 and NH groups. In order to help the hydrogen transfer reaction, the N-N bond connecting NO_2 and NH group elongate into 2.528Å with the N-N-N angle and N-N-O angle closely perpendicular. The energy barrier of the d2-TS1 is 26.6 kcal/mol at the G2M(CC1) level, and the following d2-Complex1 could dissociate into trans-HONO and trans-N_2H_2.

The d2-TS2 also has a five-member ring structure, with the same composition as d2-TS1; however, the N-N bond connecting NO_2 and NH groups shorten instead of elongating as d2-TS1. The oxygen atom of the NO_2 group is not on the top the nitrogen atom of NH_2 group, therefore, the hydrogen atom needs to get close to the oxygen by elongating the N-H to 1.610Å. The energy of hydrogen transfer is as high as 36.64 kcal/mol, and it produces the unstable intermediate d2-Complex3, whose energy is higher than d2-TS2 by 0.16 and 0.24 kcal/mol at the G2M(CC1) and CCSD(T)/6-311++G(3df,2p) levels, respectively. We believe that the minor difference is due to the calculation error of electronic energy for the unstable d2-Complex3. In order to break the N-N bond connecting NO_2 and NH groups, d2-Complex3 needs to cross the 4.93 kcal/mol barrier through d2-TS3 to form the d2-Complex4 of composing trans-HONO and cis-N_2H_2 molecules. The products are similar to those of d2-TS1; however, the highest energy barrier at d2-TS2 is higher than d2-TS1 by 10.04 and 9.56 kcal/mol at the G2M(CC1) and CCSD(T)/6-311++G(3df,2p) levels.

The other hydrogen transfer channel goes through d2-TS4 to form d2-Complex4, and it is an intramolecular hydrogen transfer from the NH group to the oxygen atom of the NO_2 group. The energy barrier is high for this kind of intramolecular transfer, which is 37.8 and 38.07 kcal/mol by G2M and CCSD(T) methods. The product intermediate, d2-Complex4, is stable; however, the dissociation energy to form H_2NN and trans-HONO would be very high, as in the $H_2NN(H)NO$ case. Therefore, the d2-Complex4 can undergo another intramolecular hydrogen transfer from NH_2 group to the nitrogen atom in the middle of the molecule.

Expectedly, the d2-TS5 creates a very high energy barrier, which is 69.38 kcal/mol above d2-Complex4. Even though the subsequent reaction, which is passing via d2-TS6 with 0.22kcal/mol height to form cis-HONO and trans-N_2H_2 molecules, has only minor barrier, this reaction channel cannot happen readily.

Finally, there is another high-barrier path via the d2-TS7, whose energies are 109.44 and 111.24 kcal/mol higher than $H_2NN(H)NO_2$ molecule by G2M and CCSD(T) methods. The structure of d2-TS7 is of four-member ring, composing of three nitrogen atoms and one oxygen atom, and the original N-O bond of NO_2 breaks as the formation of new N-O bond with the NH_2 group. This phenomenon is consistent with the channel1-4 in the monomer reaction, which has a very high barrier comparing with other hydrogen transfer reactions. After passing through d2-TS7, there are two possibilities to react further. One possibility is that d2-Complex7 undergoes the dissociation reaction to form H_2NO and HNNO molecules by breaking the longest N-N bond, which is 1.500Å. The other possibility is to produce the HNO and HNN(H)O molecules via d2-TS8, whose barrier is 11.86 kcal/mol at the G2M(CC1) level. The d2-TS8 is of four-member ring, which includes the three nitrogen atoms and one hydrogen atom; the hydrogen transfer from the H_2NO group to the nitrogen of the NO group as the longest N-N bond in d2-Complex7 breaks. Even though the HNO + HNN(H)O molecules are more stable than H_2NO and HNNO molecules, the energy barrier of d2-TS8 is higher than the dissociation energy. However, these two reaction paths are very hard to occur kinetically due to the extremely high energy barrier of d2-TS7.

In Table3-25, the difference between those determined by CCSD(T) /6-311++G(3df,2p) and G2M(CC1) are less than 1 kcal/mol. However, the energies calculated by CCSD(T) /6-311+G(d,p) have no systematic correlation with G2M(CC1). The CCSD(T)/6-311+G(d,p) energies of some of the species are lower than G2M(CC1) by over 3 kcal/mol, whereas some are higher than those by G2M(CC1) by 2~4 kcal/mol. This

non-systematic relationship appears in all of the N_2H_4+N_2O_4 isomeric reactions, therefore, the single-point energies calculated by the CCSD(T)/6-311+G(d,p) methods are again not reliable. In the next section, we will discuss the heats of reaction more precisely.

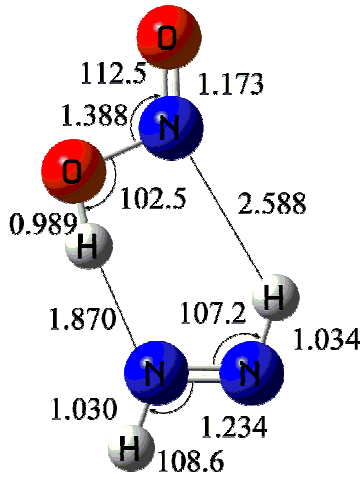

d2-Complex1 (C_1)

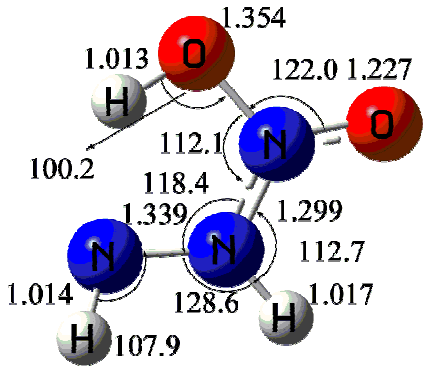

d2-Complex2 (C_1)

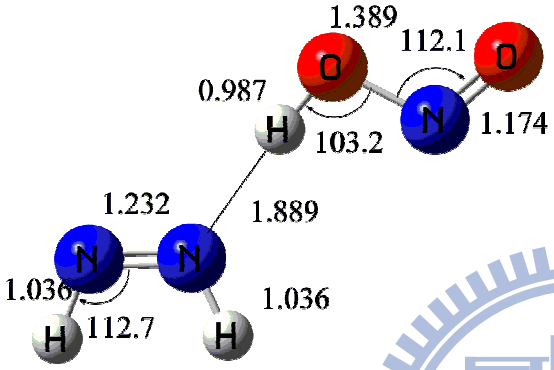

d2-Complex3 (C_1)

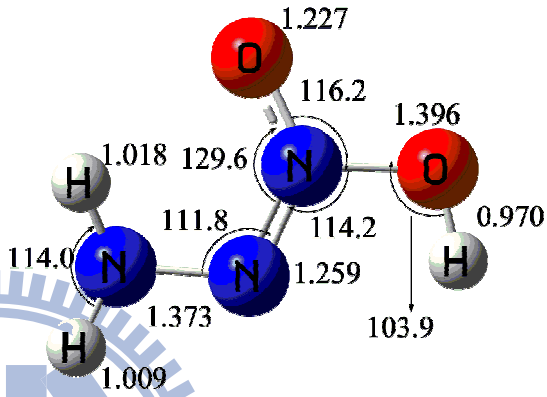

d2-Complex4 (C_1)

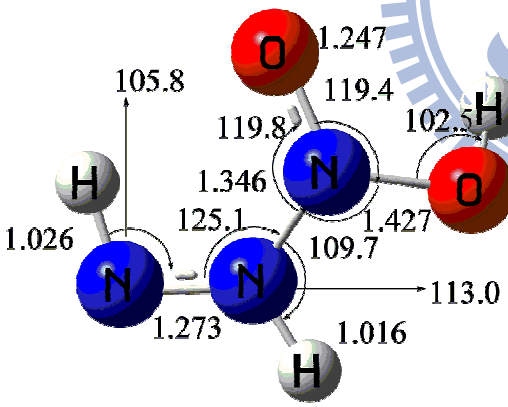

d2-Complex5 (C_1)

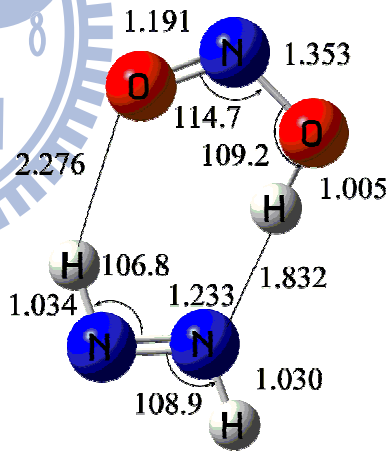

d2-Complex5 (C_1)

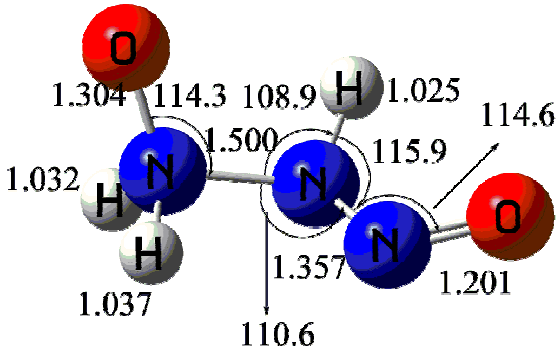

d2-Complex7 (C_1)

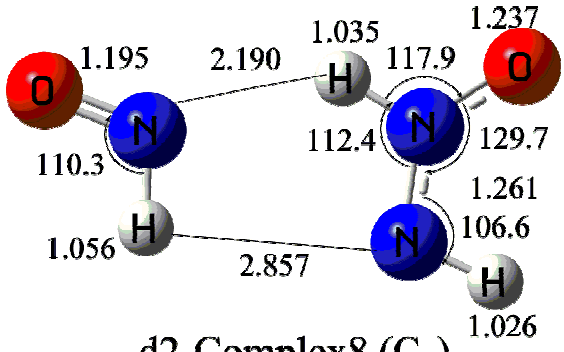

d2-Complex8 (C_1)

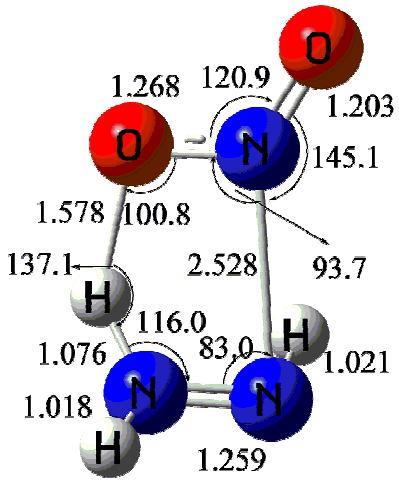

d2-TS1 (C_1)

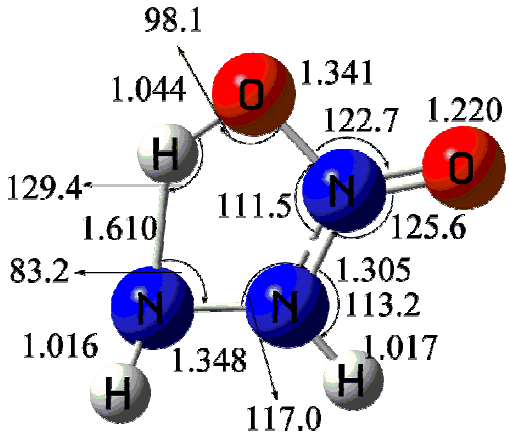

d2-TS2 (C_1)

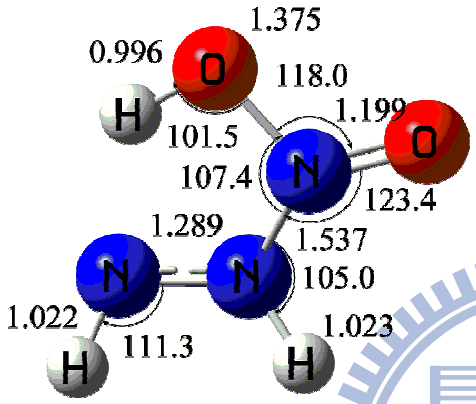

d2-TS3 (C_1)

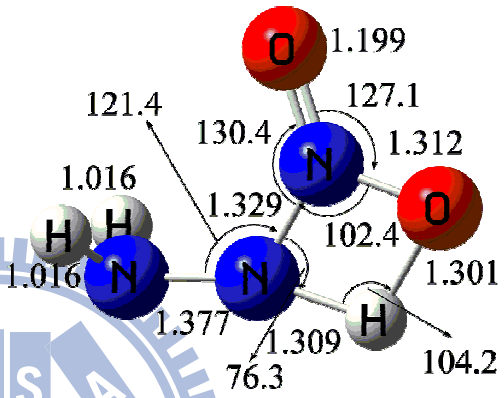

d2-TS4 (C_1)

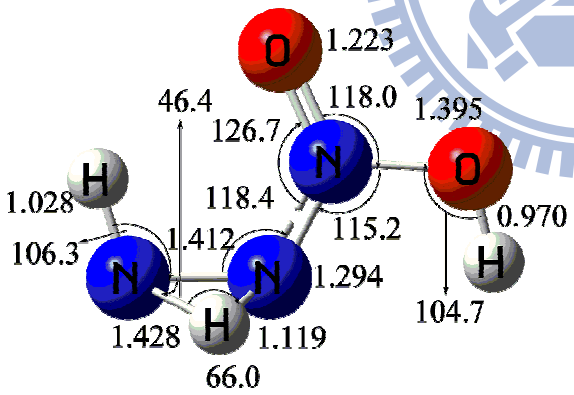

d2-TS5 (C_1)

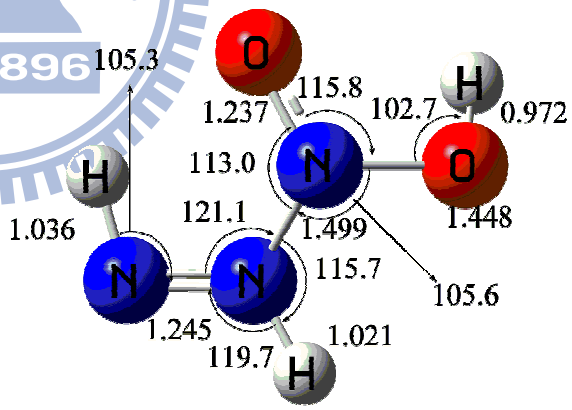

d2-TS6 (C_1)

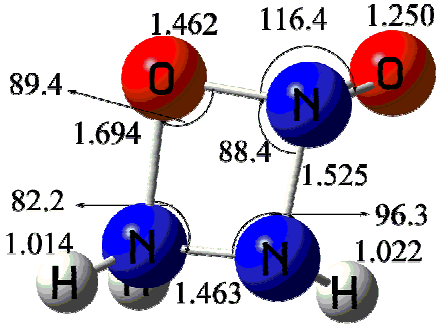

d2-TS7 (C_1)

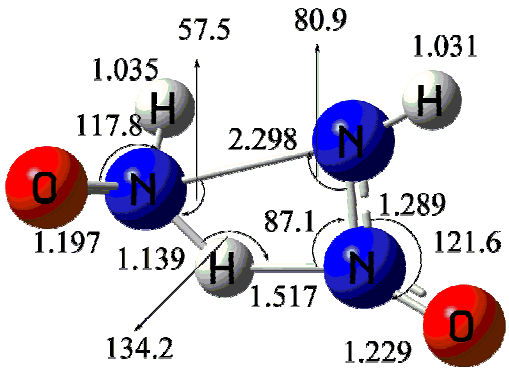

d2-TS8 (C_1)

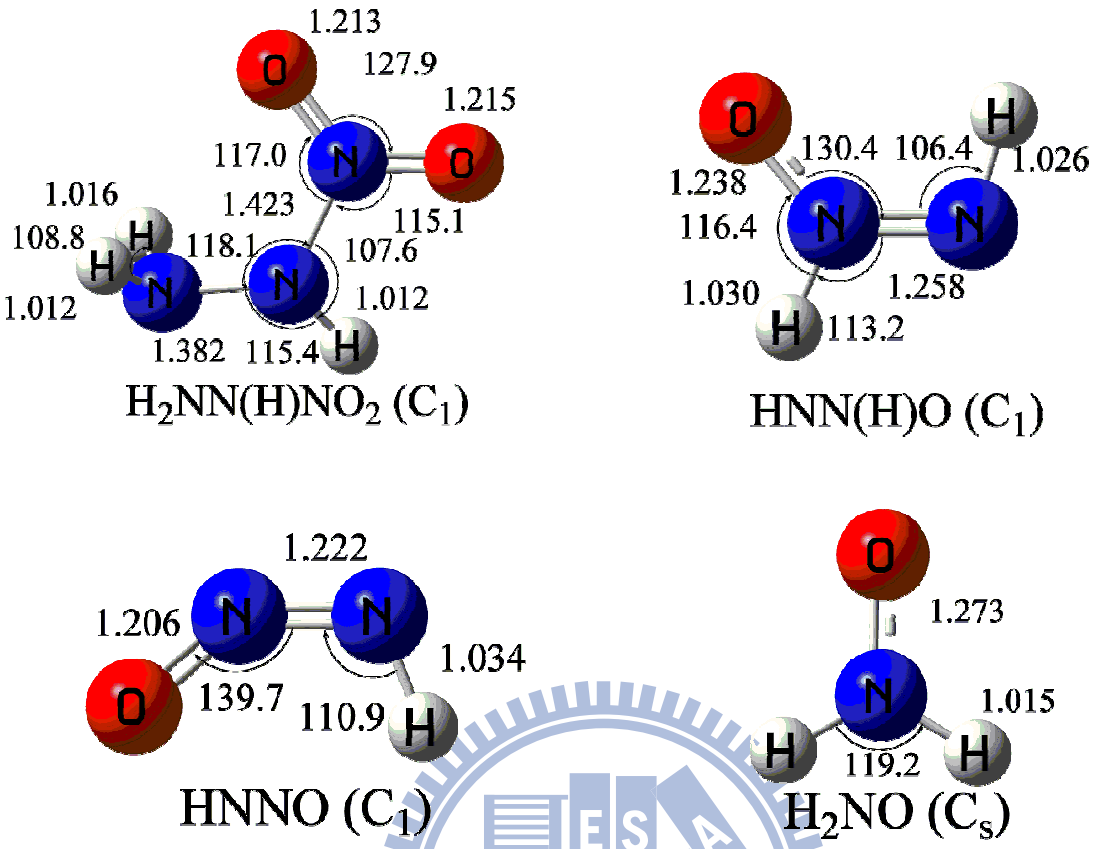

Fig3-15: The stationary points in the PES of $H_2NN(H)NO_2$ decomposition are optimized by B3LYP/6-311++G(3df,2p).

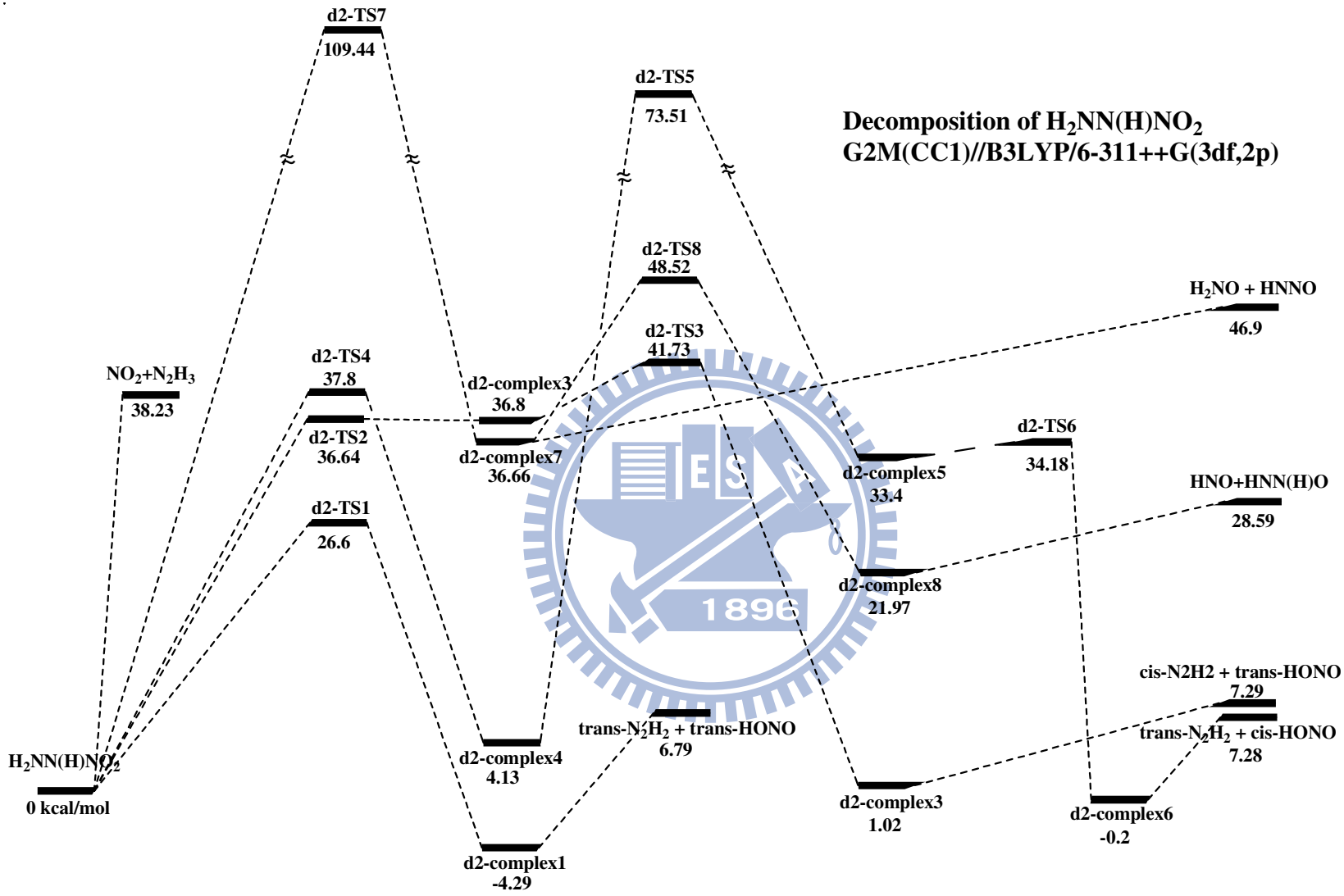

Fig3-16: Potential Energy Surface of $H_2NN(H)NO_2$ decomposition, whose energies are calculated by G2M(CC1) // B3LYP/6-311++G(3df,2p).

Table3-24: Moments of inertia (I_A, I_B, I_C) and vibration frequencies of the species in $H_2NN(H)NO_2$ decomposition computed at B3LYP/6-311++G(3df,2p).

Species or Transition States	Moments of inertia I_i(a.u)	Vibrational Frequency υ_j (cm^{-1})
$H_2NN(H)NO_2$	155.4, 394.6, 534.8	173, 313, 330, 498, 590, 790, 795, 851, 976, 1236, 1315, 1367, 1430, 1663, 1705, 3472, 3562, 3577
d2-Complex1	131.9, 869.9, 1001.8	75, 84, 151, 180, 226, 301, 699, 894, 916, 1340, 1359, 1479, 1600, 1663, 1751, 3262, 3302, 3351
d2-Complex2	156.1, 368.8, 523.3	161, 296, 395, 505, 553, 598, 749, 777, 899, 1118, 1204, 1364, 1446, 1553, 1696, 2976, 3499, 3529
d2-Complex3	61.5, 1229.1, 1290.6	27, 49, 121, 126, 219, 239, 701, 890, 920, 1276, 1357, 1464, 1553, 1668, 1744, 3163, 3236, 3397
d2-Complex4	153.9, 387.9, 539.8	290, 347, 371, 394, 533, 643, 666, 752, 974, 1134, 1286, 1329, 1393, 1600, 1700, 3458, 3626, 3734
d2-Complex5	165.3, 392.0, 546.0	152, 248, 315, 413,460, 590, 637, 907, 916, 1037, 1256, 1343, 1474, 1529, 1540, 3399, 3528, 3695
d2-Complex6	179.2, 670.6, 849.8	82, 129, 186, 191, 238, 362, 713, 958, 997, 1344, 1356, 1471, 1599, 1662, 1667, 3089, 3258, 3303
d2-Complex7	92.3, 639.0, 664.8	110, 225, 337, 401, 621, 696, 803, 1031, 1132, 1205, 1316, 1396, 1454, 1621, 1644, 3196, 3250, 3405
d2-Complex8	123.7, 1093.3, 1217.0	22, 52, 111, 114, 177, 318, 684, 908, 1137, 1270, 1426, 1530, 1553, 1621, 1687, 2971, 3263, 3406
d2-TS1	144.5, 598.0, 726.4	375i, 155, 240, 250, 349, 431, 778, 822, 1063, 1141, 1277, 1483, 1553, 1567, 1693, 2613, 3454, 3488
d2-TS2	153.4, 366.7, 517.2	274i, 282, 426, 540, 566, 581, 767, 881, 944, 1100, 1186, 1337, 1447, 1542, 13663, 2565, 3499, 3503
d2-TS3	161.2, 403.2, 554.6	552i, 203, 284, 449, 568, 686, 719, 767, 853, 983, 1293, 1328, 1413, 1478, 1623, 3254, 3387, 3417
d2-TS4	168.6, 379.6, 538.3	1847i, 102, 195, 309, 657, 744, 750, 814, 1005, 1012, 1232, 1302, 1323, 1606, 1669, 2275, 3451, 3539
d2-TS5	158.4, 400.2, 552.3	1604i, 253, 256, 313, 475, 505, 628, 661, 863, 956, 1114, 1259, 1317, 1412, 1622, 2672, 3369, 3738
d2-TS6	168.1, 403.9, 547.8	374i, 192, 282, 336, 449, 539, 611, 834, 880, 1034, 1261, 1307, 1452, 1509, 1530, 3272, 3462, 3687
d2-TS7	167.8, 340.1, 428.1	1250i, 103, 425, 503, 608, 664, 692, 838, 885, 1022, 1046, 1198, 1319, 1466, 1600, 3393, 3423, 3576

d2-TS8	106.8, 776.9, 838.4	380i, 94, 160, 280, 317, 537, 710, 777, 896, 1252, 1343, 1373, 1508, 1597, 1697, 1890, 3265, 3310
NO_2	7.4, 137.6, 145.0	767, 1395, 1703
N_2H_3	8.8, 58.6, 66.5	548, 696, 1136, 1238, 1479, 1658, 3425, 3488, 3632
H_2NO	5.6, 52.6, 58.1	273, 1270, 1385, 1662, 3450, 3550
HNNO	10.6, 143.9, 154.5	595, 751, 1218, 1337, 1728, 3245
HNN(H)O	21.2, 140.8, 162.0	684, 899, 1089, 1262, 1437, 1534, 1610, 3320, 3404
HNO	3.2, 41.9, 45.1	1562, 1672, 2876
trans-HONO	19.0, 143.1, 162.1	590, 621, 819, 1303, 1783, 3773
cis-HONO	21.1, 135.9, 157.0	635, 695, 876, 1342, 1716, 3597
trans-N_2H_2	5.9, 45.4, 51.3	1341, 1351, 1588, 1652, 3235, 3036
cis-N_2H_2	6.1, 45.6, 51.8	1281, 1361, 1555, 1651, 3102, 3195

Table3-25: Relative energies of species in $H_2NN(H)NO_2$ decomposition computed at various theoretical levels. [a]

Species or Transition States	ZPE [b]	B3LYP/ 6-311++G(3df,2p)	CCSD(T)/ 6-311+G(d,p) [c]	CCSD(T)/ 6-311++G(3df,2p) [c]	G2M(CC1) [c]
$H_2NN(H)NO_2$	35.23	-316.432294	-315.6739897	-315.8661044	-315.9584804
complex1	32.36	-0.27	-9.44	-4.44	-4.29
complex2	33.39	35.35	38.84	37.24	36.8
complex3	31.67	4.6	-3.45	0.95	1.02
complex4	34.11	12.59	4.6	4.28	4.13
complex5	33.51	34.63	34.05	34.35	33.4
complex6	32.36	-0.2	-8.63	-4.4	-4.09
complex7	34.08	37.21	35.97	36.98	36.66
complex8	31.81	25.6	18.43	22.04	21.97
$NO_2+N_2H_3$	30.26	28.66	30.57	34.29	38.23
trans-HONO+ trans-N_2H_2	30.48	5.23	9.97	6.8	6.79
trans-HONO+H_2NN	29.45	25.68	29.9	26.13	26.17
trans-HONO+cis-N_2H_2	30.07	10.23	11.61	7.33	7.29
cis-HONO+trans-N_2H_2	30.44	5.77	2.62	7.16	7.28
H_2NO+HNNO	29.21	34.05	40.46	43.34	46.9
HNN(H)O+HNO	30.52	28.59	22.56	26.27	26.05
TS1	31.96	23.37	24.93	27.44	26.6
TS2	32.65	34.67	38.24	37	36.64
TS3	32.46	41.73	42.06	43.16	42.44
TS4	31.43	37.21	39.17	38.07	37.8
TS5	30.65	77.48	74.81	74.19	73.51
TS6	32.36	34.18	32.95	34.13	33.13
TS7	32.54	112.89	111.53	111.24	109.44
TS8	30.03	48.82	49.88	52.61	52.42

[a]: The relative energy (kcal/mol) is based on the energy of $H_2NN(H)NO_2$ as reference, whose energy unit is hartree/molecule.

[b]: The ZPE is determined by B3LYP/6-311++G(3df,2p) level, and the energy unit is kcal/mol for every specie.

[c]: The energies are including single-point energies, based on geometries of B3LYP/6-311++G(3df,2p), and ZPE.

3.3.5 The single-point energies in N_2H_4+N_2O_4 isomeric reactions

In Table3-26, the energies of the reactant and product species predicted by different computational methods are listed. The heats of reaction can be easily calculated with the heats of formation for reactants and products, and the difference between experimental and computational values is the way to determine whether a computational method performs well in this system or not. In Table3-27, the average differences in heat of reaction on monomer reactions are -0.41, 0.2, -0.33, and -0.34 kcal/mol by CCSD(T)/6-311+G(d,p), CCSD(T)/6-311++G(3df,2p), G2M(CC3), and G2M(CC1) methods, respectively. Although, the CCSD(T)/6-311+G(d,p) is the worst, the difference between the errors computed by the CCSD(T) methods is only 0.6 kcal/mol. On the other hand, the G2M methods perform well and similarly. For the N_2H_4+N_2O_4 reaction, which includes more number of molecules, the average difference between experimental and computational values is -2.94, 0.26, 0.72, and 0.88 kcal/mol by CCSD(T)/6-311+G(d,p), CCSD(T)/6-311++G(3df,2p), G2M(CC3), and G2M(CC1) methods, respectively. The CCSD(T)/6-311+G(d,p) method is still the worst; the difference is apparently large. Moreover, the error for every case is about the same, which is above -2 kcal/mol at least; therefore, the single-point energies calculated by CCSD(T)/6-311+G(d,p) in dimer reaction are not reliable. On the other hand, the CCSD(T) with a bigger basis set performs well in both dimer and monomer reactions. The large error with the G2M method is only for the case of N_2H_4+N_2O_4→trans-HONO+N_2H_3+NO_2, which is 2.67 and 2.57 by CC3 and CC1, respectively. For other cases, the G2M method provides better predictions than CCSD(T), and the most important thing is that CC3 and CC1 calculations maintain similar and stable performances. Even though the number of heavy atoms is too large to use the CCSD(T)/6-311++G(3df,2p), the G2M(CC3) method still provides reliable predictions for the N_2H_4+N_2O_4 reaction system.

Table3-26: The heats of formation based on experimental and computational studies.

	Exp [a]	CCSD(T)/ 6-311+G(d,p) [b]	CCSD(T)/ 6-311++G(3df,2p) [b]	G2M(CC3) [b]	G2M(CC1) [b]
N_2O_4	4.47	-409.3648607	-409.6067069	-409.6987294	-409.7113339
N_2H_4	26.14	-111.5732783	-111.6428137	-111.6816838	-111.6854736
cis-HONO	-16.844	-205.2927121	-205.4135918	-205.4627235	-205.4689568
trans-HONO	-17.36	-205.2944057	-205.4141683	-205.4634289	-205.4697452
N_2H_3	55.33	-110.9500308	-111.017559	-111.050437	-111.0543067
NO_2	8.58	-204.67525	-204.7939044	-204.8368898	-204.8432513
NO	21.45	-129.641594	-129.7127854	-129.7154744	-129.7437266
cis-N_2H_2	52.56	-110.3744822	-110.4402507	-110.4736947	-110.4771367
HNO	24.49	-130.2099216	-130.284393	-130.3172662	-130.3213907

[a]: The value is from reference (23), and the unit is kcal/mol.

[b]:The computational value is the sum of the zero-point energy of B3LYP/6-311++G(3df,2p) and the electronic energy at the specified method. The unit is hartree/molecule.

Table3-27: The heats of reaction of N_2H_4+NO_2 and N_2H_4+N_2O_4 reaction computed by the values from Table3-24. [a]

	Exp	CCSD(T)/ 6-311+G(d,p)	CCSD(T)/ 6-311++G(3df,2p)	G2M(CC3)	G2M(CC1)
Reactants: N_2H_4+NO_2					
cis-HONO+N_2H_3	3.76	3.63	3.49	3.40	3.40
trans-HONO+N_2H_3	3.25	2.57	3.13	2.95	2.93
Reactants: N_2H_4+N_2O_4					
trans-HONO+cis-HONO+cis-N_2H_2	-12.26	-14.72	-11.60	-12.19	-11.94
trans-HONO+[$H_2NN(H)NO_2$→ trans-HONO+cis-N_2H_2]	-12.78	-15.78	-11.96	-12.64	-12.44
cis-N_2H_2+ 2 cis-HONO	-11.75	-13.66	-11.24	-11.75	-11.45
trans-HONO+N_2H_3+NO_2	15.94	11.58	14.99	18.61	18.51

[a]: All values are in the unit of kcal/mol

3.4 Reference

(1) F.B.C. Machado and O. Roberto-Neto, Chem. Phys. Lett., 352, 120-126 (2002)

(2) M.H. Matus, A.J. Arduengo, and D.A. Dixon, J. Phys. Chem. A, 110(33), 10116-10121 (2006)

(3) S. Tsunekawa, J. Phys. Soc. Jpn., 41, 2077 (1976)

(4) S. Tsunekawa and T. Kogima, J. Phys. Soc. Jpn., 44, 1825 (1978)

(5) M. Tsuboi and J. Overend, J. Mol. Spectrosc., 52, 256 (1974)

(6) Y. Morino, T. Yijima, and Y. Murata, Bull. Chem. Soc. Jpn., 33, 46 (1960)

(7) K. Kohata, T. Fukuyama, and K. Kuchitsu, J. Phys. Chem. 86, 602 (1982)

(8) A. Yamaguchi, I. Ichisima, T. Shimanouchi, S. Mizushima, Spectochim. Acta, 16, 1471 (1960)

(9) J.R. During, M.G. Griffin, and R.W. MacNamee, J. Raman Spectrosc., 3, 133 (1975)

(10) L.V. Gurvich, I.V. Veytes, C.B. Alcock, *Thermodynamic Properties of Individual Substance,* 4th ed, Hemisphere Pub., New York, 1989

(11) M.W. Chase Jr., *NIST-JANAF Thermochemical Tables*, 4th ed., J. Phys. Chem. Ref. Data, Monograph, vol.9 (1998)

(12) N. Tanaka, Y.Hamada, Y.Sugawara, M. Tsuboi, S. Kato, and K. Morokuma, J. Mol. Spectrosc. 99, 245 (1983)

(13) J.R. During, S.F. Bush, and E.E. Mercer, J. Chem. Phys., 44, 4238 (1966)

(14) E. Catalano, R.H. Sanborn, and J.W. Frazer, J. Chem. Phys., 38, 2265 (1963)

(15) P.A. Giguere, and I.D. Liu, J. Chem. Phys., 20, 136 (1952)

(16) M.L. McKee, J. Am. Chem. Soc., 117, 1629-1637 (1995)

(17) F.R. Ornellas, S.M. Resende, F.B.C. Machado, and O. Roberto-Neto, J. Chem. Phys., 118, 4060 (2003)

(18) A. Stirling, I. Papai, and J. Mink, J. Che,. Phys., 100, 2910 (1994)

(19) Y. Morino, M. Tanimoto, S. Saito, E. Hirota, R. Awata, and T. Tanaka, J. Mol. Spectrosc, 98, 330 (1983)

(20) G.R. Bird, J.C. Baird, A.C. Jache, J.A. Hodgeson, R.F. Curl, Jr., A.C. Kunkle, J.W. Bransford, J. Rastrup-Andersen, and J. Rosenthal, J. Chem. Phys. 40, 3378 (1964)

(21) H.B. Schlegel and A. Skancke, J. Am. Chem. Soc., 115, 7465-7471 (1993)

(22) B. Ruscic and J. Berkowitz, J. Chem. Phys., 95(6), 4378 (1991)

(23) Chase, M.W., Jr., C.A. Davles, J.R. Downey, Jr., D.J. Frurip, R.A. McDonald, A.N. Syverud, *NIST-JANAF Themochemical Tables, Fourth Edition*, J. Phys. Chem. Ref. Data, 9, 1-1951 (1998).

(24) NIST Standard Reference Data, http://webbook.nist.gov/chemistry/

(25) K.J. Laidler, *Chemical Kinetics*, 3rd ed., Harper and Row: New York (1987)

(26) J.I. Steinfeld, J.S. Francisco, W.L. Hase, *Chemical Kinetics and Dynamics*, Prentice Hall: Englewood Cliffs, NJ (1989)

(27) I.C. Hisatsune, J. Phys. Chem., 65, 2249 (1961)

(28) W.F. Giauque and J.D. Kemp, J. Chem. Phys., 6, 40 (1938)

(29) A.S. Primetel, F.C.A. Lima, and A.B.F. da Silva, J. Phys. Chem. A, 111, 2913-2920 (2007)

(30) J. Koupt, Chem. Phys. Lett., 240, 553 (1995)

(31) K.B. Borisenko, M. Kolonits, B. Rozsondaia, and I. Hargittai, J. Mol. Struct., 121, 413 (1997)

(32) B.S. Cartwright and J.H. Robertson, Chem. Commum. (London), 3, 82 (1966)

(33) A. Kvick, R. K. McMullan, and M.D. Newton, J. Chem. Phys., 76, 3754 (1982)

(34) J.L. Domenech, A.M. Andrews, S.P. Belov, G.T. Fraser, and W.J. Lafferty, J. Chem. Phys., 100, 6993 (1994)

(35) Y. Elyoussoufi, M. Herman, J. Lievin, and I. Kleiner, Spectrochim. Acta, Part A, 53, 881 (1997)

(36) (a) X. Wang, Q.-Z. Qin, K. Fan, J. Mole. Struct. (Theochem), 432, 55-62, (1998)

(b) X. Wang and Q.-Z. Qin, Inter. J. Quant. Chem. 76, 77-82 (2000)

(37) R.V. St. Louis and B. Carwford, Jr., J. Chem. Phys., 42, 587 (1965)

(38) I.C. Hisatsune, J.P. Devlin, and Y. Wasa, J. Chem. Phys., 33, 714 (1960)

(39) F. Melen, M. Herman, J. Phys. Chem. Ref. Data., 21, 831 (1992)

(40) I.I. Zakjarov, A.I. Kolbasin, O.I. Zakharova, I.V. Kravchenko, and V.I.Dyshlovoi, Theoretical and Experimental Chem., 44, 26 (2008)

(41) L.H. Jones, B.I. Swanson, and S.F. Agnew, J. Chem. Phys. 82, 4389 (1985)

(42) A. Givan and A. Loewenschuss, J. Chem. Phys. 90, 6135 (1989)

(43) M. Cher, J. Chem. Phys., 37, 2564 (1962)

(44) T. Carrington and N. Davidson, J. Phys. Chem., 57, 418 (1953)

IV. Conclusion

In this work, we have studied the mechanisms for reactions of N_2H_4 with NO_2 and N_2O_4 in order to understand why hydrazine and dinitrogen tetroxide react hypergolically. Moreover, the structures of the N_2O_4 isomers, which are still unknown experimentally, have been investigated. They include $N_2O_4(D_{2h})$, trans-$ONONO_2$, and cis-$ONONO_2$. Mechanistically, reactions of N_2H_4 with these isomers and NO_2 have been considered. The results show that the reactions taking place by hydrogen transfer are the lower-energy channels. The lowest energy channel has been identified to be the N_2H_4 + trans-$ONONO_2$ reaction, in which the two reactants form an intermediate, which can undergoes the hydrogen transfer reaction barrierlessly. Therefore, it is believed that the hypergolic reaction of N_2H_4 and N_2O_4 is initiated by the reaction of N_2H_4 with trans-$ONONO_2$, because the product $H_2NN(H)NO$ can directly dissociate to the N_2H_3 and NO with only 27.83 kcal/mol dissociation energy at the G2M(CC1) level. Other decomposition channels are too high to occur.

We predict the structures of the N_2O_4 isomers by B3LYP /6-311++G(3df,2p), and the deviations of their vibrational frequencies comparing with the experimental data are less than 25 cm^{-1} on average. The trans-$ONONO_2$ structure optimized by different methods including B3LYP, PW91PW91, BHandHLYP, and CCSD have similar results, indicating that the ON-ONO_2 bond is the longest. However, the cis-$ONONO_2$ isomer has two types of structures, with two longest bonds ON-ONO_2 and ONO-NO_2. The PES of the N_2O_4 isomerization describes the relationship among these N_2O_4 isomers, and the results are in agreement with experimental observations including the cis-trans isomerization and autoionization.

In other bimolecular reactions of the N_2H_4 + N_2O_4 system, hydrogen abstraction reactions are still the major and lower-energy channels; those involving N-O bond breaking

need to overcome much higher energy barriers. For the N_2H_4 and NO_2 reaction, the products of the lowest-energy path are cis-HONO and N_2H_3, whose energy barrier is 7.57 kcal/mol calculated by G2M(CC1). Based on the Transition State Theory, the rate constant of the lowest-energy channel is $3.20\times10^{-25}T^{3.74}\exp(-1662.5/T)$ $cm^3molecule^{-1}sec^{-1}$ at T=100–4000 K. The other products, such as trans-HONO + N_2H_3, HNO_2 + N_2H_3, and $H_2NN(H)OH$ + NO, have higher energy barriers than that for cis-HONO + N_2H_3 formation.

For the N_2H_4 + $N_2O_4(D_{2h})$ and N_2H_4 + cis-$ONONO_2$ reactions, the transition states of hydrogen transfer are all ring-like structures, including four-member to seven-member rings. The lowest-energy channels for both reactions form trans-HONO and $H_2NN(H)NO_2$ molecules, whose energy barriers are higher than their intermediates by 21.1 and 14.4 kcal/mol predicted at the G2M(CC3) level for N_2H_4 + $N_2O_4(D_{2h})$ and N_2H_4 + cis-$ONONO_2$ reactions, respectively. Furthermore, the $H_2NN(H)NO_2$ may decompose to trans-N_2H_2 and trans-HONO via five-member ring TS of 26.6 kcal/mol, or it may directly dissociate to N_2H_3 radical and NO_2 molecule with the dissociation energy of 38.23 kcal/mol computed by G2M(CC1).

In all calculations, the B3LYP calculations can provide a good prediction and save the computational resources for this eight heavy-atom system; it is the advantage of DFT methods. The G2M method provides reliable calculations of the single point energy as good as CCSD(T)/6-311++G(3df,2p), and it also has smaller differences in heats of reaction comparing with experimental data.

Appendix I. Geometries of Stationary Points in Reactions

A2.1 N_2H_4+NO_2 Reaction

N_2H_4 (C_2)

0 1

N	0.00000000	0.00000000	0.00000000
N	-0.54472189	-0.64113660	1.15924094
H	1.01499390	0.00000000	0.00000000
H	-0.31477390	0.96130877	0.00000000
H	0.06900573	-0.56898526	1.96443189
H	-0.66666316	-1.62179697	0.94328899

NO_2 (C_{2v})

0 2

N	0.00000000	0.00000000	0.00000000
O	1.19004232	0.00000000	0.00000000
O	-0.83419585	0.84871551	0.00000000

Complex1 (C_1)

0 2

N	0.00000000	0.00000000	0.00000000
H	1.01509992	0.00000000	0.00000000
H	-0.32236307	0.95876991	0.00000000
N	-0.55495858	-0.66456103	-1.13734986
H	0.06168211	-0.62516363	-1.94200366
H	-0.69750017	-1.63658529	-0.89062700
O	-0.76339367	-1.36237429	3.06409103
O	-1.00681161	-2.69843036	1.34582577
N	-1.13943267	-1.70050759	1.98779595

Complex2 (Cs)

0 2

N	0.00000000	0.00000000	0.00000000
H	1.01968248	0.00000000	0.00000000
H	-0.26270017	0.98526140	0.00000000
N	-0.42406447	-0.55195252	-1.26517439
H	-1.43921838	-0.54489968	-1.25740058
H	-0.15571623	-1.53102158	-1.25739461
N	1.98317756	2.58122225	-0.73802318
O	0.82537312	2.85857765	-0.56905883
O	2.54944932	1.53394878	-0.56908261

Complex3 (C_1)

0 2

N	0.00000000	0.00000000	0.00000000
H	1.01883051	0.00000000	0.00000000
H	-0.84604857	1.56936011	0.00000000
N	-0.42488392	-1.25579101	-0.17222791
H	-1.41106572	-1.40054109	-0.02210501
H	0.17644330	-2.04076084	0.03912968
N	-0.56989347	3.48984053	0.07369767
O	-1.39652783	2.41253084	0.00291955
O	0.58717108	3.22210923	0.11578940

Complex4 (C_1)

0 2

N	0.00000000	0.00000000	0.00000000
H	1.01056090	0.00000000	0.00000000
H	-0.46442431	0.89797537	0.00000000
N	-0.69116453	-0.98063693	-0.58868243
H	-0.08966011	-1.79583697	-0.68273074
H	-2.33202530	-0.48745816	-0.93386529
O	-3.70130265	2.07159062	-0.73091655
O	-3.17773271	0.03509070	-1.05684625
N	-2.81800172	1.29455882	-0.65392500

Complex5 (C_1)

0 2

N	0.00000000	0.00000000	0.00000000
H	1.01059178	0.00000000	0.00000000
H	-0.47316043	0.89427447	0.00000000
N	-0.69524692	-0.99233305	-0.56517150
H	-2.37531415	-0.40945092	-0.91742942

H	-0.08928612	-1.80502518	-0.65597507
O	-4.20739850	0.17577433	-1.34471250
O	-2.63553550	1.46119208	-0.55987206
N	-3.08084850	0.38550795	-0.94802084

Complex6 (C_1)

0 2

N	0.00000000	0.00000000	0.00000000
H	1.01847254	0.00000000	0.00000000
H	-0.26485750	0.98318140	0.00000000
N	-0.34680567	-0.46113670	-1.35009925
H	-0.15804753	-1.47117879	-1.33571273
H	-1.38199231	-0.35162440	-1.39591228
O	-2.42778804	0.90010508	-2.47418379
O	0.24824588	0.14811715	-2.36594749
N	-1.58569665	1.29702627	-3.17740326

$H_2NN(O)H_2$ (Cs)

0 1

N	0.00000000	0.00000000	0.00000000
H	1.01920186	0.00000000	0.00000000
H	-0.24953050	0.98818339	0.00000000
N	-0.33017496	-0.42391249	-1.38480775
H	-0.06077961	-1.41982707	-1.39365345
H	-1.36173626	-0.40655220	-1.39365022
O	0.20980612	0.26937893	-2.36770766

TS1 (C_1)

0 2

N	2.21007300	0.00739800	-0.53834300
H	2.96975500	-0.66085300	-0.45101700
H	2.65228900	0.91961700	-0.57883600
N	1.47665900	-0.05086500	0.70820100
H	0.90826400	0.79037300	0.76595700
H	0.80851700	-0.81736300	0.62204300
N	-1.76466600	0.00632100	-0.20689900
O	-1.29915300	-1.08634800	-0.03068600
O	-1.30000700	1.08987900	0.01832800

TS2 (C_1)

0 2

N	0.00000000	0.00000000	0.00000000
H	1.01849545	0.00000000	0.00000000
H	-0.34449470	1.09139080	0.00000000
N	-0.47588778	-0.72569465	-1.03712176
H	-1.47570523	-0.86413454	-1.01992010
H	0.06737095	-1.52790763	-1.31859779
N	0.61113507	2.97552121	-0.51311794
O	-0.50599540	2.46409838	-0.18773140
O	1.57107503	2.23116813	-0.61332168

TS3 (C_1)

0 2

N	-1.72626200	-0.80616200	0.06060100
H	-2.58090200	-1.27875000	0.31065600
H	-1.05917700	-1.29019500	-0.52027200
N	-1.77235600	0.53215100	-0.13295000
H	-2.39461200	0.97852200	0.53182200
H	-0.76376700	0.92699400	-0.13655100
O	2.22679000	-0.52979200	0.02561900
O	0.75150400	1.02825500	0.03063800
N	1.06606200	-0.20088600	-0.01846700

TS4 (C_1)

0 2

N	0.00000000	0.00000000	0.00000000
H	1.01307190	0.00000000	0.00000000
H	-0.43361948	0.91915170	0.00000000
N	-0.64219540	-0.85808012	-0.81639386
H	-1.18448328	-0.26263267	-1.70120027
H	-0.03478024	-1.62556040	-1.08864045
O	-1.99872604	0.82383403	-3.59217659
O	-1.39580610	1.85534747	-1.78448368
N	-1.56249483	0.83308613	-2.46052765

TS5 (C_1)

0 2

N	0.00000000	0.00000000	0.00000000
H	1.01611152	0.00000000	0.00000000
H	-0.30897838	0.96746169	0.00000000
N	-0.43907266	-0.56886743	-1.19289998
H	-0.26359545	-1.56728295	-1.23518078
H	-1.41910812	-0.28014028	-1.41809247
O	-1.91413651	0.74719196	-2.76377940
O	0.19047799	0.08536953	-2.52246549
N	-0.93166197	0.36219098	-3.42209332

TS6 (C_1)

0 1

N	0.00000000	0.00000000	0.00000000
H	1.01423263	0.00000000	0.00000000
H	-0.29353736	0.97752680	0.00000000
N	-0.41725539	-0.55397481	-1.21345303
H	0.23677865	-0.91143166	-2.04504882
H	-1.40630200	-0.77309880	-1.19340188
O	-0.13192708	0.26902985	-2.43505682

NO (C_1)

0 2

N	0.00000000	0.00000000	0.00000000
O	1.14463700	0.00000000	0.00000000

N_2H_3 (C_1)

0 2

N	0.00000000	0.00000000	0.00000000
H	1.01258167	0.00000000	0.00000000
H	-0.42282211	0.91526553	0.00000000
N	-0.68954091	-0.92239768	0.69867227
H	-0.07034688	-1.72893980	0.79848878

cis-HONO (C_1)

0 1

H	0.00000000	0.00000000	0.00000000
N	1.91042837	0.00000000	0.00000000
O	0.70186949	0.68164381	0.00000000
O	1.79615677	-1.17093862	-0.00000000

trans-HONO (C_1)

0 1

H	0.00000000	0.00000000	0.00000000
N	1.89534734	0.00000000	0.00000000
O	0.65704761	0.71055331	0.00000000
O	2.79881935	0.73219332	-0.00019577

HNO_2 (C_{2v})

0 1

H	0.00000000	0.00000000	0.00000000
O	1.91231819	0.00000000	0.00000000
O	0.66658895	1.79260407	0.00000000
N	0.85550353	0.59472736	0.00000000

$H_2NN(H)OH$ (C_1)

0 1

N	1.19043000	-0.15319500	-0.02108700
H	1.36131500	-0.71358400	0.80391900
H	1.15032500	-0.76528700	-0.83407100
N	0.00697600	0.56083300	0.15414100
H	-1.60935400	-0.32235800	0.72132500
H	-0.04041800	1.22534500	-0.61044400
O	-1.15546400	-0.28469800	-0.12651300

A2.2 N_2O_4 Isomers

$N_2O_4(D_{2h})$

0 1

N	0.00000000	0.00000000	0.00000000
N	1.80007200	0.00000000	0.00000000
O	2.25489700	1.09359700	0.00000000
O	2.25489700	-1.09359700	0.00000000
O	-0.45482500	1.09359700	0.00000000
O	-0.45482500	-1.09359700	-0.00000000

trans-$ONONO_2$ (C_s)

0 1

N	0.00000000	0.00000000	0.00000000
O	1.19966850	0.00000000	0.00000000
O	-0.77102768	0.91523496	0.00000000
N	0.38137710	-2.49581696	0.00144223
O	-0.22751915	-3.44683747	0.00100714
O	-0.66176246	-1.25536698	-0.00008869

cis-$ONONO_2$ (C_s)

0 1

N	0.00000000	0.00000000	0.00000000
O	1.17702044	0.00000000	0.00000000
O	-0.84057884	0.82389502	0.00000000
N	-0.84654162	-2.07319749	1.13355663
O	-0.58237455	-1.42639481	2.08020412
O	-0.61942181	-1.51687617	-0.07853316

cis-$ONONO_2$_2 (C_1)

0 1

N	0.00000000	0.00000000	0.00000000
O	1.20892355	0.00000000	0.00000000
O	-0.75626308	0.93109366	0.00000000
N	0.12563524	-2.47905369	-0.85933482
O	1.02234688	-2.17537162	-1.45535887
O	-0.62243349	-1.24906634	0.01590401

cis-$ONONO_2$_3 (C_s)

0 1

N	0.00000000	0.94562700	0.00000000
O	1.16461100	0.60517300	0.00000000
O	-0.44983000	2.05819400	0.00000000
N	-0.45638800	-1.72788300	0.00000000
O	0.63649500	-1.93043100	0.00000000
O	-0.95193700	-0.04846100	0.00000000

i-TS1 (C_s)

0 1

N	0.00000000	0.00000000	0.00000000
O	1.16203260	0.00000000	0.00000000
O	-0.92286866	0.70613815	0.00000000
N	-0.65675574	-1.93909753	-0.39165029
O	-1.01351973	-2.99245717	-0.81054912
O	-0.59828946	-1.76647212	0.87633430

i-TS2 (C_1)

0 1

N	0.00000000	0.00000000	0.00000000
O	1.18720389	0.00000000	0.00000000
O	-0.82853799	0.85059233	0.00000000
N	0.74500347	-2.54126021	-0.40673260
O	0.03748693	-2.63548238	0.47941119
O	-1.87365324	-2.18058269	-0.46257476

i-TS3 (C_1)

0 1

N	-0.87309600	0.00612100	-0.06191600
O	-1.07102800	1.16854800	-0.23476000
O	-1.41830200	-0.80069600	0.62364100
N	1.60787500	-0.22630600	-0.25069800
O	1.58609100	0.36551000	0.73051400
O	0.26030700	-0.54070000	-0.84585600

i-TS4 (C_1)

0 1

N	0.00000000	0.00000000	0.00000000
O	1.21579974	0.00000000	0.00000000
O	-0.74177089	0.94502020	0.00000000
N	0.52064332	-2.55066968	0.03143088
O	1.02519055	-2.61358091	1.01976574
O	-0.63278296	-1.21412245	-0.01019251

NO (C_1)

0 2

N	0.00000000	0.00000000	-0.61047300
O	0.00000000	0.00000000	0.53416400

NO_3 (C_{3h})

0 2

N	0.00000000	0.00218100	0.00000000
O	-0.84406000	-0.89428800	0.00000000
O	1.19616500	-0.28715100	0.00000000
O	-0.35210500	1.17953100	0.00000000

NO^+ (C_1)

1 1

N	0.00000000	0.00000000	-0.56340500
O	0.00000000	0.00000000	0.49298000

NO_3^- (C_{3h})

-1 1

N	0.00000000	0.00009500	0.00000000
O	-0.77423300	0.98977700	0.00000000
O	1.24419000	0.17487200	0.00000000
O	-0.46995700	-1.16473200	0.00000000

N_2O_4_ PW 91PW91 (D_{2h})

0 1

N	0.00000000	0.00000000	0.92918200
N	0.00000000	0.00000000	-0.92918200
O	0.00000000	1.10389800	-1.38796000
O	0.00000000	-1.10389800	-1.38796000
O	0.00000000	1.10389800	1.38796000
O	0.00000000	-1.10389800	1.38796000

trans-$ONONO_2$_ PW91PW91 (C_s)

0 1

N	-1.06037300	0.03451500	-0.00002400
O	-1.04287700	1.23914700	-0.00008400
O	-1.97843200	-0.74473300	0.00030800
N	1.46957800	0.39545200	0.00012800
O	2.44030700	-0.20903300	0.00018200
O	0.22294800	-0.66160100	-0.00049600

cis-$ONONO_2$_ PW91PW91 (C_{2v})

0 1

N	-0.91090600	0.00000300	0.00030000
O	-1.35358200	-1.10229000	-0.00075900
O	-1.35334600	1.10239900	-0.00029500
N	1.63345000	0.00000800	0.00085100
O	1.03850400	0.00018100	-1.06343300
O	1.03619800	-0.00029900	1.06348000

cis-$ONONO_2$_2_ PW91PW91 (C_1)

0 1

N	0.91156100	0.06685800	-0.06367000
O	0.61740500	1.20848800	-0.35340500
O	1.90613900	-0.37209600	0.46126400
N	-1.65366400	-0.52318300	-0.07064500
O	-1.81601900	0.49643000	0.40499400
O	-0.05818500	-0.93353700	-0.39532800

cis-$ONONO_2$_3_ PW91PW91 (C_s)

0 1

N	0.00000000	0.95405200	0.00000000
O	1.16977400	0.60395300	0.00000000
O	-0.45666100	2.07477000	0.00000000
N	-0.45368500	-1.74657200	0.00000000
O	0.65679200	-1.93907000	0.00000000
O	-0.97293100	-0.04619700	0.00000000

N_2O_4_BHandHLYP (D_{2h})

0 1

N	0.00000000	0.00000000	0.84008800
N	0.00000000	0.00000000	-0.84008800
O	0.00000000	1.07644100	-1.29198100
O	0.00000000	-1.07644100	-1.29198100
O	0.00000000	1.07644100	1.29198100
O	0.00000000	-1.07644100	1.29198100

N	0.00000000	0.00000000	0.84761600
N	0.00000000	0.00000000	-0.84761600
O	0.00000000	1.09362900	-1.30863800
O	0.00000000	-1.09362900	-1.30863800
O	0.00000000	1.09362900	1.30863800
O	0.00000000	-1.09362900	1.30863800

trans-$ONONO_2$_BHandHLYP (C_s)

0 1

N	-0.99887800	0.02293400	-0.00011400
O	-1.02005100	1.20486900	-0.00038800
O	-1.88900000	-0.74912600	0.00068800
N	1.38365400	0.38395100	0.00104400
O	2.33735300	-0.20933600	-0.00009400
O	0.23501800	-0.60243000	-0.00102000

trans-$ONONO_2$_CCSD (C_1)

0 1

N	-1.00636300	0.02395100	-0.03240300
O	-1.02470900	1.22378500	-0.09183100
O	-1.89241400	-0.75246900	0.17177200
N	1.36763000	0.30038600	0.28663100
O	2.36508200	-0.15507500	-0.03251600
O	0.23593100	-0.60003500	-0.26987300

cis-$ONONO_2$_BHandHLYP (C_1)

0 1

N	-0.82729600	-0.00002300	0.06336700
O	-1.20532300	-1.06902400	-0.24941400
O	-1.20213900	1.07298500	-0.23944900
N	1.55199300	-0.00230900	0.31681300
O	1.50732200	0.00401700	-0.81720600
O	0.26603000	-0.00593800	0.97341200

cis-$ONONO_2$_CCSD (C_1)

0 1

N	-0.84085500	0.01766600	-0.07362100
O	-0.89537900	1.17529800	-0.37650400
O	-1.53297100	-0.63214000	0.65256800
N	1.57954800	-0.31846800	-0.19825400
O	1.56402700	0.44385800	0.66224100
O	0.21796600	-0.72381400	-0.70041400

cis-$ONONO_2$_3_BHandHLYP (C_s)

0 1

N	-0.91868200	-0.05822300	0.00000000
O	-0.52413000	-1.18836000	0.00000000
O	-2.04008600	0.31724500	0.00000000
N	1.64853900	0.56592300	0.00000000
O	1.92559200	-0.49236300	0.00000000
O	0.00000000	0.91924100	0.00000000

cis-$ONONO_2$_3_CCSD (C_s)

0 1

N	0.00000000	0.93749800	0.00000000
O	1.16780100	0.60575400	0.00000000
O	-0.45672400	2.04452500	0.00000000
N	-0.46220700	-1.70356500	0.00000000
O	0.63501700	-1.91730400	0.00000000
O	-0.94166400	-0.06266700	0.00000000

N_2O_4_CCSD (D_{2h})

0 1

A2.3 N_2H_4 and N_2O_4 Reactions

A.2.3.1 trans-$ONONO_2$ + N_2O_4 and

cis-$ONONO_2$ +N_2O_4 Reaction

C_s-Complex1 (C_1)

0 1

N	0.00000000	0.00000000	0.00000000
O	1.27477331	0.00000000	0.00000000
O	-0.63069617	1.03430668	0.00000000
N	0.30366649	-2.97407015	-1.00256561
O	-0.26593110	-3.79285962	-0.46616035
O	-0.59032416	-1.13109651	0.01255127
H	0.94286895	-2.57884258	1.81265292
N	1.65879995	-3.10324858	1.31830120
H	1.37074041	-4.07848045	1.25896991
N	1.79377790	-2.55892283	0.05439522
H	1.70185199	-1.48711316	0.04816388
H	2.62130279	-2.90636101	-0.42191950

C_s-Complex2 (C_1)

0 1

N	2.04917400	0.00956800	-0.09409700
O	1.29563500	-0.97241000	0.54099300
O	3.20503600	-0.25516100	-0.21644300
N	-2.19728200	-0.91238700	0.05861400
O	-2.53133400	-0.59897400	-1.05259700
O	1.44984400	1.00576000	-0.44293400
H	-0.71385500	1.62709400	-0.12589700
N	-1.58821600	1.41730100	0.34800700
H	-2.33402600	1.49807300	-0.34169000
N	-1.54955500	0.07481700	0.76134100
H	0.38103000	-0.61490800	0.56253400
H	-1.68544500	-0.06907300	1.75584900

C_s-Complex3 (C_1)

0 1

N	-0.37726700	0.68710900	0.06263100
O	-0.03588900	0.76215600	1.18350300
O	-0.44408700	1.41768300	-0.85371600
N	-2.16698500	-1.07111200	-0.14133600
O	-2.81241100	-0.17583500	0.28368100
O	-0.86748600	-0.85869000	-0.33890600
N	3.12387300	-0.58916000	0.52841100
H	4.13108300	-0.52216000	0.42445600
H	2.84099200	0.02696300	1.27944700
N	2.42774200	-0.19177100	-0.65918100
H	2.94291100	0.50046100	-1.19480800
H	2.31245400	-1.01324800	-1.23927500

C_s-Complex4 (C_1)

0 1

N	1.85920800	-0.50565700	0.01420700
O	1.80176400	-1.61199000	-0.46854800
O	2.58506400	-0.09475400	0.88522100
N	-2.73629100	-0.12952000	-0.35298500
O	-3.84419500	-0.21204400	0.00814000
O	-1.84486000	-0.00585400	0.73104800
H	2.08545100	2.02323900	-0.51739600
N	1.11830900	1.78166400	-0.32275000
H	0.88915500	2.04893400	0.62550000
N	0.85502800	0.43723200	-0.50540300
H	0.74057400	0.18358300	-1.48229200
H	-0.97114800	0.05534000	0.29581600

C_s-Complex5 (C_1)

0 1

N	-1.32413400	-0.65719100	-0.10875300
O	-2.43064800	-0.63439600	0.34702100
O	-0.64424100	-1.66474500	-0.31639800
N	-0.58491100	1.09843300	-0.58667800
O	1.03550800	0.75118600	0.80475000
O	-1.26115400	1.86466200	-0.11403800
N	2.75740900	-0.23859700	-0.52261100
H	2.31442000	0.08943800	-1.37704300
H	3.30883500	0.54260800	-0.17387700
N	1.67892300	-0.38493400	0.43261700
H	0.99258500	-1.05943700	0.02317600
H	2.09743200	-0.83023600	1.25503800

C_s-Complex6 (C_1)

0 1

N	-2.16541400	-0.20627300	-0.32184200
O	-1.70623300	-0.35591200	0.98004900
O	-3.24163100	-0.65026800	-0.46807200
N	1.57373500	-1.03758900	0.01347900
O	2.47878400	-1.66864900	-0.33624900
O	1.93940500	0.37708900	0.08026200
H	-0.29686100	1.42873300	-1.13541500
N	0.28771400	1.95344100	-0.49630000
H	1.03140300	2.43672900	-0.99109900
N	0.75719800	1.11506000	0.50300200
H	-0.80941500	0.05128200	0.94546700
H	1.13963500	1.69269900	1.24474900

C_s-Complex7 (C_1)

0 1

N	-1.13333700	-0.75549400	0.01064700
O	-1.47470700	-1.61199200	-0.75290500
O	-0.65599600	-0.91515400	1.13046800
N	-1.24314900	1.09376900	-0.48201700
O	-1.33114900	1.69156800	0.47340900
O	0.96654200	0.86544800	-0.84869200
N	2.47143200	-0.72020100	0.09857600
H	1.83317300	-1.49093900	-0.08687900
H	2.96618100	-0.54662700	-0.77409100
N	1.61761600	0.44526000	0.26032700
H	0.94341300	0.17583500	1.00257000
H	2.23176900	1.17943200	0.62742600

C_s-Complex8 (C_1)

0 1

N	3.67507900	0.17295000	-0.01037900
O	4.74345200	-0.30805600	-0.01713200
O	2.66643500	-0.79316100	-0.00731300
N	-3.99409900	-0.59543900	-0.02320400
O	-2.79700000	-1.25032800	0.04090200
O	-3.90427400	0.58713200	-0.05685000
N	0.42475500	1.08049100	0.01335600
H	1.84637100	-0.25336500	-0.00160600
H	0.71830700	2.07258700	-0.00849500
N	-0.79437200	0.92273800	0.05318300
H	-2.07367000	-0.57175800	0.04582500
H	-1.33945300	1.80264900	0.05671900

C_s-TS1 (C_1)

0 1

N	0.00000000	0.00000000	0.00000000
O	1.29740421	0.00000000	0.00000000
O	-0.60120825	1.04902354	0.00000000
N	0.53589387	-3.06168433	-1.00874828
O	0.02585584	-3.88891583	-0.41684774
O	-0.57379641	-1.11876790	0.00695695
H	1.20416130	-2.53604194	1.78584579
N	1.92531232	-2.98787819	1.23229400
H	1.75246533	-3.99094967	1.21115324
N	1.90832777	-2.44540819	-0.03569032
H	1.68797946	-1.31670511	-0.02817546
H	2.73792653	-2.70293653	-0.56556823

C_s-TS2(C_1)

0 1

N	-0.79411700	0.91906700	0.04235100
O	-0.58940100	1.71894300	-0.80809300
O	-1.01270000	0.96009500	1.20615600
N	2.25598000	-0.64475500	-0.21847600
O	2.75552000	0.27737300	0.37505400
O	0.96255500	-0.68724200	-0.24730400
H	-2.27862300	-1.23466200	1.02216500
N	-1.64262300	-1.59276600	0.31603400
H	-0.73792300	-1.82162200	0.72565600
N	-1.41312800	-0.65132200	-0.65101000
H	-2.22314800	-0.43883400	-1.22953500
H	-0.53087900	-0.86980000	-1.14707800

C_s-TS3 (C_1)

0 1

N	-0.48922400	0.50539200	0.06919200
O	-1.13020900	1.25257100	-0.66693100
O	-0.02434800	0.84197000	1.21625200
N	-1.78143000	-1.07920700	0.35850700
O	0.42300700	-0.39608900	-0.58479500
O	-2.71560200	-0.70744800	-0.15928700
N	2.89271100	-0.68751200	0.11846400
H	2.55926300	-1.08577800	0.99063700
H	2.95757600	-1.42624500	-0.57527000
N	1.97754100	0.25899200	-0.29278000
H	1.60560400	0.83753000	0.49473700
H	2.25759400	0.76280400	-1.12569300

C_s-TS4 (C_1)

0 1

N	1.38831200	-0.66982700	-0.02333200
O	0.56530600	-1.55576300	0.42007000
O	2.48644600	-1.01636900	-0.34771900
N	0.52598600	1.44298900	0.42515100
O	0.87945300	2.23412200	-0.28483500
O	-1.20463700	1.02431200	-0.07288700
H	-1.79724000	-1.29498000	-1.21597400
N	-2.39348300	-0.96203400	-0.46400900
H	-3.06603300	-0.31192900	-0.86225500
N	-1.56075000	-0.22650900	0.42236700
H	-0.58604700	-0.87307100	0.55086100
H	-2.08368200	-0.10278000	1.28910600

C_s-TS5 (C_1)

0 1

N	0.34995900	0.46088800	0.11404900
O	0.14769100	1.62509100	-0.27052800
O	0.41844800	0.11031300	1.32166600
N	2.13047400	-0.15021800	-0.73071800
O	2.69930300	-0.60455800	0.13636000
O	-0.30018300	-0.57378100	-0.67629400
N	-2.82136800	0.07437200	-0.09540900
H	-2.50227300	0.98999800	0.20904900
H	-2.99834500	0.12680500	-1.09376800
N	-1.77925000	-0.82236200	0.12122700
H	-1.36500500	-0.73712500	1.06116100
H	-2.01514900	-1.77494700	-0.13013200

C_s-TS6 (C_1)

0 1

N	1.59047200	0.01501400	-0.16616100
O	2.72255700	-0.35412800	-0.26650200
O	1.41412600	1.19591000	0.37442100
N	-0.46018600	-1.54825300	-0.26005100
O	-0.63082700	-1.65001700	0.87231700
O	-1.37698800	-0.42218200	-0.91074700
N	-1.02578600	1.72663700	0.16383400
H	0.23793100	1.45032400	0.28807800
H	-1.22116300	2.24799700	-0.68624900
N	-1.76412900	0.57296100	0.10961900
H	-1.67372600	0.07075100	1.00367200
H	-2.75657400	0.70974300	-0.09209600

$HONO_2$ (C_s)

0 1

N	0.15135700	0.03281700	0.00000100
O	-1.14471600	-0.52128000	-0.00000500
O	1.02400900	-0.77833500	0.00000200
O	0.20340000	1.23840100	-0.00000200
H	-1.72104900	0.25999700	0.00003500

$H_2NN(H)NO$ (C_s)

0 1

N	0.00000000	0.00000000	0.00000000
H	1.01223451	0.00000000	0.00000000
N	-0.59174751	1.24859386	0.00000000
H	-0.72878939	1.60578679	0.94157471
H	-1.49082457	1.19179266	-0.46081390
N	-0.43048695	-0.94546440	0.97239083
O	0.33631278	-1.86688479	1.16972090

O	-1.52331992	-0.76755782	1.46744523

trans-HONO (C_1)

0 1

H	-1.71587800	0.43962200	0.00012800
N	0.17891700	0.48537600	-0.00001800
O	-1.04186900	-0.25486300	-0.00001400
O	1.09980100	-0.22479400	0.00001400

$H_2NN(H)NO_2$ (C_1)

0 1

N	-0.59856600	0.06210500	-0.02039200
O	-1.61145200	-0.60276300	0.06844500
O	-0.49998400	1.27099100	-0.02578300
H	1.74371500	0.50919600	0.93181100
N	1.80069800	-0.06244400	0.09335800
H	2.06399600	0.52776100	-0.68526500
N	0.60056400	-0.68487300	-0.19233800
H	0.46491200	-1.58629500	0.24775900

cis-HONO (C_1)

0 1

H	0.94274500	1.03421900	0.00001300
N	-0.17093000	-0.51802600	0.00000300
O	1.08743700	0.06658100	-0.00000200
O	-1.05571700	0.25741400	-0.00000100

cis-N_2H_2 (C_{2v})

0 1

N	-0.61718800	-0.11947800	0.00000000
H	-1.02333500	0.83629000	-0.00000200
N	0.61720500	-0.11947600	0.00000000
H	1.02322000	0.83638800	0.00000200

$H_2NN(H)ONO$ (C_1)

0 1

N	-1.18567700	-0.09243500	-0.44454600
O	-2.18584500	-0.23329300	0.13427800
O	-0.14720600	0.34922200	0.45165300
H	1.81641400	-1.32855400	-0.44155100
N	2.01835800	-0.45616900	0.02804100
H	2.07607700	-0.60305200	1.03283300
N	1.07687200	0.49272000	-0.33622400
H	1.40504400	1.39535500	-0.00962600

N_2O_4_PW91PW91 (D_{2h})

0 1

N	0.00000000	0.00000000	0.92918200
N	0.00000000	0.00000000	-0.92918200
O	0.00000000	1.10389800	-1.38796000
O	0.00000000	-1.10389800	-1.38796000
O	0.00000000	1.10389800	1.38796000
O	0.00000000	-1.10389800	1.38796000

N_2H_4_PW91PW91 (C_2)

0 1

N	-0.71112700	-0.07603300	-0.10039400
N	0.71112700	-0.07601000	0.10041100
H	-1.06264700	0.84237700	-0.38290100
H	-1.14612600	-0.31018000	0.79103100
H	1.06264800	0.84246000	0.38271600
H	1.14612600	-0.31035500	-0.79096200

C_s-Complex1_PW91PW91 (C_1)

0 1

N	1.67652000	0.01929500	0.03262800
O	1.33661600	-1.09170300	-0.49782900
O	2.84055200	0.28221400	0.29339000
N	-1.19286600	0.97249900	-0.71634100
O	-1.86181300	1.43640400	0.09774100
O	0.74729500	0.87414400	0.31274600
H	-1.15523300	-0.97362100	1.50443900
N	-1.85522400	-1.19206200	0.79105500
H	-2.65419000	-0.55989700	0.93735100

N	-1.28889800	-0.94250600	-0.44749400
H	-0.23129300	-1.13351300	-0.49853400
H	-1.83719600	-1.34202600	-1.21057400

C_s-Complex2 _PW91PW91

0 1

N	2.06087300	-0.02172200	-0.06211500
O	1.18301600	-1.07005200	0.30308800
O	3.19791000	-0.36696200	-0.23268900
N	-2.24550500	-0.83519900	0.27706000
O	-2.67181300	-0.70906500	-0.85835500
O	1.56441200	1.09275000	-0.15701300
H	-0.56824800	1.68002300	-0.28279700
N	-1.52354600	1.45448400	0.01207000
H	-2.07914300	1.24848300	-0.83199900
N	-1.48094100	0.23290400	0.70564300
H	0.30368000	-0.62166300	0.42217800
H	-1.52064900	0.30651800	1.72375200

C_s-TS1_PW91PW91 (C_1)

0 1

N	-1.73864900	0.06712700	-0.04444700
O	-1.23723000	-1.11286200	0.30357600
O	-2.93958600	0.15820200	-0.20751700
N	1.36152700	0.96894600	0.64149800
O	1.97159500	1.35881700	-0.26235400
O	-0.93365800	1.01889200	-0.18964600
H	1.30556400	-1.16915400	-1.43756200
N	1.90901300	-1.27495900	-0.62010200
H	2.77002500	-0.73804700	-0.78639600
N	1.23528200	-0.81350100	0.49255400
H	-0.01337900	-0.97577300	0.42696700
H	1.67862200	-1.13470800	1.35799700

$H_2NN(H)NO$_PW91PW91 (C_1)

0 1

N	-0.84228000	0.55759900	-0.00087200
O	-1.27114500	-0.59755900	0.01634100
H	1.80286400	-0.65701300	0.77227000
N	1.32505100	-0.47154800	-0.11420700
H	0.65363800	-1.24375800	-0.25479200
N	0.49597700	0.64669800	0.05509900
H	0.86142500	1.55199300	-0.22834400

$HONO_2$_PW91PW91 (C_s)

0 1

N	0.16195600	0.03152200	-0.00002500
O	-1.18244100	-0.49144500	-0.00002700
O	1.00657200	-0.81964300	0.00002200
O	0.24919600	1.24269100	-0.00000300
H	-1.72031100	0.32652500	0.00023300

A2.3.2Decomposition of $H_2NN(H)NO$

$H_2NN(H)NO$ (C_s)

0 1

N	0.00000000	0.00000000	0.00000000
O	1.21449462	0.00000000	0.00000000
H	0.67307493	2.64331755	0.00000000
N	0.12801267	2.28989062	-0.78251754
H	0.80043033	2.00513381	-1.49139352
N	-0.56071557	1.15237827	-0.36058654
H	-1.56539344	1.14330710	-0.43205469

d-complex1 (C_s)

0 1

N	0.00000000	0.00000000	0.00000000
O	1.20269464	0.00000000	0.00000000
H	-0.11738512	3.06490330	0.00000000
N	0.07455260	2.32052132	0.65744296
H	-0.11707951	2.60831394	1.60804973
N	-0.60533812	1.15812523	0.32739359
H	-1.61378420	1.09447647	0.31086474

d-complex2 (C_s)

0 1

N	0.00000000	0.00000000	0.00000000
O	1.35720976	0.00000000	0.00000000
H	-0.26521826	3.08073553	0.00000000
N	0.32889539	2.25966405	0.00052307
H	1.63452086	0.94569670	-0.00025343
N	-0.43545400	1.20222911	0.00027829
H	-1.45265308	1.23856682	0.00122174

d-complex3 (C_1)

0 1

N	0.00000000	0.00000000	0.00000000
O	1.26342643	0.00000000	0.00000000
H	0.91665180	2.09388753	0.00000000
N	-0.06025885	2.14560568	0.27589920
H	-0.58937974	2.95698342	0.00490785
N	-0.75962265	1.00998830	0.09894244
H	-0.50459330	-0.88306906	-0.08600266

d-complex4 (C_s)

0 1

N	0.00000000	0.00000000	0.00000000
O	1.26538819	0.00000000	0.00000000
H	0.83961531	2.17767849	0.00000000
N	-0.17598196	2.30930825	0.00000000
H	-1.68426919	1.02513898	0.00047259
N	-0.67421007	1.12740370	0.00013443
H	-0.55758353	-0.85263843	0.00084800

d-complex5 (C_1)

0 1

N	0.00000000	0.00000000	0.00000000
O	1.21193454	0.00000000	0.00000000
H	1.61185070	1.92370959	0.00000000
N	1.04442454	2.79406253	-0.10268993
H	-0.70626551	3.29412736	-0.39444332
N	-0.11407266	2.45508581	-0.29881623
H	-0.34704604	0.02933363	-0.99549537

d-TS1 (C_1)

0 1

N	0.00000000	0.00000000	0.00000000
O	1.30169441	0.00000000	0.00000000
H	0.29932529	3.03128937	0.00000000
N	0.56353455	2.13242586	-0.38174390
H	1.44778447	1.16915858	-0.10735966
N	-0.39308022	1.21587527	-0.17495401
H	-1.39104365	1.37531951	-0.21267637

d-TS2 (C_1)

0 1

N	-0.86626700	0.52716200	0.01124000
O	-1.31757800	-0.59836500	-0.02623200
H	2.22338200	-0.20438800	-0.32846100
N	1.29224000	-0.50568400	-0.07673700
H	1.30658500	-1.00458600	0.80830900
N	0.45913200	0.61548900	-0.00255400
H	0.81492500	1.53712400	0.20636400

d-TS3 (C_1)

0 1

N	0.00000000	0.00000000	0.00000000
O	1.23613751	0.00000000	0.00000000
H	1.22419580	1.97939455	0.00000000
N	0.24992672	2.23523084	0.16740706
H	-0.10654367	3.16101291	0.01040271
N	-0.62039608	1.25185506	0.06337151
H	4 -0.70684532	0.41713834	-0.96696886

d-TS3 (C_1)

0 1

N	0.00000000	0.00000000	0.00000000
O	1.25837324	0.00000000	0.00000000
H	0.94490073	2.08138443	0.00000000
N	-0.05329229	2.29129287	0.14654991
H	-1.02641781	1.77218013	-0.70472698

N	-0.71446871	1.07724649	0.13715148
H	-0.53104569	-0.86995538	-0.02549344

d-TS5 (C_1)

0 1

N	0.00000000	0.00000000	0.00000000
O	1.24743587	0.00000000	0.00000000
H	1.36318517	1.81558264	0.00000000
N	0.51437372	2.44495360	0.06227596
H	-1.36977876	2.07753688	-0.04114587
N	-0.42528014	1.69835484	-0.15784437
H	-0.39020239	-0.27865323	-0.93038216

trans-N_2H_2 (C_{2h})

0 1

H	0.00000000	0.00000000	0.00000000
N	1.05694148	0.00000000	0.00000000
H	2.32820757	1.46019384	0.00000000
N	1.34633747	1.18719032	-0.09680587

cis- N_2H_2 (C_{2v})

0 1

H	0.00000000	0.00000000	0.00000000
N	1.03847619	0.00000000	0.00000000
N	1.52135971	1.13617027	0.00000000
H	0.80087205	1.88399125	0.00000000

NNH_2 (C_{2v})

0 1

H	0.00000000	0.00000000	0.00000000
N	1.04344395	0.00000000	0.00000000
H	1.43878658	0.96574622	0.00000000
N	1.71751876	-1.00416564	-0.00166675

HON (C_1)

0 1

N	0.00000000	0.00000000	0.00000000
O	1.25145900	0.00000000	0.00000000
H	1.62922500	0.92488000	0.00000000

HNO (C_1)

0 1

N	0.00000000	0.00000000	0.00000000
O	1.19674500	0.00000000	0.00000000
H	-0.34442400	1.00429500	0.00000000

A.2.3.3 N_2O_4 (D_{2h}) + N_2H_4 Reaction

D_{2h}-Complex1

0 1

N	0.00000000	0.00000000	0.00000000
H	1.01235717	0.00000000	0.00000000
H	-0.31415293	0.96622512	0.00000000
N	-0.43988856	-0.71613490	1.15985092
H	-1.34888690	-1.11364349	0.95791082
H	-0.52969477	-0.11303912	1.97095320
O	-0.24876672	-0.25484515	-3.39869321
N	-1.13706456	-0.65079150	-2.72231847
O	-2.23030550	-0.26214460	-2.47990128
N	-0.75770214	-2.18999074	-1.91616340
O	0.31577919	-2.60229722	-2.19498850
O	-1.64970404	-2.58326150	-1.24102970

D_{2h}-Complex2

0 1

N	0.00000000	0.00000000	0.00000000
H	1.01539567	0.00000000	0.00000000
H	-0.74253937	1.90283048	0.00000000
N	-0.54686290	-0.54718880	1.14508905
H	-0.55981648	-1.56221011	1.12877314
H	-1.48476056	-0.18763632	1.27689967
O	-1.31846684	2.67847358	0.15676020
N	-2.36765571	2.13698283	0.91060600
O	-3.16857792	2.94157293	1.18974225

N	-0.37204376	-0.63326199	-1.27630655
O	0.37832725	-0.38649055	-2.19204217
O	-1.38931838	-1.27984636	-1.28367830

D_{2h}-Complex3

0 2

N	0.00000000	0.00000000	0.00000000
H	1.01721440	0.00000000	0.00000000
H	-1.25591063	1.14706432	0.00000000
N	-0.43943886	-1.25899531	0.03255080
H	-1.43721070	-1.34815477	-0.11359212
H	0.15195576	-2.02551453	-0.25557582
N	-3.19862049	1.20983737	-0.13703510
O	-2.01764930	1.82757672	-0.00379603
O	-3.14160839	0.01612593	-0.21744709

D_{2h}-Complex4

0 1

N	0.00000000	0.00000000	0.00000000
H	1.03138220	0.00000000	0.00000000
H	-0.70433782	1.84131974	0.00000000
N	-0.40118132	-1.16347728	0.00082228
H	-1.43256491	-1.16349824	0.00082230
H	0.30319596	-3.00485168	0.00105130
N	-0.40709202	-4.79276565	0.00215899
N	0.00702022	3.62886646	-0.00063250
O	-1.05980932	2.76704225	-0.00097677
O	1.06349624	3.09395278	0.00079742
O	-1.46382223	-4.25841988	0.00259322
O	0.65926401	-3.93034431	0.00111304

D_{2h}-Complex5

0 1

N	0.00000000	0.00000000	0.00000000
H	1.01495053	0.00000000	0.00000000
H	-0.86993694	1.73863796	0.00000000
N	-0.43011958	-0.56060123	1.19276361
H	-0.23643605	-1.55556453	1.25640232
H	-1.41619478	-0.37043159	1.32318584
O	-1.41199736	2.53347626	0.21373793
N	-2.45204863	2.00615558	0.96744755
O	-3.21436314	2.82922442	1.31135361
N	-1.27659948	-0.18391616	-1.96882748
O	-1.54989126	-0.83963924	-2.88264452
O	-0.28329613	-0.86357192	-1.13794553

D_{2h}-TS1

0 1

N	0.00000000	0.00000000	0.00000000
H	1.01601395	0.00000000	0.00000000
H	-0.48051195	0.95300824	0.00000000
N	-0.55729530	-0.85909462	0.91487088
H	-0.49853578	-1.81907760	0.58306940
H	-1.53023206	-0.60858295	1.05442677
O	-1.69059917	1.86423788	-0.45496614
N	-1.97381194	1.16198928	-1.46575939
O	-2.90732216	1.41266758	-2.17427856
N	-0.41161887	-0.44302930	-1.74483542
O	0.37935179	0.05247316	-2.49216788
O	-1.00405009	-1.48070858	-1.75654151

D_{2h}-TS2

0 1

N	0.00000000	0.00000000	0.00000000
H	1.02059285	0.00000000	0.00000000
H	-0.60672428	1.38797298	0.00000000
N	-0.42476209	-0.62970943	-1.07597872
H	-1.42008435	-0.56322418	-1.24951355
H	0.18848521	-0.95005071	-1.81205901
N	-3.15675111	2.39200236	1.98987525
N	-2.41827406	2.11225714	-0.07444788
O	-1.10515321	2.32494018	-0.04358733
O	-2.79621554	1.04056945	-0.46355578
O	-4.09256987	1.69651589	2.25849118
O	-2.61907400	3.26416214	2.60658354

D_{2h}-TS3

0 1

N	0.00000000	0.00000000	0.00000000
H	1.01252150	0.00000000	0.00000000
H	-0.39023710	0.96603782	0.00000000
N	-0.52768175	-0.87460659	-0.87481343
H	-1.50774923	-0.70494114	-1.06424695
H	0.01219245	-1.05870964	-1.74666088
N	-0.29419178	0.66124629	-3.44604711
N	0.51294116	2.36652492	-1.77903662
O	-0.48961004	2.43896419	-1.09080317
O	1.55001045	1.86124153	-1.42850889
O	-1.44810016	0.55406049	-3.11326436
O	0.55988826	-0.18883743	-3.26738103

D_{2h}-TS4

0 1

N	0.00000000	0.00000000	0.00000000
H	1.01328132	0.00000000	0.00000000
H	-0.61529519	1.05045492	0.00000000
N	-0.50232648	-1.05435293	0.64054241
H	0.02542528	-1.91700296	0.58652540
H	-1.50038596	-1.16701148	0.51709243
O	-1.26753936	2.10459586	-0.24554055
N	-1.30867371	1.97522259	-1.52741565
O	-1.86912952	2.80349971	-2.17523167
N	-0.47677399	-0.12137323	-2.96694664
O	-0.85438263	-0.29893263	-4.09162936
O	-0.07966269	-0.93603719	-2.16695428

A.2.3.4 $H_2NN(H)NO_2$ Decomposition

d2-Complex1 (C_1)

0 1

N	0.00000000	0.00000000	0.00000000
H	1.03356188	0.00000000	0.00000000
N	-0.36554484	1.17809712	0.00000000
H	0.94171799	2.51524037	-0.00047479
H	-1.39564132	1.20331981	0.00029266
N	2.72696530	1.95645883	-0.00146909
O	3.83592052	2.33998232	-0.00274097
O	1.80643359	2.99479120	-0.00156513

d2-Complex2 (C_1)

0 1

N	0.00000000	0.00000000	0.00000000
H	1.01713619	0.00000000	0.00000000
N	-0.83288530	1.04663247	0.00000000
H	-2.03368002	-0.19788747	0.01777853
H	-0.36679249	1.81341201	-0.47333767
N	-0.49867814	-1.19381332	0.11182974
O	0.14292722	-2.22712813	0.26783977
O	-1.85314705	-1.18414412	0.13772995

d2-Complex3 (C_1)

0 1

N	0.00000000	0.00000000	0.00000000
H	1.03568914	0.00000000	0.00000000
N	-0.51076494	1.12124526	0.00000000
H	-0.94991111	-1.63230185	0.00000000
H	0.19363075	1.88145985	0.00000000
N	-0.25483976	-3.37755380	-0.00013790
O	-0.56725198	-4.50967374	0.00010095
O	-1.35624963	-2.53153766	0.00013951

d2-Complex4 (C_1)

0 1

N	0.00000000	0.00000000	0.00000000
H	2.15462604	0.00000000	0.00000000
N	-1.35556970	0.21863235	0.00000000
H	-1.65973949	0.81406689	0.76697340
H	-1.82951771	-0.67129515	-0.04259768
N	0.62345358	0.92568371	0.58286900
O	2.01296346	0.80187947	0.52798334
O	0.18964004	1.90679564	1.17875213

d2-Complex5 (C_1)

0 1

N	0.00000000	0.00000000	0.00000000
H	2.83886437	0.00000000	0.00000000
N	-1.02100992	0.76041469	0.00000000
H	-0.71307241	1.64245001	0.42417397
H	-0.06468907	-0.93950184	-0.38247363
N	1.10814304	0.19133438	0.74038514
O	2.15904135	-0.64450884	0.25806678
O	1.37884167	1.33134804	1.16780092

d2-Complex6 (C_1)

0 1

N	0.00000000	0.00000000	0.00000000
H	1.83213642	0.00000000	0.00000000
N	-0.60430618	1.07425371	0.00000000
H	0.11206020	1.82057589	-0.00127063
H	-0.68540458	-0.76912940	0.00141923
N	3.24828382	1.31505075	-0.00008911
O	2.83681160	0.02600249	0.00065801
O	2.36813442	2.11815893	-0.00081438

d2-Complex7 (C_1)

0 1

N	0.00000000	0.00000000	0.00000000
H	1.02489323	0.00000000	0.00000000
N	-0.48621297	1.41863797	0.00000000
H	-0.62401115	1.62598099	-1.00127064
H	-1.42083917	1.31104246	0.43651913
N	-0.59340890	-0.70934081	0.99370746
O	0.03014585	-1.66597035	1.36615065
O	0.30764663	2.25873207	0.60384366

d2-Complex8 (C_1)

0 1

N	0.00000000	0.00000000	0.00000000
H	1.02561527	0.00000000	0.00000000
N	-3.08015599	0.07977564	0.00000000
H	-2.65823314	1.04751374	0.01839848
H	-1.39045074	-1.31323584	-0.01901756
N	-0.36045111	-1.20859794	-0.01745252
O	0.32530310	-2.23795406	-0.03226651
O	-4.27355495	0.14759226	-0.00627314

H_2NO (C_s)

0 2

N	0.00000000	0.00000000	0.00000000
H	1.01513819	0.00000000	0.00000000
H	-0.49469353	0.88642392	0.00000000
O	-0.62608610	-1.06625676	0.30137749

HNN(H)O (C_1)

0 1

N	0.00000000	0.00000000	0.00000000
H	1.02607510	0.00000000	0.00000000
H	-1.37771032	1.32951148	0.00000000
N	-0.35456496	1.20672914	0.00036754
O	0.32356044	2.24188817	0.00117696

HNNO (C_1)

0 2

N	0.00000000	0.00000000	0.00000000
H	1.03398181	0.00000000	0.00000000
N	-0.43505179	1.14146282	0.00000000
O	-0.03345059	2.27878908	-0.00212162

d2-TS1 (C_1)

0 1

N	0.00000000	0.00000000	0.00000000
H	1.02104352	0.00000000	0.00000000
N	-0.40106780	1.19331483	0.00000000
H	0.22612146	1.90162548	0.51149290
H	-1.41049829	1.29427658	0.08716768
N	1.20976789	0.73162529	2.09610742
O	1.88170039	0.36718699	3.02491056
O	1.02784469	1.96550860	1.86891328

d2-TS2 (C_1)

0 1

N	0.00000000	0.00000000	0.00000000
H	1.01656404	0.00000000	0.00000000
N	-0.84932107	1.04659022	0.00000000
H	-1.96861420	-0.10618895	0.10813989
H	-0.53905590	1.70495266	-0.70904279
N	-0.51442712	-1.18012623	0.21585348
O	0.11770583	-2.20316090	0.42275495
O	-1.85241656	-1.12880462	0.28226684

d2-TS3 (C_1)

0 1

N	0.00000000	0.00000000	0.00000000
H	1.02298860	0.00000000	0.00000000
N	-0.69811321	1.08405072	0.00000000
H	-1.82104828	0.12926546	-1.09498306
H	-0.11164669	1.90364080	-0.16818517
N	-0.39763251	-1.05382052	-1.04571381
O	-0.02534437	-2.19288493	-1.00938340
O	-1.70562870	-0.81285323	-1.39538831

d2-TS4 (C_1)

0 1

N	0.00000000	0.00000000	0.00000000
H	1.30855337	0.00000000	0.00000000
N	-1.31257088	0.41766919	0.00000000
H	-1.79991294	0.09527381	0.83108195
H	-1.79997816	0.09507354	-0.83096605
N	0.31532732	-1.29146140	0.00028931
O	1.62668637	-1.26182931	0.00025653
O	-0.38683757	-2.26307747	0.00057958

d2-TS5 (C_1)

0 1

N	0.00000000	0.00000000	0.00000000
H	2.22213028	0.00000000	0.00000000
N	-1.40687305	0.11558611	0.00000000
H	-1.63725615	0.83052621	0.70174481
H	-0.50478899	-0.92168299	0.38556931
N	0.68301899	0.79058350	0.76319108
O	2.05997005	0.56682691	0.77043938
O	0.24876194	1.72126248	1.42689769

d2-TS6 (C_1)

0 1

N	0.00000000	0.00000000	0.00000000
H	2.83513762	0.00000000	0.00000000
N	-0.88870343	0.87143335	0.00000000
H	-0.42450307	1.73466791	0.33413736
H	-0.23933531	-0.96645072	-0.22607518
N	1.16858552	0.08548548	0.93509956
O	2.22323963	-0.68703836	0.31331872
O	1.46055961	1.24909425	1.23814313

d2-TS7 (C_1)

0 1

N	0.00000000	0.00000000	0.00000000
H	1.02209185	0.00000000	0.00000000
N	-0.44850413	1.39223790	0.00000000
H	0.27195258	2.11290944	-0.07813083
H	-1.22873780	1.54099565	-0.62974988
N	-0.30558646	-0.27559216	1.46829505
O	0.74296922	-0.24190832	2.14717549
O	-1.12899062	0.93225050	1.48195046

d2-TS8 (C_1)

0 1

N	0.00000000	0.00000000	0.00000000
H	1.03103975	0.00000000	0.00000000
N	-2.20421120	0.64854267	0.00000000
H	-2.00851589	0.74422696	-1.01177250
H	-1.84330631	-0.29315430	0.53010430
N	-0.48157447	-0.91763335	0.76586944
O	0.24530342	-1.73536020	1.32626968
O	-2.66050009	1.59536267	0.57263806